Analysis of Stress Concentration in a Thick Walled Cylinder Containing Elliptical Hole
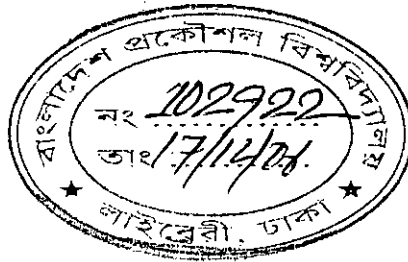
By

Safina Hussain

Submitted as the partial fulfillment for the degree of
MASTER OF SCIENCE IN MECHANICAL ENGINEERING

DEPARTMENT OF MECHANICAL ENGINEERING
BANGLADESH UNIVERSITY OF ENGINEERING AND TECHNOLOGY
Dhaka, Bangladesh.

December, 2006

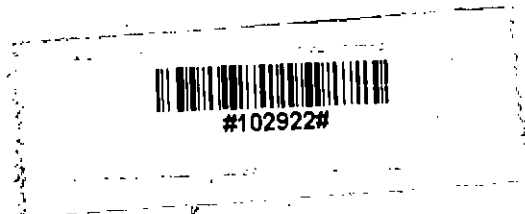The thesis titled "**Analysis of Stress Concentration in a Thick Walled Cylinder Containing Elliptical Hole**", **submitted by Safina Hussain, Roll no**: 040410067P Session April, 2004 has been accepted as satisfactory in partial fulfillment of the requirement for the degree of MASTER OF SCIENCE IN MECHANICAL ENGINEERING on 13.12.2006

BOARD OF EXAMINERS

1. _____ Chairman

   Dr. Abu Rayhan Md. Ali
   Professor
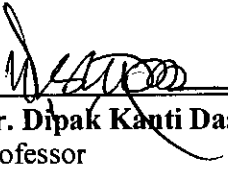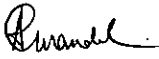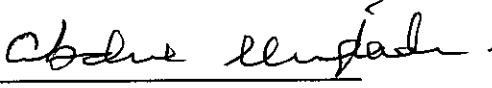   Department of Mechanical Engineering
   Bangladesh University of Engineering and Technology (BUET)
   Dhaka, Bangladesh.

2. _____ Member
   (Ex-officio)
   Dr. Md. Maksud Helali
   Professor and Head
   Department of Mechanical Engineering
   Bangladesh University of Engineering and Technology (BUET)
   Dhaka, Bangladesh.

3. _____ Member

   Dr. Dipak Kanti Das
   Professor
   Department of Mechanical Engineering
   Bangladesh University of Engineering and Technology (BUET)
   Dhaka, Bangladesh.

4. _____ Member

   Dr. Amalesh Chandra Mandal
   Professor
   Department of Mechanical Engineering
   Bangladesh University of Engineering and Technology (BUET)
   Dhaka, Bangladesh.

5. _____ External

   Dr. Abdul Muqtadir
   Professor
   Department of Civil Engineering
   Bangladesh University of Engineering and Technology (BUET)
   Dhaka, Bangladesh

CANDIDATE'S DECLERATION

It is hereby declared that this thesis or any part of it has not been submitted elsewhere for any degree or diploma.

Safina Hussain

Safina Hussain

ACKNOWLEDGEMENT

ABSTRACT

Pressure vessels used in industries usually incorporate openings in the main shell that causes local stress concentration around the opening which in turn reduces the pressure carrying capacity of the vessel. Therefore the aim of the present work is to investigate the stress concentration factor and also the stress distribution around the elliptical radial and offset holes having blended features at the intersection using finite element method. Two different orientations of the cross holes are investigated, one with the major axis of the hole along the longitudinal axis of the cylinder and another along the circumferential direction of the cylinder A finite element package ANSYS is used for the present computation. The cylindrical pressure vessels of different ratios of outer to inner diameter are analyzed using three dimensional solid isoparametric finite elements. After imposing boundary conditions and loading the vessel with internal pressure, the stress concentration factors (SCF) are obtained for some noticeable configurations of cross hole and cylinder. The comparison of principal and von Mises SCFs between equivalent circular (obtained by Hamilton *et al.* [11]) and elliptical radial cross holes show that elliptical cross holes reduce the SCFs around 30% and 28% respectively compared to the circular ones. Elliptical holes of circumferential orientation show about 55% reduction in SCF values than the longitudinal orientation, thus establishing that the circumferential orientation of the hole must be preferred over the longitudinal orientation. Again, the smaller offset cross holes provide a maximum reduction in principal and von Mises SCF values around 15% ad 9% respectively in comparison with the radial cross holes; thus making offset cross holes a better proposition than the radial ones.

Nomenclature

a	Inner radius of the cylinder
b	Outer radius of the cylinder
L	Cylinder half length
K	Stress concentration factor
K_e	Von Mises equivalent stress concentration factor
K_{S1}	Maximum Principal Stress concentration factor
r	Radial; distance from the cylinder axis.
R_a	Major radius of the ellipse
R_b	Blend corner radius
R_c	Minor radius of ellipse
SCF	Stress concentration factor
v	Poisson's ratio
E	Modulus of elasticity
σ_{ec}	Maximum von Mises equivalent stress of the plain cylinder
$\sigma_{\theta c}$	Maximum hoop/ principal stress of the plain cylinder
σ_{emax}	Maximum von Mises equivalent stress at the cross hole
$\sigma_{\theta max}$	Maximum hoop stress at the cross hole intersection
σ_{VM}	von Mises equivalent stress
σ_1	Principal stress
σ_{1max}	Maximum principal stress in the vessel
Orientation A	Major axis of the elliptical hole along the hoop direction of the cylinder
Orientation B	Major axis of the elliptical hole along the longitudinal axis of the cylinder
Smaller hole	$R_c = 0.4$ mm, $R_a = 0.8$ mm
Larger hole	$R_c = 2$ mm, $R_a = 4$ mm
FE method	Finite Element Method

CONTENTS

LIST OF FIGURES

LIST OF TABLES

CHAPTER 1

INTRODUCTION

Pressure vessels are being increasingly used for storage, industrial processing and power generation and it is clear that there is a need to determine the operating stresses in such vessels using analytical and experimental techniques. Pressure vessel systems are an essential feature of industrial life and are safe when used according to established practice. They are, however, a potential source of danger when misused. Knowledge of the behavior of the material used in the construction of a pressure vessel is essential if failure and disasters are to be avoided and the vessel is to be designed economically. To achieve these objectives as well as achieve good design, the magnitude of stresses and strains together with their distribution as well as stress concentration factors across the pressure vessel wall must be determined during the design stage.

Usually the stresses acting in principal direction are evaluated from basic established equations. The working stresses are kept below the yield stress of the material and to ensure that yielding does not occur in the region of discontinuities, or due to unknown factors, a safety factor is incorporated into the design. Safety factors can vary enormously from 2 to 20 in some pressure vessels [19]. Economic factors and safety demands have accelerated the need to collect and understand pressure vessel material behavior and to improve stress analysis techniques. Although there is no ideal material for a pressure vessel, selection of material must comply with its applications and the environment it will encounter in service.

In the construction of high pressure systems, the simplest and commonest form of container continues to be the thick walled cylinder with end closures. While many such cylinders may be 'perfect' in the sense that no geometric discontinuity, or stress-raiser, is introduced into the main cylindrical barrel, many other cases arise where for practical reasons some kind of transverse pressure tapping or cross-bore is unavoidable. A particular case is that of a thick-walled cylinder or pipe where it is necessary to introduce a small transverse hole or cross bore through the vessel wall for a specific purpose. In particular, vessels subjected to pressure fluctuations frequently must be connected to other parts of a system, and it may be necessary to consider the effect of such connections by passages which leave the cylinder in a more-or-less radial direction. High-pressure cylindrical vessels, e.g. as used in the petrochemical and pharmaceutical industries, usually incorporate openings in the main shell for variety of reasons such as, access, transfer of fluid, instrumentation, bursting caps, etc. The presence of an opening in the shell causes local stress concentration factor (SCF) depending on the size, shape and location of the opening. The sides holes or cross holes are major source of weakness in the vessel due to the high stress concentrations that occur. The severity of these high stress concentrations depends on the geometrical configuration of the cross bore at its junction with the main bore, and such concentrations reduce the pressure-carrying capacity of the vessel as well as reducing its fatigue life. It is clearly desirable to know how great such stress concentrations are, and to what degree any stress concentration factor, calculated on the usual assumptions of perfect elasticity, homogeneity, and isotropy and so on, is reflected in the lowered resistance of the member to an applied stress system. The peak stress occurring at the stress concentration may be critical in determining the design life of a vessel. It is therefore important to minimize the stress raising effect at the opening.

Most side wall openings in high pressure vessels are either circular or elliptical in cross section. Elliptical openings are one of the design possibilities of such openings. Many arrangements of opening may be employed for different practical purposes and there is a general terminology describing different types of opening. A single opening in one side of a vessel is called a side hole. Two holes symmetrically opposed about an axial plane of symmetry are called cross holes; i.e. the projected bores are coincident across the main bore of the vessel. Diametrically opposed cross

holes are referred to as radial cross holes. Cross holes on any other chord of the main cylinder are called offset cross holes.

Sectional view of a cylindrical vessel with radial cross holes is shown in figure 1.1. When the vessel is pressurized, the stress concentrates around the hole due to the discontinuity in geometry. In practice, a smooth blend is often incorporated in the design at the junction between the cross hole and the main bore [17], as illustrated in figure 1.2. This is intended to alleviate the local stress concentration factors (SCF) (chamfers have also been incorporated at this location for the same reason [16] as shown in figure 1.3. Elliptical cross holes provide lower SCF than their circular counterparts but are less widely used due to higher manufacturing costs [14]. Offset cross holes are cheaper to manufacture than radial cross hole. Figure 1.4 shows the sectional view of offset cross hole.
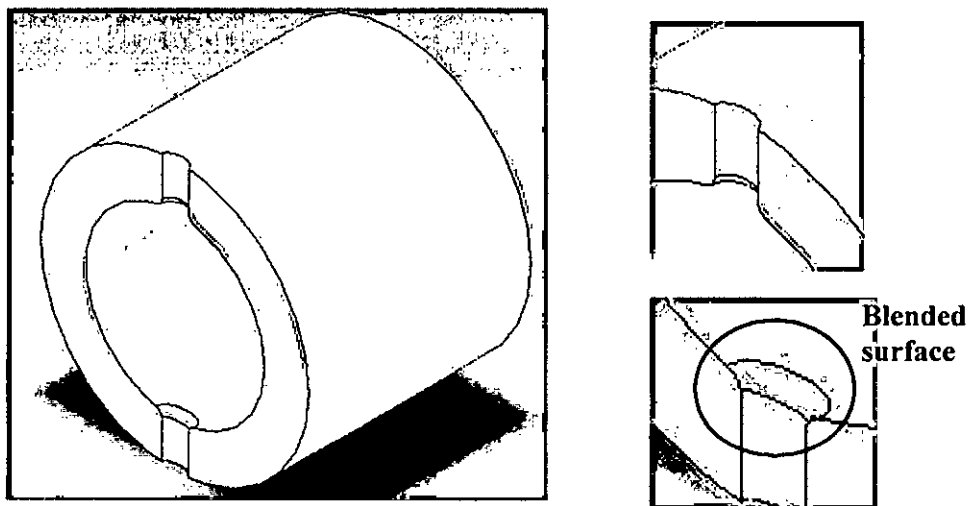
Figure 1.1: Radial elliptical cross holes having blended surface at the intersection.
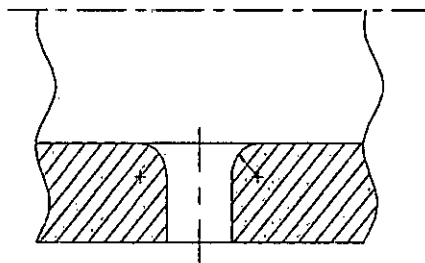
Figure 1.2: Cross holes having blended surface at the intersection

3
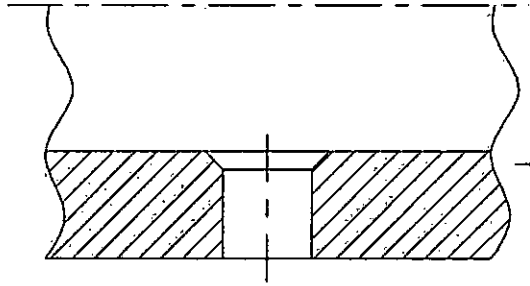
Figure 1.3: Cross holes having chamfer at the intersection
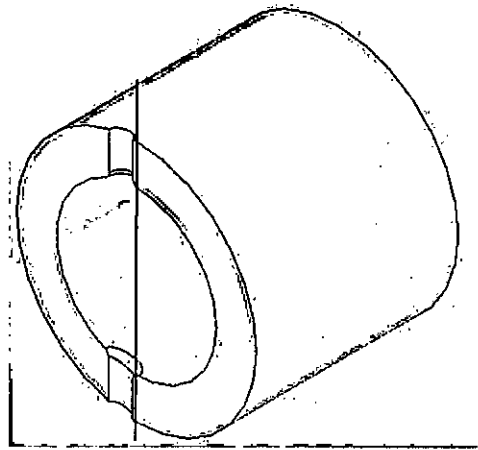
Figure1.4: Offset cross holes having blended surface at the intersection

1.1 MOTIVATION OF THE PRESENT RESEARCH WORK

The thick walled cylindrical pressure vessels with cross holes has received significant attention because it is obvious that such radial passages or holes, which have for brevity in the title been called cross bores, introduce geometric discontinuities to the cylinder configurations and hence a stress singularity locus. Unfortunately, the stress concentration that exists at the intersection of the holes and the main cylinder bore reduces the pressure capability of such configurations below that of the main cylindrical configuration [8]. A proper understanding of the severity of the stress in these regions of high stress fields would lead to usage of less conservative safety factors in the design vessels, improved plant availability and enhanced safety. For high pressure applications, a realistic picture of the state of stress in a vessel with side ports is needed because fatigue life is very critical and present day limitations of strength and ductility in commercial pressure vessel

4

materials prevent high factors of safety. At the point of discontinuities, the stress and strain must be precisely evaluated and this leads to better design methods and consequential increase in pressure vessel life. For these reasons these stress concentrations have been the concern of investigators and researchers over the years.

All of the earlier works to evaluate the stress distribution or the stress concentration factor due to the presence of side holes and cross holes were either analytical or experimental in nature [1-7]. One of the first attempts to analyze this problem by the use of finite element method was by Masu and Craggs [8]. The authors examined the stress concentrating effects on thick pressure vessels due to radial circular cross holes for two outer to inner radius ratio of the main cylinder (b/a); b/a =1.4 and 2. The numerical results showed good agreement with the experimental results, which was incorporated in the same paper. Stress analysis in the wall of cylinders containing an offset circular cross hole was done by Masu [10] using finite element method. The same author also examined the effects of cross hole diameter size on the principle stress distributions as well as the stress concentration factors along the radial and offset circular cross hole, which was published in the same year. Recently, another work by Hamilton *et al.* [11] studied the stress concentration factors for internally pressurized thick cylindrical vessels having radial and offset circular cross holes using finite element method. They considered chamfered and blended surface between the intersection of the inner bore of the main cylinder and the cross hole and compared their results with that of the plain cylinder. In their analysis they showed that the circular cross holes, having chamfered and blended intersection, have less SCFs in the main bore than that of circular crosshole without any of these features at the intersection.

Now-a-days, sideholes or crossholes of elliptical cross section are used in pressure vessels for various practical purposes. A noteworthy investigation of cylinders having elliptical side branches were performed by Fenner and Nadiri [14], who used boundary element method for the solution. From their study it is obtained that the elliptical side branches gives less stress concentration factor than those of circular ones. So, elliptical cross holes is the topic of interest in the present study. However, no significant finite element analysis has been reported on elliptical openings in pressure vessels so far. Therefore the aim of the present work is to investigate the

5

stress concentration factor and also the stress distribution around the elliptical radial and offset holes having blending features at the intersection using Finite Element Method.

1.2 OBJECTIVES

The specific objectives of the present research work are as follows:

(i) To investigate the stress concentration factor, stress distribution and the location of the maximum stress around an elliptical radial and offset cross holes with blending features at the intersection of the main bore and the cross hole of an internally pressurized thick walled cylinder by commercial finite element software. Two different orientation of the hole are investigated, one with the major axis of the hole along the hoop direction of the cylinder and another along the longitudinal direction of the cylinder.

(ii) To observe the effect of the main cylinder radius ratio (b/a) on stress concentration factors along with the change of cross hole diameter.

(iii)To compare the results obtained for elliptical cross holes with the circular cross holes as obtained in the literature.

CHAPTER 2

LITERATURE REVIEW

The problem of the stress concentration at the intersection of the side hole and cross hole of cylinders under internal pressure has been one of much concern to the high-pressure industry. As a result, this problem has become the concern of many researchers. One of the first noteworthy papers was that by Fessler and Lewin [1], who derived an approximate method of calculation (based on the theoretical solution for a hole in an infinite plate under uniform tension) and compared results with experimental data of stresses in a junction formed from 'Araldite' casting-resin B by the frozen stress photo-elastic model. They considered analytically the approximate stresses at a junction between a small branch pipe and a large pipe and the corrections in the simple theory appropriate to certain particular cases where the bores of the pipes were comparable. The comparison showed a theoretical value of the hoop stress-concentration factor of 3.70, which was 32% greater than the measured experimental value of 2.80 for a cylinder of K=3 and K_S= 2, where,

$$K = \frac{outside \quad diameter}{bore \quad diameter}$$

$$K_s = \frac{bore \quad diameter}{sidehole \quad diameter}$$

Thus the maximum stresses predicted by the theory of Fessler and Lewin [1] proved to be too large. However, their theory provided the equations to calculate asymptotic

stress-concentration factors for cylinders with side holes sufficiently small compared with the bore.

In a valuable but brief contribution to the discussion of an earlier paper by Lake [2], the same equation was derived in a more straightforward manner. He showed that in a particular case the theoretical stress concentration factor on the von Mises (or Maxwell) basis due to a small radial hole in a thick tube was 2.9. Following this, Morrison *et al.* [4] also presented the same equation using the same technique as Lake.

Probably the most extensive effort devoted to the subject of the stress-concentration problem was done by Faupel and Harris [3] who have carried out a project similar to, but more elaborate than, that undertaken by Fessler and Lewin [1], including a theoretical analysis and both photo-elastic and strain-gauge experimental observations. Their results are in reasonable agreement with each other, but an error was made by Faupel and Harris [3] in the theoretical work. They predicted a universal value of hoop stress concentration factor 2.5 for all closed-end cylinders with small side holes. The approach consisted in superimposing on the whole system to a fictitious volumetric tension which facilitates calculation, and as a result, the hoop stress concentration at a small circular cross-bore was found to be 2.5. If, however, the fictitious volumetric tension was removed, the hoop stress factor gave a change in value as

$$(4K^2+1)/(K^2+1)$$

Where, K= the ratio of external to internal diameter of the main tube. The degree of the discrepancy, of course, were changing with K; for a very thin tube the error was small; for a tube with K=2 it was 36%.

But as Morrison *et al.* [4] pointed out, if the fictitious volumetric tension, used by Faupel and Harris [3] to facilitate calculation, was removed, the hoop stress concentration factor could be obtained in a rather simpler manner. Morrison *et al.* [4] provided both the analytical and experimental solution to the problem. The method

8

they explained not only provided the direct stress concentration factor, but also the shear stress and Maxwell (von Mises) equivalent stress concentration factors, the ones which in the opinion of Morrison *et al* [4] were more likely to be of relevance in any problems concerning the behavior under static or repeated stress of any ductile material. In experimental method, the authors presented single series of tests on cylinder of outer to inner diameter ratio of 2.25. The side holes in this study were in form of circular holes of diameter 1 inch. These cylinders were, however, machined from material about which ample information was available so the test results can be compared directly with those from plain cylinders and the effective stress concentration factor for use in design were directly deduced. The investigation was primarily experimental; but the they drew attention to the elastic stress analysis which, exploiting solution for uniaxial stress concentration around a circular hole, provided a valuable assessment of effects at the outlet of the side hole to the main bore. A result from the analytical solution was of particular importance because independently of the value of the ratio of bore diameter to outer diameter for the vessel, the side hole introduced a shear stress 2.5 times the value arising in the undrilled cylinder. In other words, in systems limited by shear stress and loaded by internal pressure only, the introduction of a side hole immediately reduced the safe working pressure to 40 % of its original full value.

Cole [5] first studied the effect of offset branch holes in a cylinder. He showed that the round section cross-bore having its axis offset from the radial center-line has the low stress concentration. In a comparison of the internal pressure at a cylider for an offset cross hole and radial cross-hole, he observed a ratio of 1: 1.668, thus making an off-axis cross-hole an attractive proposition. He then suggested that a cylinder with an offset transverse hole has a better fatigue life than a rounded radial cross-hole. From the results of his investigation it is obtained that, the safe working pressures for an undrilled cylinder and a cylinder having a diametral round cross-hole having all the parameters same, if expressed in terms of ratios, were 1: 0.4. Thus, for the cylinder having a diametral round cross-bore, the allowable pressure was shown to be practically 40 % greater than that corresponding to the undrilled cylinder. Cole [5] further reported that during a fatigue test at low cycle pressures,

fatigue crack was found to form at the internal outlet of the cross bore and then propagate slowly in a radial direction (regardless of cross bore position) through the cylinder wall and form a hair crack on the outer surface of the cylinder at failure. As the cyclic pressure approached a level that caused overall yielding at the cylinder bore, unstable fracture of the cylinder was found to occur before the fatigue crack had completed its propagation through the cylinder wall, and the crack width usually extended over the full length of the cylinder test section.

A more sophisticated approximate analysis was presented by Gerdeen [6] who took into account the effect of transverse shear deformation in the cylinder due to circular side hole. There have been no successful attempts to account for the side hole effects including the shear and bending effects for side holes; which were not infinitely small compared to the cylinder bore until the analysis performed by Gerdeen. The analysis was performed for a number of geometries of the cylinder and the hole; diameter ratios of 1.5, 2, 3, 4, 5 and 6 and with bore radius of the cylinder to the side hole radius ratio of 1.5, 2, 3, 5 and 8. The distribution of hoop stress concentration factor showed that the stress concentration factors increased with the increasing side hole ratio (decreasing side hole diamtere for a fixed bore diameter). Thus he showed that it is advantageous to use as small a side hole ratio as possible to reduce the stress concentration factors from internal pressure loading. These calculations supported experimental measurements that show that for large side hole ratios the stress concentrations were lower. For either an internal pressure or an external pressure acting separately, the theoretical results obtained by the authors indicated that the best configuration was one for which the internal intersecting bores have identically the same diameter. The experimental results obtained by Gerdeen and Smith [7] also verified the theoretical analysis performed by Gerdeen. Both plastic and steel materials were used for the experiment and the loading considered were both internal and external in nature.

The finite element method to analyze the stress distribution and stress concentration on cylinders having side holes or cross holes was first attempted by Masu and Craggs [8]. The finite element analysis of the present problem by Masu and Craggs [8]

10

reported an investigation of fatigue strength of thick walled cylinders that contain a small traverse circular hole or cross hole in the cylinder wall. Experimental tests have been carried out on high strength steel cylinders containing a small diameter cross hole in order to observe the effect of cross bore on fatigue life; this work was supplemented by a three dimensional finite element analysis of the problem. The results obtained by the authors justified the previous analytical or experimental works which showed that the introduction of cross hole increases the stress concentration factor than that of plain cylinder.

Another numerical study was made by Masu [9] where a three dimensional finite element analyses were performed for closed ended thick walled cylinder with a cross bore under internal pressure. Cylinders having either a round cross bore or optimally offset circular cross bore were investigated. The effects of cross bore diameter size on the principal stress distribution as well as the stress concentration factors along the cross bores were also investigated. The results showed that the hoop stress distributions as well as the stress concentration factors in a thick walled cylinder depend on cross bore diameter size. The maximum hoop stresses in the circular radial cross bore cylinders approached 1.5 times that in offset cross hole cylinders. The stress concentration factor at the bore of the circular radial cross bore, and an optimally offset circular cross bore were found to be 2.30 and 1.33 respectively. The present observations were in general supportive of experimental observations by Ficenec [15] where an improvement of fatigue life upto 170% was obtained by offsetting the cross hole.

In the same year, Masu [10] investigated the cross bore diameter size effects on the principle stress distribution as well as the stress concentration factors along the plain cross bores. The results showed a dependency of the stress distributions, as well as the stress concentration factors on cross bore diameter size. The stress concentration factor was found to increase with the increasing cross bore size for a particular thickness ratio. This behavior contradicted other previous observations that the stress concentration in a plate decreases with increasing hole size due to the fact that there is less abrupt change in cross sectional area with a large hole. However the previous

11

observations were based on uniaxial loads and they assumed plane stress conditions. But as the stress state they considered was complex in this case where also shear stresses were involved so their effect cannot be ignored as they dictated the outcome of the stress found on the cross bore surface.

In industry, it has been common practice to incorporate a chamfer [16] or smooth blend radius [17] at the junction between the cross hole, side hole and main bore. Although this would seem to be in keeping with standard engineering practice to minimize stress concentration effects, there is no clear theoretical or experimental justification for this design in details in the literature.

Hamilton *et al.* [11] used finite element method to study the elastic stress concentration factors for internally pressurized thick walled cylinders having radial and offset circular cross holes. Three forms of intersection between the cross hole and main bore were considered: plain, chamfered and blend radiused intersection. The effects on the stress concentration factor of such blending is of particular interest to the pressure vessel designer, particularly if the effect of blending geometry is to reduce the stress concentration factor at the cross bore – main cylinder bore intersection. Thus a study was carried out to observe effects of blending geometry on the stress field and its consequent influence on fatigue life. The authors carried out the study on five outer to inner radius of the main cylinder; $b/a = 1.5, 1.75, 2, 2.25$ and 2.5. Two circular cross holes of different radii were modeled; the radius of the circular holes were taken as $R_c = 0.45mm$ and $R_c = 2$ mm. The results obtained from the study showed that introduction of a cross bore into a cylinder wall greatly increases the hoop stress that would otherwise be present in a plain cylinder. Attempts to reduce the hoop stress in a plain cross bore cylinder by using blending features were seen to be successful over a region close to the main bore. The results of this investigation carried out by the authors also confirmed the fact that offsetting the cross holes gives less stress concentration factor.

One of the earlier works regarding elliptical side holes or cross holes in a cylinder, were by Murthy [12] and Murthy and Bapu Rao [13] where they obtained analytical

12

solutions for the stresses around a small elliptical hole in a long thin circular cylindrical shell under axial tension. But there analysis was for thin cylinder which was under axial tension. Fenner and Nadiri [14] performed an extensive work to compute the stress concentration factors at the intersection between elliptical side branches and thick walled tubes or pressure vessels. They used boundary integral equation (boundary element) method to obtain the effect of the elliptical side branches on cylinders. In their investigation, they considered the aspect ratios of the elliptical branches to be 0.9 and 0.8 and main cylinder radius ratio to be 1.5. The results of their investigation showed that the elliptical holes give less stress concentration factors compared to that of circular ones.

Until now, no noteworthy finite element analysis of thick walled cylinders having elliptical cross hole has been found in the literature. So in this present study the finite element method is employed to solve this phenomenon. In this present study an extensive finite element investigation of the elastic stress concentration effect of radial and offset elliptical cross holes in cylindrical vessels is presented, with particular consideration given to the effect of incorporating supposed local stress reducing features.

CHAPTER 3
THEORITICAL BACKGROUND

In this chapter, the governing basic equations for the applied mechanics with appropriate boundary conditions and also the solution procedure applicable to the present problem will be discussed. The generalized governing equations are based on constitutive relation of stress-strain and the equilibrium equations. Also, the formulation of the three-dimensional stress-analysis using finite element will be discussed in this chapter.

3.1 FUNDAMENTAL EQUATIONS

The problem that dealt in this present study is three dimensional in nature. This problem is governed by the constitutive relation of stress-strain and the equilibrium equations.

3.1.1. STRESS-STRAIN RELATIONS

For linear elastic materials, the stress-strain relations come from the generalized Hooke's law. For isotropic materials, the two material properties are Young's modulus (or modulus of elasticity) E and Poisson's ratio υ. Considering an elemental cube inside a body, Hooke's law gives, for the triaxial stress system,

$$\varepsilon_x = \frac{\sigma_x}{E} - \upsilon\frac{\sigma_y}{E} - \upsilon\frac{\sigma_z}{E} \dots\dots\dots\dots\dots\dots\dots\dots\dots(3.1)$$

$$\varepsilon_y = -\upsilon \frac{\sigma_x}{E} + \frac{\sigma_y}{E} - \upsilon \frac{\sigma_z}{E} \quad\text{...(3.2)}$$

$$\varepsilon_z = -\upsilon \frac{\sigma_x}{E} - \upsilon \frac{\sigma_y}{E} + \frac{\sigma_z}{E} \quad\text{...(3.3)}$$

$$\gamma_{yz} = \frac{\tau_{yz}}{G}$$

$$\gamma_{xz} = \frac{\tau_{xz}}{G} \quad\text{...(3.4)}$$

$$\gamma_{xy} = \frac{\tau_{xy}}{G}.$$

Where, σ_x, σ_y and σ_z are normal stresses, ε_x, ε_y and ε_z are normal strains, τ_{yz}, τ_{xz} and τ_{xy} are shear stresses and γ_{yz}, γ_{xz} and γ_{xy} are the engineering shear strains.

The shear modulus (or modulus of rigidity), G, is given by,

$$G = \frac{E}{2(1+\upsilon)} \quad\text{...(3.5)}$$

From Hooke's law relationships, note that,

$$\varepsilon_x + \varepsilon_y + \varepsilon_z = \frac{(1-2\upsilon)}{E}(\sigma_x + \sigma_y + \sigma_z) \quad\text{...............................(3.6)}$$

Substituting for $(\sigma_y + \sigma_z)$ and so on into Eq. a, we get the inverse relations,

$$\sigma = D\ \varepsilon \quad\text{...(3.7)}$$

This is the constitutive relation of stress and strain in form of linear elasticity.

D is the symmetric (6×6) material matrix given by,

$$D = \frac{E}{(1+\upsilon)(1-2\upsilon)}\begin{bmatrix} 1-\upsilon & \upsilon & \upsilon & 0 & 0 & 0 \\ \upsilon & 1-\upsilon & \upsilon & 0 & 0 & 0 \\ \upsilon & \upsilon & 1-\upsilon & 0 & 0 & 0 \\ 0 & 0 & 0 & 0.5-\upsilon & 0 & 0 \\ 0 & 0 & 0 & 0 & 0.5-\upsilon & 0 \\ 0 & 0 & 0 & 0 & 0 & 0.5-\upsilon \end{bmatrix} \quad\text{..............(3.8)}$$

The above mentioned matrix is used to calculate the stresses from strains in each elements in finite element (FE) method.

3.1.2. THE EQUILIBRIUM EQUATIONS:

$$\frac{\partial \sigma_x}{\partial x} + \frac{\partial \tau_{xy}}{\partial y} + \frac{\partial \tau_{xz}}{\partial z} + f_x = 0 \dots\dots\dots\dots\dots\dots\dots(3.9)$$

$$\frac{\partial \tau_{xy}}{\partial x} + \frac{\partial \sigma_y}{\partial y} + \frac{\partial \tau_{yz}}{\partial z} + f_y = 0 \dots\dots\dots\dots\dots\dots\dots(3.10)$$

$$\frac{\partial \tau_{xz}}{\partial x} + \frac{\partial \tau_{yz}}{\partial y} + \frac{\partial \sigma_z}{\partial z} + f_z = 0 \dots\dots\dots\dots\dots\dots\dots(3.11)$$

Where, f_x, f_y and f_z are the distributed body forces per unit volume.

The differential equations of equilibrium can be written as,

$$\overline{\nabla^T}\sigma + b = 0$$

Where, b is the body force vector.

The equations given here have to be solved by given certain boundary conditions. These boundary conditions may be expressed in terms of prescribed traction vector $\vec{t}$ or prescribed displacement **u**. That is for three dimensional problems, it is obtained that,

$$\vec{t} = S\,n = h \text{ on } S_h$$
$$u = g \text{ on } S_g$$

where h and g are given vectors, S_h is that part of the boundary S, on which the traction vector $\vec{t}$ is prescribed and S_g is that part of the boundary S on which displacement vector u is given. The sum of S_h and S_g constitutes the entire boundary S.

It is no surprise that exact analytical solutions of the three-dimensional elasticity problems present a formidable task, and as a consequence they are scarce. Moreover, these solutions are confined to physically simple problems with uncomplicated geometry. But when the geometry is arbitrary and also the boundary conditions are complicated, the exact solution of the problem cannot be obtained. This inability to

16

obtain an exact solution may be attributed to either the complex nature of governing differential equations or the difficulties that arise from dealing with the boundary and initial conditions. To deal with such problems, numerical approximations are therefore made. Numerical solutions approximate exact solutions only at discrete points, called nodes. The first step of any numerical procedure is discretization. This process divides the medium of interest into a number of small sub regions and nodes. There are two common classes of numerical methods:

(1) Finite difference methods and

(2) Finite element methods.

With finite difference methods, the differential equation is written for each node, and the derivatives are replaced by difference equations. This approach results in a set of simultaneous linear equations. Although finite difference methods are easy to understand and employ in simple problems: they become difficult to apply for problems with complex geometries or complex boundary conditions. This situation is also true for problems with no isotropic material properties.

The advantage of the FE method is that in principle any problem can be solved, irrespective of the geometry and even considering complex constitutive relations. The expense that has to be paid for this gain in generality is that the FE method provides an approximate solution, which, however, converges towards the exact solution for a decreasing element size.

In the present numerical computation of the problem Finite element method (FEM) is used.

3.2. FINITE ELEMENT METHOD

The finite element method has become a powerful tool for the numerical solution of a wide range of engineering problems. Applications range from deformation and stress analysis of automotive, aircraft, building and bridge structures to field analysis of heat flux, fluid flow, magnetic flux, seepage, and other flow problems. With the advances in computer technology and CAD systems, complex problems can be modeled with relatively easier. Several alternative configurations can be tested on a computer before the first prototype is built. All of these suggest the need to keep

17

pace with these developments by understanding the basic theory, modeling techniques and computational aspects of the finite element method.

All the physical phenomena encountered in engineering mechanics are modeled by differential equations, and usually the problem addressed is too complicated to be solved by classical analytical methods. The finite element method is a numerical approach by which general differential equations can be solved in an approximate manner.

The differential equations which describe the physical problem considered are assumed to hold over a certain region. This region may be one, two, or three dimensional. It is a characteristic feature of the finite element method that instead of seeking approximations that hold directly over the entire region, the region is divided into smaller parts, so called finite elements, and the approximation is then carried out over each element. For instance, even though the parameters vary in a highly non linear in manner over the entire region, it may be for approximation to assume that the parameters vary in a liner manner over each element. The collection of all elements is called a finite element mesh. The material properties and the governing relationships are considered over these elements and expressed in terms of unknown values at element corners.

When the type of approximation which is to be applied over each element has been selected, the corresponding behavior of each element can then be determined. This can be performed because the approximation made over each element is fairly simple; as a result can be determined easily. Having determined the behavior of all elements, these elements are then patched together, using some specific rules, to form the entire region, which eventually enable us to obtain an approximate solution for the behavior of the entire body.

The finite element method can be applied to obtain approximate solutions for arbitrary differential equations. For some physical problems differential equations can be solved by finite element method for both the boundary value problems and initial value problems.

18

A system with a finite number of unknowns is called a discrete system in contrast to the original continuous system with an infinite number of unknowns. The determination of the values of the variable at the nodal points follows from the solution of a certain system of equations. A system often involves thousands of equations, so such systems cannot be solved by hand and therefore the FE method relies entirely on the availability of efficient computers.

The finite element method can be applied to arbitrary differential equations and arbitrary geometries of bodies consisting arbitrary materials. It is therefore no surprise that the FE method today is the most powerful approach for solving differential equations that occur in engineering, physics and mathematics.

In the next section, the three dimensional modeling of finite element method will be discussed as for the analysis made in this research work is based on three dimensional FE method. The formulation and equations used to analyze a three dimensional FE problem are discussed below.

3.2. THREE DIMENSIONAL FINITE ELEMENTS MODELING

Most engineering problems are three dimensional. So far, we have studied the possibilities of finite element analysis of simplified models, where rod elements, constant-strain triangles, axisymmetric elements, beams, and so on give reasonable results. In this chapter, we deal with the formulation of three-dimensional stress-analysis problems. The ten-node tetrahedral element is presented in this section. Problem modeling is also discussed. In addition, frontal solution method is introduced.

If u, v and w are displacements in the x, y and z directions respectively, then

$$u = [u, v, w]^T \quad\dots\dots\dots\dots\dots\dots\dots\dots\dots\dots\dots\dots\dots(3.9)$$

. The stresses and strains are given by,

$$\sigma = [\sigma_x \quad \sigma_y \quad \sigma_z \quad \tau_{yz} \quad \tau_{xz} \quad \tau_{xy}]^T$$
$$\varepsilon = [\varepsilon_x \quad \varepsilon_y \quad \varepsilon_z \quad \tau_{yz} \quad \tau_{xz} \quad \tau_{xy}]^T \quad\dots\dots\dots\dots\dots\dots(3.10)$$

The stress-strain relations are given by, from 3.7 as

$$\sigma = D\varepsilon$$

Where, D is a (6×6) symmetric matrix. For isotropic materials, D is given by equation (3.8)

The strain-displacement relations are given by,

$$\varepsilon = \left[\frac{\partial u}{\partial x}, \frac{\partial v}{\partial y}, \frac{\partial w}{\partial z}, \frac{\partial v}{\partial z} + \frac{\partial w}{\partial y}, \frac{\partial u}{\partial z} + \frac{\partial w}{\partial x}, \frac{\partial u}{\partial y} + \frac{\partial v}{\partial x} \right]^T \dots\dots\dots\dots(3.11)$$

The body force and traction vectors those act on a three dimensional body are given by,

$$f = [f_x, f_y, f_z]^T$$
$$T = [T_x, T_y, T_z]^T \dots\dots\dots\dots\dots\dots\dots\dots\dots\dots(3.12)$$

Now, for the formulation of FE method, the volume is divided into ten-node tetrahedral. Each node is assigned a number in the x-, y-, and z-coordinates .

For each local node I three degrees of freedom are assigned q_{3i-2}, q_{3i-1}, and q_{3i}, and for the corresponding global node I, the assigned degree of freedoms are Q_{3I-2}, Q_{3I-1}, Q_{3I}. Thus, the element and global displacement vectors are,

$$q = [q_1, q_2, q_3 \dots\dots q_{12}]^T$$
$$Q = [Q_1, Q_2, Q_3, \dots\dots\dots Q_N]^T \dots\dots\dots\dots\dots\dots\dots\dots(3.13)$$

Where N is the total number of degrees of freedom for the structure, three per node. Ten Lagrange-type shape functions are considered N_1, N_2, N_3 ………N_9 and N_{10}, where shape function N_i has a value of 1 at node I and is zero at the other nine nodes. Specifically, N_1 is 0 at nodes 2, 3……9 and 10 and linearly increases to 1 at node 1. Using the master element, the shape functions can be defined as,

20

$$N_1 = -\xi + 2\xi^2,$$

$$N_2 = -\eta + 2\eta^2,$$

$$N_3 = -\zeta + \zeta^2,$$

$$N_4 = 4\xi\eta$$

$$N_5 = 4\eta\zeta$$

$$N_6 = 4\zeta\xi$$

$$N_7 = 4\xi - 4\xi^2 - 4\xi\eta - 4\xi\zeta$$

$$N_8 = 4\eta - 4\eta^2 - 4\xi\eta - 4\eta\zeta$$

$$N_9 = 4\zeta - 4\zeta^2 - 4\eta\zeta - 4\xi\zeta$$

$$N_{10} = 1 - 3\xi - 3\eta - 3\zeta + 2\xi^2 + 2\eta^2 + 2\zeta^2 + 4\xi\eta + 4\eta\zeta + 4\xi\zeta$$

..(3.14)

The displacements u, v, and w at x can be written in terms of the unknown nodal values as,

$$u = Nq \dots\dots\dots\dots\dots\dots\dots (3.15)$$

where

$$N = \begin{bmatrix} N_{i=1} \\ \cdot \\ \cdot \\ N_{i=10} \end{bmatrix}^T \dots\dots\dots\dots\dots\dots (3.16)$$

Where, $N_{i=1} = \begin{bmatrix} N_1 & 0 & 0 \\ 0 & N_1 & 0 \\ 0 & 0 & N_1 \end{bmatrix}$ and so on.

It is easy to see that the shape functions can be used to define the coordinates x, y, and z of the point at which the displacements u, v, and w are interpolated. This is called the isoparametric formulation when the co-ordinates and also the

21

corresponding displacements can be expressed using same shape functions. The isoparametric transformation is given by,

$$x = \sum_{i=1}^{10} x_i N_i$$

$$y = \sum_{i=1}^{10} y_i N_i \quad \dots\dots\dots\dots\dots\dots\dots\dots\dots\dots\dots\dots\dots(3.17)$$

$$z = \sum_{i=1}^{10} z_i N_i$$

Using the chain rule for partial derivatives, say, of u,

$$\begin{Bmatrix} \dfrac{\partial u}{\partial \xi} \\ \dfrac{\partial u}{\partial \eta} \\ \dfrac{\partial u}{\partial \zeta} \end{Bmatrix} = J \begin{Bmatrix} \dfrac{\partial u}{\partial x} \\ \dfrac{\partial u}{\partial y} \\ \dfrac{\partial u}{\partial z} \end{Bmatrix} \quad \dots\dots\dots\dots\dots\dots\dots\dots\dots\dots\dots\dots\dots(3.18)$$

Thus, the partial derivatives with respect to ξ, η and ζ are related to x, y, and z derivatives by the foregoing relationship. The Jacobian matrix of the transformation is given by,

$$J = \begin{bmatrix} \dfrac{\partial x}{\partial \xi} & \dfrac{\partial y}{\partial \xi} & \dfrac{\partial z}{\partial \xi} \\ \dfrac{\partial x}{\partial \eta} & \dfrac{\partial y}{\partial \eta} & \dfrac{\partial z}{\partial \eta} \\ \dfrac{\partial x}{\partial \zeta} & \dfrac{\partial y}{\partial \zeta} & \dfrac{\partial z}{\partial \zeta} \end{bmatrix} \quad \dots\dots\dots\dots\dots\dots\dots\dots\dots\dots(3.19)$$

The volume of the element is given by,

$$V_e = \left| \int_0^1 \int_0^{1-\xi} \int_0^{1-\xi-\eta} \det \ Jd \ \xi \, d\eta \, d\zeta \right| \quad \dots\dots\dots\dots\dots\dots(3.20)$$

22

Since detJ is constant,

$$V_e = |\det J| \int_0^1 \int_0^{1-\xi} \int_0^{1-\xi-\eta} d\xi \, d\eta \, d\zeta \quad \text{............}(3.21)$$

Thus obtained,

$$V_e = \frac{1}{6}|\det J| \quad \text{............................}(3.22)$$

The inverse relation corresponding of the partial derivative of u is given by,

$$\begin{Bmatrix} \dfrac{\partial u}{\partial x} \\ \dfrac{\partial u}{\partial y} \\ \dfrac{\partial u}{\partial z} \end{Bmatrix} = A \begin{Bmatrix} \dfrac{\partial u}{\partial \xi} \\ \dfrac{\partial u}{\partial \eta} \\ \dfrac{\partial u}{\partial \zeta} \end{Bmatrix} \quad \text{............................}(3.23)$$

Where A is the inverse of the Jacobian matrix J

$$A = J^{-1}$$

Using the strain-displacement relations, the relation among derivatives in x, y, and z and ξ, η, and ζ and the assumed displacement field u=Nq,

$$\varepsilon = Bq \quad \text{............................}(3.24)$$

Where B is a (6×30) matrix.

All the terms of B are constants. Thus this equation gives constant strains after the nodal displacements are calculated.

Now, the element stiffness matrix will be calculated. Element stiffness matrix is important to obtain the value of displacements in each elements of FE method.

23

The element strain energy in the total potential is given by,

$$U_e = \frac{1}{2} \int_e \varepsilon^T D\varepsilon dV$$

$$= \frac{1}{2} q^T B^T DBq \int_e dV$$

$$= \frac{1}{2} q^T V_e B^T DBq \qquad \qquad \dots\dots\dots\dots\dots\dots(3.25)$$

$$= \frac{1}{2} q^T k^e q$$

Where the element stiffness matrix k^e is given by,

$$k^e = V_e B^T DB \dots\dots\dots\dots\dots\dots\dots(3.26)$$

In which V_e is the volume of the element given by $\frac{1}{6}|\det J|$. In the Galerkin approach, the internal virtual work of the element comes out to be,

$$\int_e \sigma^T \varepsilon(\phi)dV = \psi^T V_e B^T DBq \dots\dots\dots\dots\dots\dots(3.27)$$

Equation 3.27 gives the element stiffness matrix. This element stiffness is required to obtain the displacements in each node of an element.

Now, the force terms will be calculated.

The potential term associated with body force is,

$$\int_e u^T f dV = q^T \int\int\int N^T f \det J d\xi d\eta d\zeta$$

$$= q^T f^e \qquad \qquad \dots\dots\dots\dots\dots\dots(3.28)$$

Using the integration formula,

24

$$f^e = \frac{V_e}{4}\left[f_x, f_y, f_z, f_x, f_y, f_z, \ldots, f_z\right]^T \ldots\ldots\ldots\ldots\ldots\ldots(3.29)$$

For this equation, the element body force vector f^e is of dimension 12×1. It is noted that $V_e f_x$ is the x component of the body force, which is distributed to the degrees of freedom q_1, q_4, q_7, and q_{10}.

It is now consider uniformly distributed traction on the boundary surface. The boundary surface of a tetrahedron is a triangle. Without loss of generality, if A_e is the boundary surface on which traction is applied, formed by local nodes, then,

$$\int_{A_e} u^T T dA = Q^T \int_{A_e} N^T T dA = q^T T^e \ldots\ldots\ldots\ldots\ldots\ldots(3.30)$$

The element traction load vector is given by,

$$T^e = \frac{A_e}{3}\left[T_x, \quad T_y, \quad T_z, \quad T_x, \quad T_y, \quad T_z, \quad T_x, \quad T_y, \quad T_z, \quad 0 \quad 0 \quad 0\right]\ldots(3.31)$$

The stiffnesses and forces are gathered into global locations using element connectivity. Point loads are added into proper locations of the force vector. Boundary conditions are considered using penalty or other approaches. The energy and Galerkin approaches yield the set of equations,

$$KQ = F \ldots\ldots\ldots\ldots\ldots\ldots\ldots\ldots\ldots\ldots\ldots\ldots(3.32)$$

Where, K is the element stiffness matrix, Q the displacement matrix which gives the values of displacements in each node of an element and F is the force matrix which contains all the force effects on a body (body force+ traction force+ point force).The above equation 3.32 gives a set of equations for each node of an element and for all the elements of a discritized body the same set of equations are obtained. Then all the equations of all elements are globalized and by applying boundary conditions to these equations, the values of the displacements are obtained from the known stiffness matrix and the force terms(obtained from boundary conditions)

As we are dealing with solid mechanics problem so the quantity we want to calculate is the stress.

As mentioned above, after these equations of (3.32) are solved, the element nodal displacements q can be obtained. Since $\sigma = D\varepsilon$ and $\varepsilon = Bq$, the element stresses are given by,

$$\sigma = DBq \dots\dots\dots\dots\dots\dots\dots\dots\dots\dots\dots\dots\dots(3.33)$$

The three principal stresses can be calculated by using the relationships of. the three invariants of the (3×3) stress tensor are,

$$I_1 = \sigma_x + \sigma_y + \sigma_z$$
$$I_2 = \sigma_x\sigma_y + \sigma_y\sigma_z + \sigma_z\sigma_x - \tau_{yz}^2 - \tau_{xz}^2 - \sigma_{xxy}^2 \qquad \dots\dots\dots(3.34)$$
$$I_3 = \sigma_x\sigma_y\sigma_z + 2\tau_{yz}\tau_{xz}\tau_{xy} - \sigma_x\tau_{yz}^2 - \sigma_y\tau_{xz}^2 - \sigma_z\tau_{xy}^2$$

We define,

$$a = \frac{I_1^2}{3} - I_2$$

$$b = -2\left(\frac{I_1}{3}\right)^3 + \frac{I_1 I_2}{3} - I_3$$

$$c = 2\sqrt{\frac{a}{3}}$$

$$\theta = \frac{1}{3}\cos^{-1}\left(-\frac{3b}{ac}\right)$$

The principal stresses are given by,

$$\sigma_1 = \frac{I_1}{3} + c\cos\theta$$

$$\sigma_2 = \frac{I_1}{3} + c\cos\left(\theta + \frac{2\pi}{3}\right) \dots\dots\dots\dots\dots\dots\dots\dots\dots(3.35)$$

$$\sigma_3 = \frac{I_1}{3} + c\cos\left(\theta + \frac{4\pi}{3}\right)$$

This is the procedure of solving three dimensional models using Finite element method. Now solving of these equations requires computer as these large volumes of equations is not possible to solve by hand. So in the following section, the computer programs and soft wares those are used for solving these problems are discussed.

3.3. COMPUTER PROGRAMS

Computer use is an essential part of the finite element analysis. Well-developed, well-maintained, and well-supported computer programs are necessary in solving engineering problems and interpreting results. Many available commercial finite element packages fulfill these needs. It is also the trend in industry that the results are acceptable only when solved using certain standard computer program packages. The commercial packages provide user-friendly data-input platforms and elegant and easy to follow display formats. However, the packages do not provide an insight into the formulations and solution methods. Specially developed computer programs with available source codes enhance the learning process.

3.3.1. ANSYS

ANSYS is a comprehensive general-purpose finite element computer program that contains over 100,000 lines of code. ANSYS is capable of performing static, dynamic, heat transfer, fluid flow, and electromagnetism analyses. ANSYS has been a leading FEA program for well over 20 years. Today, ANSYS is used in many engineering fields, including aerospace, automotive, electronics, and nuclear. In order to use ANSYS or any other "canned" FEA computer program intelligently, it is imperative that one first fully understands the underlying basic concepts and limitations of the finite element methods. ANSYS is a very powerful and impressive engineering tool that may be used to solve a variety of problems.

3.3.2. BASIC STEPS IN THE FINITE ELEMENT METHOD

The basic steps involved in any finite element analysis consist of the following:

Preprocessing Phase

1. Create and discretize the solution domain into finite elements; that is, subdivided the problem into nodes and elements.

2. Assume a shape function to represent the physical behavior of an element; that is, an approximate continuous function is assumed to represent the solution of an element.

3. Develop equations for an element.

4. Assemble the elements to present the entire problem. Construct the global stiffness matrix.

5. Apply boundary conditions, initial conditions and loading.

Solution Phase

6. Solve a set of linear or nonlinear algebraic equations simultaneously to obtain nodal results. such as displacement values at different nodes or temperature values at different nodes in a heat transfer problem.

Postprocessing Phase

7. Obtain other important information. At this point, you may be interested in values of principal stresses. heat fluxes, etc.

ANSYS uses the same procedure to solve any problem.

3.3.3. THREE DIMENSIONAL ELEMENTS USED IN ANSYS

A number of three dimensional elements are used in ANSYS, among them some are used for solving solid mechanics problems. Some of thses structural elements are described below.

SOLID45 is a three-dimensional brick element used to model isotropic solid problems It has eight nodes, with each node having three translational degrees of

freedom in the nodal x-, y-, and z-directions, as shown in Figure 3.3.1. (The element's faces are shown by the circled numbers) This element may be used to analyze large-deflection, large-strain, plasticity, and creep problems.
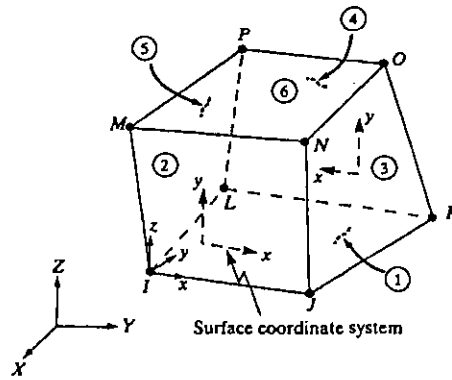

Figure 3.3.1:Solid45 element used by ANSYS

SOLID65 is used to model reinforced-concrete problems or reinforced composite materials, such as fiberglass. This element is similar to the SOLID45 elements, and it has eight nodes, with each node having three translational degrees of freedom in the nodal x, y, and z-directions, as shown in Figure 3.3.2. The element may be used to analyze cracking in tension or crushing in compression.
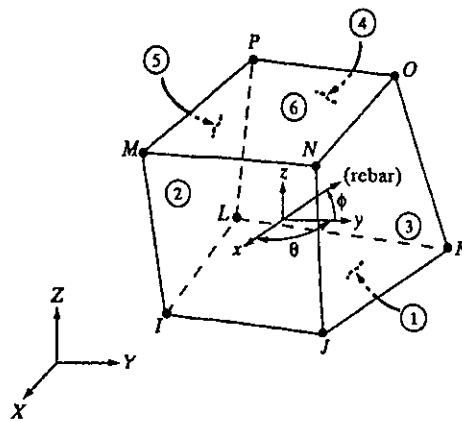

Figure 3.3.2:Solid65 element used by ANSYS

SOLID72 is a four-node tetrahedral element, with each node having three translational degrees of freedom in the nodal x, y, and z-directions, as well as rotations about the nodal x, y, and z-directions, as shown in Figure 3.3.3. As in

29

previous examples, the element's faces are shown by the circled numbers Distributed surface loads (pressures) may be applied to the element's surfaces.
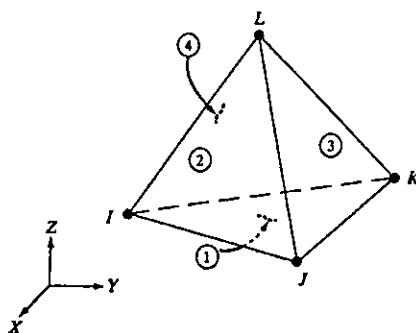

Figure 3.3.3:Solid72 element used by ANSYS

SOLID92 is a ten-node tetrahedral element that is more accurate than the SOLID72 element, but it requires more solution time. Each node has three translational degrees of freedom in the nodal x-, y-, and z-directions, as shown in Figure 10.11. This element may be used to analyze large-deflection, large-strain, plasticity, and creep problems.
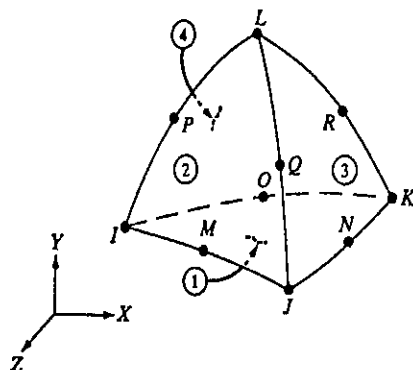

Figure 3.3.4:Solid92 element used by ANSYS

In the present study SOLID92 is used to describe the three dimensional model. SOLID92 has a quadratic displacement behavior and is well suited to model irregular meshes (such as produced from various CAD/CAM systems).

In the next section, the ,methods ANSYS uses to solve equations described in section 3.2 are discussed.

3.3.4. THE FRONTAL SOLVER

There are number of solver used by the software ANSYS to solve the equations of a given problem such as, Frontal Solver (direct elimination solver), Sparse Direct Solver (direct elimination solver), Preconditioned Conjugate Gradient (PCG) Solver(iterative solver), Incomplete Cholesky Conjugate Gradient (ICCG) Solver(Iterative solver) and Jacobi Conjugate Gradient (JCG) Solver (iterative solver). The frontal solver is the default, but one can select a different solver. In the present study the frontal solver method is used to get the solution.

The frontal solver does not assemble the complete global matrix. Instead, ANSYS performs the assembly and solution steps simultaneously as the solver processes each element. The method works as follows:

- After the individual element matrices are calculated, the solver reads in the degrees of freedom (DOF) for the first element.

- The program eliminates any degrees of freedom that can be expressed in terms of the other DOF by writing an equation to the .TRI file. This process repeats for all elements until all degrees of freedom have been eliminated and a complete triangularzed matrix is left on the .TRI file.

- The program then calculates the nodal DOF solution by back substitution, and uses the individual element matrices to calculate the element solution. Frontal solution shows the main steps in a frontal solution and the files produced at each step.
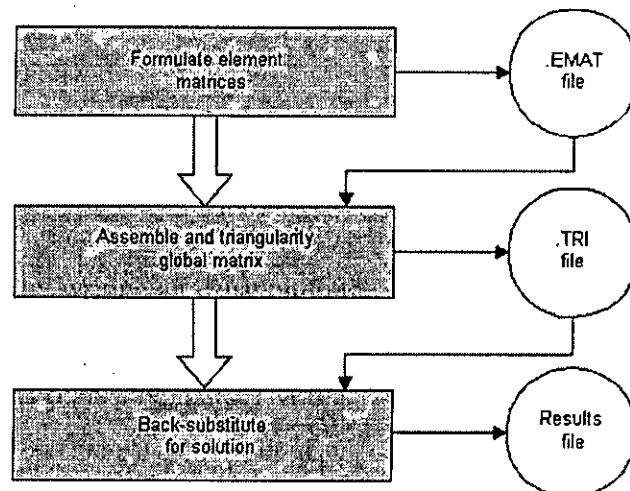

Figure 3.4.1.Typical steps and files in a frontal solution

3.4. von Mises equivalent stress

von Mises stress is used as a criterion in determining the onset of failure in ductile materials. The failure criterion states that the von Mises stress σ_{VM} should be less than the yield stress σ_Y of the material. In the inequality form, the criterion may be put as,

$$\sigma_{VM} \leq \sigma_Y \quad \text{............................ ....} \quad (3.36)$$

The von Mises stress σ_{VM} is given by,

$$\sigma_{VM} = \sqrt{I_1^2 - 3I_2} \quad \text{...............................} \quad (3.37)$$

Where I_1 and I_2 are the first two invariants of the stress tensor. For the general state of stress I_1 and I_2 are given by,

$$\begin{aligned} I_1 &= \sigma_x + \sigma_y + \sigma_z \\ I_2 &= \sigma_x\sigma_y + \sigma_y\sigma_z + \sigma_z\sigma_x - \tau_{yz}^2 - \tau_{xz}^2 - \sigma_{xy}^2 \end{aligned} \quad \text{.............} \quad (3.38)$$

In terms of the principal stresses σ_1, σ_2 and , the two invariants can be written as,

$$\begin{aligned} I_1 &= \sigma_1 + \sigma_2 + \sigma_3 \\ I_2 &= \sigma_1\sigma_2 + \sigma_2\sigma_3 + \sigma_3\sigma_1 \end{aligned} \quad \text{........................} \quad (3.39)$$

It is easy to check that von Mises stress can be expressed in the form of principal stresses,

$$\sigma_{VM} = \frac{1}{\sqrt{2}}\sqrt{(\sigma_1 - \sigma_2)^2 + (\sigma_2 - \sigma_3)^2 + (\sigma_3 - \sigma_1)^2} \quad \text{...........} \quad (3.40)$$

Or,

$$\sigma_{VM} = \left(\sigma_{XX}^2 + \sigma_{YY}^2 + \sigma_{ZZ}^2 - \sigma_{XX}\sigma_{YY} - \sigma_{YY}\sigma_{ZZ} - \sigma_{XX}\sigma_{ZZ} + 3\tau_{XY}^2 + 3\tau_{XZ}^2 + 3\tau_{YZ}^2\right)^{0.5} \quad (3.41)$$

3.5. ELASTIC STRESS CONCENTRATION FACTORS

To obtain stress concentration factors usually the Principal stress concentration factor and the von Mises stress concentrations factors are used. The stress concentration effect of the cross holes in a cylinder is quantified here in terms of two elastic Stress concentration factors (SCF). The Principal Stress concentration factor is given as,

$$K_{S1} = \frac{\sigma_{1\max}}{\sigma_{\theta C}} \dots\dots\dots\dots\dots\dots\dots\dots\dots\dots\dots\dots(3.42)$$

Where, $\sigma_{1\max}$ is the maximum value of principal stress in the vessel and $\sigma_{\theta C}$ is the value of maximum principal stress at the inner surface of the plain cylinder (the hoop stress at the bore). The von Mises equivalent stress concentration factor is defined as,

$$K_e = \frac{\sigma_{e\max}}{\sigma_{ec}} \dots\dots\dots\dots\dots\dots\dots\dots\dots\dots\dots\dots(3.43)$$

Where, $\sigma_{e\max}$ is the maximum value of equivalent stress in the vessel with a cross hole and σ_{ec} is the value of equivalent stress at the inner surface of a similar plain cylinder.

The von Mises equivalent stress concentration factors are particularly of more interest as any problems concerning the behavior under static or repeated stress of any ductile material, the von Mises equivalent is more accurate than the principal stress which is also discussed in reference [4]. From section 3.4 it is seen that to calculate von Mises Equivalent stress all the three principal stresses are taken into account, i.e.; all the three principal stresses are given the equal importance. So for this present study the von Mises stress concentration factor is calculated along with the principal stress concentration factor.

CHAPTER 4
COMPUTATIONAL DETAILS

In the present investigation, an extensive parametric finite element investigation of the elastic stress concentration effect due to elliptical shaped cross holes in internally pressurized cylindrical vessels is presented. Two different orientation of the cross hole are considered; one major axis of the elliptical hole along the hoop direction of the cylinder (circumferential orientation) as shown in figure 4.1. In another orientation of the cross hole major axis of the elliptical hole is along the longitudinal direction of the cylinder (longitudinal orientation) as shown in figure 4.2. In figures 4.3 and 4.5, the sectional views of the main cylinder for both the orientations are shown. Figures 4.4 and 4.6 show the close view of the blended intersection between the main bore of the cylinder and the cross hole. Particular consideration is given to the effect of incorporating local stress reducing features, i.e. blended surface at the intersection of the cross hole and the inner surface of the main cylinder as shown in figure 4.2 and 4.4 for both the orientation.

Two thick cylindrical vessel configurations are investigated, one with elliptical cross hole along the radial center direction of the cylinder (Radial cross hole), (shown in figure 4.5 and 4.7) and one elliptical cross hole offset from the radial center line of the cylinder (offset cross hole) (shown in figure 4.6 and 4.8) for two different orientation of holes; orientation A and orientation B. The main cylinder has inner radius a and outer radius shown in figure 4.10 Five cylinder radius ratios were considered for each type of vessel:

$$b/a = 1.5, 1.75, 2, 2.25, 2.5$$

Two elliptical cross hole of different geometrical dimension are modeled:

$$R_c = 0.4 \text{ mm (smaller hole) and}$$

R$_c$ = 2 mm (larger hole)

Where, R$_c$ is the minor axis radius of the elliptical hole.

In this present investigation, the elliptical hole with minor axis radius R$_c$ = 0.4 mm is termed as smaller hole and R$_c$ = 2 mm is termed as larger hole. The reason behind using these two dimensions of elliptical holes is because the smaller hole is perhaps typical for an instrumentation tapping and the larger hole is more typical for a fluid entry or exit port.
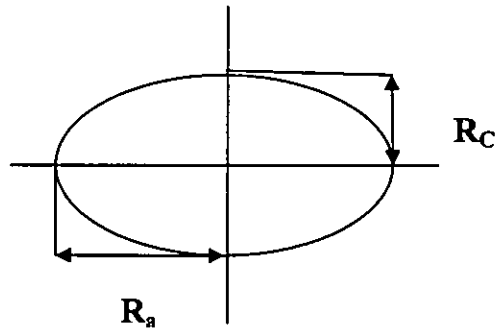

R$_C$

R$_a$

Figure 4.11: The dimension of the elliptical hole

Rb

2L
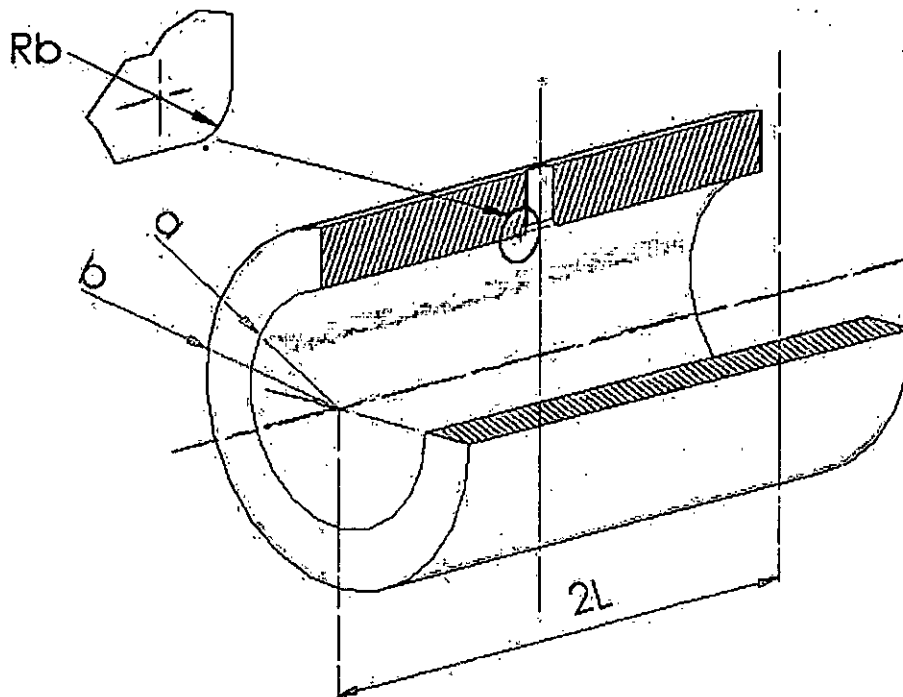
Figure 4.12: Vessel with cross hole configurations showing all the dimensions of the vessel

All through the finite element investigations, the major to minor axis ratio of the elliptical hole, $R_a/R_c = 2$ is used where R_a is the major axis radius of the elliptical hole as shown in figure 4.9.

The intersection between the inner surface of the main bore and cross holes is modeled as a smooth blend having blend radius of $R_b = 0.4$ mm for smaller hole and $R_b = 2.0$ mm for the larger hole. These blended surfaces are incorporated in all the vessel configurations, radiuses different for smaller and larger holes.

The two hole dimensions; smaller hole and larger hole, are used for both the radial and offset configurations of holes and for orientation A only. For orientation B the finite element investigations are done on cylinders containing only the larger cross holes. For offset smaller and larger holes, for both orientation, the offset distance used is 0.112b [suggested by reference [10] as the optimum distance]. When all the different parameters are combined, they define a range of 30 different vessel configurations on which finite element analysis has been performed.

4.1: MODELING THE PROBLEM IN ANSYS

4.1.1 Pre-processing of the model

The vessels were analyzed using the commercial program ANSYS. The models being three dimensional in nature, three dimensional isoparametric tetrahedral element models are used for the study. Model size is minimized by invoking symmetry boundary conditions. The radial elliptical cross hole configurations of both the orientation have three plane of symmetry and the offset cross hole configurations have two planes of symmetry. Thus only quarter and half models required for the radial and offset geometries respectively. A model length of L= 2b is used for all cases.
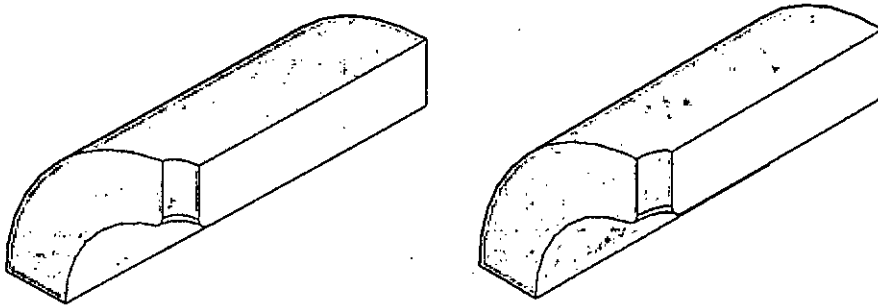
Figure 4.13: The quarter models of radial cross hole for orientation A and B .
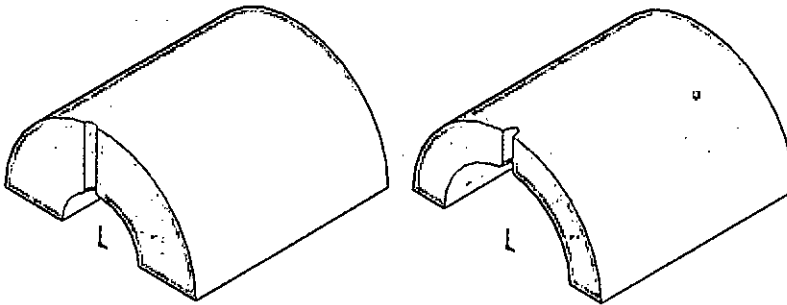

Figure 4.14: The half models of offset cross hole for orientation A and B

The geometries of the models for the present study are drawn by CAD software 'SolidWorks'. It is an alternative to creating a model directly with ANSYS. The models are generated first by 'SolidWorks' software and then it is imported into ANSYS for analysis, by saving them in the IGES file format. Creating a model using a CAD package has the following advantages:

- The effort of duplication can be avoided by using existing CAD models to generate solid models for analysis, so the models can be created in a easy manner.

-

- More familiar tools can be used to create models.

However, models imported from CAD systems may require extensive repair if they are not of suitable quality for meshing. But once successfully imported, the model can be meshed just as any model created in ANSYS. It is also possible to generate the models in ANSYS, but there is no such short cut way of drawing elliptical shaped cross holes and also generating the model every time can be avoided. By using Solid works the main model is generated once and after that only the dimensions of the various features are edited to get different b/a ratio or the smaller and larger holes.

As stated earlier, the models are imported into ANSYS in the IGES file format. The Initial Graphics Exchange Specification (IGES) is a vendor neutral standard format used to exchange geometric models between various CAD and analysis systems. ANSYS's IGES import capability is among the most robust in the industry. Moreover, because the filter can import partial files, at least some portion of the model can generally be imported. ANSYS provides the following two options for importing IGES files:

- DEFAULT--This option uses an enhanced geometry database and should, in almost all cases, be the choice of the user. The option is designed to convert IGES files, if possible, without user intervention. The conversion includes automatic merging and the creation of volumes to prepare the models for meshing. If the DEFAULT option encounters problems translating the IGES file, ANSYS will alert user to this and activate a suite of enhanced topological and geometric tools designed specifically for interactive repair of imported models.

- ALTERNATE--This option uses the standard ANSYS geometry database, and is provided largely for backward compatibility. Occasionally, ANSYS will be unable to translate an IGES model using the DEFAULT option and the user will be instructed to try to ALTERNATE option. The ALTERNATE option has no capabilities for automatically creating volumes and models imported through this translator will require manual repair. However, the enhanced set of topological or geometric repair tools

is not available for models imported through this translator; the user must use the standard PREP7 geometry tools to repair the model.

In the present study, the DEFAULT options of the ANSYS importing of IGES files are used.

As stated earlier, in the pre-processing stage of the finite element analysis, the tetrahedral elements are selected for all the models. The material properties of the steel material have been used. After successful import of the model in ANSYS, it is meshed by a suitable element. In Finite element method the mesh generation is the technique to subdivide a domain into a set of sub domains, called finite elements. The structures are meshed using a 10 node tetrahedron element (SOLID92). Figure 4.13 show the view of the model after it is meshed. The regions around the cross hole, where the largest strain gradient occurs and where the stress is likely to concentrate, are refined to increase the accuracy of the solution. From figure 4.13, it is easily visible that the node density is higher around the regions around the cross holes.
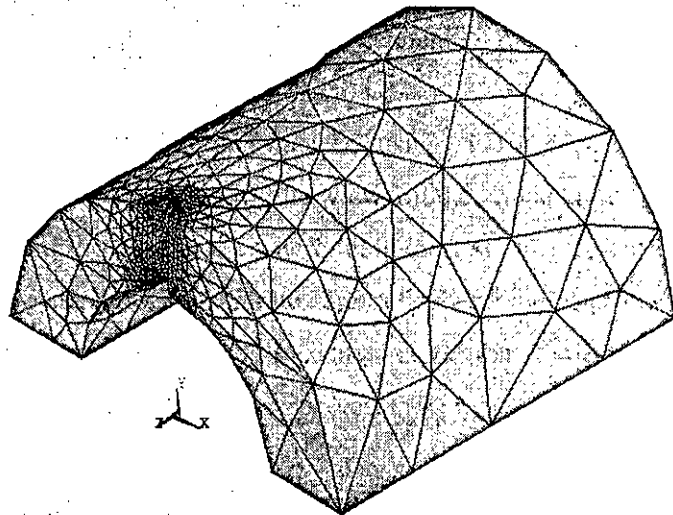
Figure 4.15: Model after it is meshed

4.1.2: Boundary conditions and the solution:

After the meshing of the model is completed by tetrahedral elements, the proper boundary conditions are applied to the model. Both the 1/8 th model for radial cross holes and the 1/4 th model for offset cross holes have 7 sides: 1 and 2 the inside surface and the outer surface of the main cylinder respectively, 3 the end remote from the hole, 4 and 5 the two sides along the length of the model (on longitudinal planes of symmetry), 6 the cross hole surface, 7 the surface on the transverse plane of symmetry. Symmetry boundary conditions are applied to symmetry surfaces (side 4, 5 and 7). The cut end of the cylinder (side 3) is constrained such that the plane section remains plane upon loading. The vessel is loaded by internal pressure, assuming a closed-end condition for the main cylinder. In the finite element models, internal pressure is applied to the main bore (side 1), the cross hole (side 6) and the junction between the cross hole and the inner surface of the main cylinder. The closed end boundary condition was represented by applying a uniform axial thrust to the end of the cylinder (side 3).

After applying the boundary conditions, the solution phases of the finite element analysis are executed. In this phase, computer takes over and solves the simultaneous equations that the finite element method generates. For the present investigations, the frontal solver is used for the solution of the finite element models.

4.1.3: Post processing:

The general post processor contains the commands that allow displaying results of an analysis. All the vital information can be obtained by using the post processing command. In the present study, the quantities that are of importance are the von Mises equivalent stress and the Principal stress that is developed in the cylinder containing the cross hole due to the application of internal pressure. The von Mises equivalent stress distribution or the Principal stress distribution in the models of the cylinders can be obtained easily by the contour plot of these stresses. From the contour plot, the location where the stress either von Mises equivalent stress or the Principal stress, is concentrating can be easily observed.

Again, after solution of a finite element analysis is made, the von Mises equivalent stress or the Principal stress at each node point can be obtained. So the values of the stresses where they are concentrating are readily available. The maximum values of these stresses are required because they are needed to calculate the stress concentration factors.

To calculate stress concentration factors, from the definition, it is apparent that the value of the maximum Principal stress and the value of the maximum von Mises equivalent stress at the inner surface of a plain cylinder (cylinder without cross hole) are required. For this, 5 models of the cylinders without any cross holes for 5 outer to inner radius ratios (b/a) are analyzed and corresponding maximum values of the stresses at the bore of the cylinders are obtained. These values are then used to calculate the Principal stress concentration factor (K_{s1}) and von Mises equivalent stress concentration factor (K_e) for different models using the formula stated in the previous chapter.

CHAPTER 5

RESULTS AND DISCUSSION

In the preceding chapters the computational technique for determination of the stress concentration factor, stress distribution and the location of the maximum stress around elliptical radial and offset cross holes of an internally pressurized thick walled cylinder has been presented. Two different orientation of the hole have been investigated, one with the major axis of the cross hole along the circumferential direction of the cylinder and another major axis of the cross hole along the longitudinal direction of the cylinder. The different geometries of the thick walled cylindrical vessel and different dimensions of the elliptical hole for two different orientations are summarized in the table 5.1.

A 1/8th model of the cylinder for radial elliptical cross holes and 1/4th model for offset cross holes for both the orientations are used for the present investigation. The inner diameter of the main cylinder is 20 mm and the outer diameter is calculated using the five thickness ratio given in the previous chapter.

This chapter is divided into two sections; the first section deals with results obtained from the finite element analysis of the models of different geometry and orientation and in the second section the results obtained are compared with the published data available in literature.

Table 5.1: Geometrical Characteristics of Various Test Cases Investigated

			Elliptical cross hole along the radial center direction of the cylinder (Radial cross hole)					Elliptical cross hole offset from the radial center line of the cylinder (offset cross hole)				
		b/a	1.5	1.75	2	2.25	2.5	b/a	1.5	1.75	2	2.25	2.5
Orientation A		Smaller hole	$R_c = 0.4$ mm $R_a = 0.8$ mm $R_b = 0.4$ mm					Smaller hole	$R_c = 0.4$ mm $R_a = 0.8$ mm $R_b = 0.4$ mm				
		Larger hole	$R_c = 2.0$ mm $R_a = 4.0$ mm $R_b = 2.0$ mm					Larger hole	$R_c = 2.0$ mm $R_a = 4.0$ mm $R_b = 2.0$ mm				
Orientation B		Larger hole	$R_c = 2.0$ mm $R_a = 4.0$ mm $R_b = 2.0$ mm					Larger hole	$R_c = 2.0$ mm $R_a = 4.0$ mm $R_b = 2.0$ mm				

5.1 Circumferential Orientation

5.1.1. Radial Cross hole

Figure 5.1 shows the von Mises equivalent stress distribution as a contour plot for a radial elliptical cross hole with the major axis of the elliptical hole along the hoop direction of the cylinder(orientation A). In this case the main cylinder ratio is b/a = 2, the minor axis radius of the hole is $R_c = 2$ mm and the fillet radius is $R_b = 2$ mm between the hole and inner surface of the cylinder. From the contour plot of von Mises equivalent stress (σ_{VM}), it is observed that the highest stress occurs at the junction between the crosshole and outer surface of the cylinder, on the transverse plane of symmetry. The same stress distribution occurs for all the other test cases. This is an interesting finding of this thesis work as the finite element Analysis by Hamilton *et al.* [11] for circular cross hole shows that von Mises equivalent stress (σ_{VM}) concentrates around the intersection of the cross hole and inner surface of the main cylinder, with same boundary conditions and same finite element solution technique being carried out. But in case of

42

elliptical cross hole the stress is observed to be concentrating at the junction between the hole and the outer surface of the cylinder rather than the inner surface, which is observed in case of circular cross holes. The reason behind this phenomenon is due to the elongation of the effective major to minor axis ratio of the elliptical hole, as it intersects with the inner radius, which does not happen in the intersection between the hole and the outer surface of the main cylinder. As a result the stress concentrates at the outer surface of the cylinder which is also observed in other test cases.

The Principal stress concentration factors (K_{s1}) and von Mises equivalent stress concentration factors (K_e) for all the larger cross hole and smaller cross hole configurations are plotted against main cylinder radius ratio, which are shown in figures from 5.5 to 5.8. All these figures illustrate that the SCFs, either the Principal or the von Mises, increases with the increase of the main cylinder radius ratio (b/a). Table 5.2 shows the values of Principal stress concentration factors (K_{s1}) and von Mises equivalent stress concentration factors (K_e) obtained from the present study –

]

Table 5.2: The values of K_{s1} and K_e for different b/a ratio

Circumferential Orientation

b/a ratio	Smaller radial cross hole		Larger radial cross hole	
	K_{s1}	K_e	K_{s1}	K_e
1.5	1.77	1.71	1.92	1.72
1.75	1.803	1.75	2.2	1.815
2.0	2	1.795	2.36	1.93
2.25	2.11	1.9	2.45	1.952
2.5	2.2	2.	2.52	2.012

The data in table 5.2 depicts that both the Principal SCFs (K_{s1}) and the von Mises equivalent SCFs (K_e) are greater in values for larger radial cross holes than for smaller radial cross holes.

Figure 5.2 depicts the contour plot of Principal stress (σ_1) distribution for an elliptical radial cross hole where the major axis of the cross hole is along the hoop direction of the cylinder (Circumferential Orientation). In this case the main cylinder ratio is b/a = 2, the minor axis radius of the hole is R_c = 2 mm and the fillet radius is R_b = 2 mm between the hole and inner surface of the cylinder.

5.1.2. Offset Cross hole

Figure 5.3 shows the von Mises equivalent stress (σ_V) distribution as a contour plot for an elliptical cross hole offset at a distance 3.36 mm from the radial center line with the major axis along the hoop direction of the cross hole(Circumferential Orientation). In this case the main cylinder ratio is b/a = 1.5, the minor axis radius of the hole is Rc = 0.4 mm and the fillet radius is Rb = 0.4 mm between the hole and inner surface of the cylinder. The offset distances for each b/a ratio are calculated from the relation R_b = 0.112b. So the offset distances for b/a = 1.5, 1.75, 2.0, 2.25 and 2.5 are 3.36 mm, 3.92 mm, 4.48 mm, 5.04 mm respectively. The results obtained from the investigation of the offset holes for circumferential orientation was seen to have similar effects on the location and magnitude of the peak stress. The stresses are observed to be concentrating at the outer cylinder-hole intersection as the previous analysis on the radial elliptical cross holes. The calculated stress concentration factors for both smaller and larger elliptical cross holes offset from the radial center line of the cylinder are shown in table 5.3:

Table 5.3: The values of K_{sl} and K_c for different b/a ratio

(circumferential orientation)

b/a ratio	Smaller offset cross hole		Larger offset cross hole	
	K_{sl}	K_c	K_{sl}	K_c
1.5	1.71	1.66	1.88	1.65
1.75	1.815	1.71	2.04	1.72
2.0	1.93	1.7	2.1	1.746
2.25	1.95	1.68	2.23	1.77
2.5	2	1.7	2.35	1.82

Figures 5.8 to 5.12 show the effect of outer to inner radius ratio of the main cylinder on the Principal SCFs and the von Mises Equivalent SCFs. These graphs also demonstrate the increasing nature of the SCFs with the increment of the b/a ratio same as those of radial cross holes.

5.2 Longitudinal orientation

5.2.1. Radial Cross hole

Figure5.4 presents the contour plot of von Mises (σ_{VM}) distribution for a radial elliptical cross hole; where the major axis of the cross hole is along the longitudinal direction of the cylinder. In this case the main cylinder ratio is b/a = 2, the minor axis radius of the hole is Rc = 2 mm and the fillet radius is Rb = 2 mm between the hole and inner surface of the cylinder. Considering this contour plot of von Mises stress distribution of orientation B, it is observed that the von Mises stress (σ_V) is highest around the major axis of the elliptical hole at the outer intersection of the hole and the cylinder. Similar results are obtained for all other finite element analysis of this orientation. The reason behind this occurrence can be explained by the theory of a flat plate having a hole loaded by internal pressure. A flat plate here may be considered to be a section of a thin cylinder of infinite radius. Under internal pressure, the plate is subjected to an in-plane biaxial state of stress (σ_θ, $\sigma_\theta/2$), where σ_θ is equivalent to the hoop stress of a pressurized thin cylinder. The maximum SCF at the hole can be found from the well known solution for a small hole in an infinite plate and stress superposition. This is illustrated in figure 5.13, which shows a maximum SCF of 2.5 for a circular hole. The solution for an elliptical hole is found in a similar manner. The maximum SCF depends on the major-minor axis ratio of the ellipse. If it is parallel to the higher axial stress σ_θ, the SCF will be lower than that for a circular hole; for an axis ratio of 2, the corresponding maximum SCF value is 1.5. If the major axis is perpendicular, the SCF will be greater than that for a circular hole, the corresponding maximum SCF value is 4.5. The solution for a cross

45

hole in a thick cylinder subject to internal pressure is more complex but a similar approach can be employed.

It can be concluded that in case of the elliptical hole, there are different SCF values on each hole axis. The small effective radius of curvature at the ends of the hole gives a higher SCF than at the middle of the ellipse. The ellipse should be oriented in such a way that the larger SCF is applied to the smaller bulk stress, i.e. the major axis of the elliptical hole should be placed along the hoop direction of the cylinder for less stress to build up. So if the orientation of the ellipse is placed the other way round then the maximum stress that will be developed will be greater than this orientation and also that given by a circular hole. So the results, obtained for longitudinal orientation of the cross hole, validate the above discussion that in this orientation the stress is concentrating around the major axis of the elliptical hole at the outer intersection of the hole and the cylinder.

For the finite element analysis of the models of longitudinal orientation only the larger holes are taken into account. The calculated stress concentration factors for larger elliptical cross holes along the radial center line of the cylinder are shown in table 5.4:

Table 5.4: The values of K_{s1} and K_e for different b/a ratio

longitudinal orientation

b/a ratio	Larger radial cross hole	
	K_{s1}	K_e
1.5	4.627	4.15
1.75	4.89	4.229
2.0	5.1	4.44
2.25	5.2	4.5
2.5	5.36	4.4667

Figures 5.14 and 5.15 present the variation of the Principal SCFs and the von Mises equivalent SCFs with the change of outer to inner radius ratio of the main cylinder.

]

5.2.2 Offset Cross hole

The offset distances for longitudinal orientation of cross holes each b/a ratio are same as that are calculated for the offset cross holes of circumferential orientation.

Table 5.5: The values of K_{s1} and K_e for different b/a ratio
longitudinal orientation

b/a ratio	larger radial cross hole	
	K_{s1}	K_e
1.5	4.29	3.84
1.75	4.66	3.88
2.0	4.85	3.94
2.25	5.08	3.99
2.5	5.18	4.1

The finite element analysis of offset cross holes of longitudinal orientation leads to the similar results as for other test cases. The calculated stress concentration factors for the larger elliptical cross holes offset from the radial center line of the cylinder are shown in table 5.5:

The corresponding figures 5.16 and 5.17 describe the effect of outer to inner radius ratio of the main cylinder on the Principal SCFs and the von Mises Equivalent SCFs.

5.3. Comparison of K_{s1} s and K_e s for different orientation

As in case of longitudinal orientation of cross holes only the large holes of both radial and offset configuration have been analyzed using finite element method so the SCFs are

compared for only the larger cross holes. In figures 5.18 and 5.19, the variation of the Principal SCFs (K_{s1}) and the von Mises SCFs (K_c) are observed for the radial cross holes of both the orientation. As for the reason described in section 5.2.1 it is obvious that the values of both the stress concentration factors for different b/a ratio will be higher for longitudinal orientation than that for the circumferential orientation.

Figures 5.20 and 5.21 present the variation of the Principal SCFs (K_{s1}) and the von Mises SCFs (K_c) for the offset cross holes of both the orientation. These figures are indicating the same outcomes for those obtained for radial cross holes.

5.4. <u>Comparison of K_{s1} s and K_c s between radial and offset crossholes</u>

In figures 5.22 and 5.23 for orientation A, the comparison of the Principal SCFs and the von Mises SCFs between smaller radial and smaller offset cross holes for different b/a ratio are observed. It is observed from both the figures that smaller offset cross holes show less stress concentration factor than that the radial cross holes which substantiates the findings of the reference [10] that offsetting circular cross holes led to reduced SCF, which in turn results in a significant increase in the fatigue life of vessels. Though the findings of the reference [10] were based on circular cross holes, same results are also obtained for the elliptical offset cross holes.

Figures 5.24 and 5.25 also indicate the similar results for larger radial and offset cross holes as those for larger radial and offset cross holes for circumferential orientation.

In the figures 5.26 and 5.27, the Principal SCFs (K_{s1}) and von Mises SCFs (K_c) are plotted against main cylinder radius ratio for larger cross holes of radial and offset configuration for longitudinal orientation. These figures are also of same nature as the previous ones for the circumferential orientation.

5.5 Comparison of the SCFs between radial and offset cross holes

In figures 5.28 and 5.29 the Principal SCFs (K_{s1}) and the von Mises SCFs (K_e) for smaller and larger radial cross holes for different orientation are plotted against different b/a ratios. It is noticed from the figures that for all conditions the SCFs are increased with the increasing b/a ratio. In case of comparing the SCFs between large and small radial cross holes for circumferential orientation, it is seen from the figures that both the SCFs are higher for larger holes than those of smaller holes. Again, Comparing between all the three cases, large and small hole of circumferential orientation and large hole of longitudinal orientation, it is observed that the small radial cross holes of circumferential orientation provides less stress concentration of all the 3 cases. Although the SCFs of radial small cross holes of longitudinal orientation is not calculated in this present study, but showing the trend it can be said that the SCFs for this cross hole of longitudinal orientation would have been definitely greater than that of the same of circumferential orientation.

The figures 5.30 and 5.31 illustrate the Principal SCFs (K_{s1}) and the von Mises SCFs (K_e) for smaller and larger offset cross holes for different orientation. The natures of the figures are same as that obtained for the radial cross holes. Here also the small offset cross hole of circumferential orientation shows the less SCFs among all for different b/a ratios.

From all the figures from 5.28 to 5.31 it can be observed that the von Mises equivalent SCFs does not vary much for both the small and large radial and offset cross holes of circumferential orientation where as the Principal SCFs shows a significant differences in the values for the same condition. As the concept of the von Mises equivalent stress in this study is included as the complex stress state that occurs in the cylinders due to the cross holes can be explained accurately by this theory, so it can be said that the values of the von Mises equivalent SCFs are some what independent of the hole sizes for different b/a ratios.

5.6: Comparison of the SCFs between cross hole sizes and orientation

Figures from 5.32 to 5.36 represent the comparison of Principal SCFs and von Mises equivalent SCFs between different cross hole sizes and two orientation of the hole for each outer to inner radius ratio (b/a) of the cylinder. Each figure demonstrates the comparison of both SCFs for all the geometries and orientation of the cross hole taken into consideration in this study for each b/a ratio. Actually each figure summarizes all the results obtained for each b/a ratio which are shown as bar charts. From each figure it is evident that the smaller offset cross hole of orientation A shows smallest SCF among all other configurations. And in each case the von Mises equivalent SCF is always less than the Principal SCF for all the configurations of the cross holes.

5.7: Comparison of the SCFs with published data available in literature

In this section the SCFs for elliptical cross holes in a cylinder are compared with the SCFs obtained by Hamilton *et al.*[11] for mainly circular cross holes. Before making any comparison, the validity of the finite element computer program (ANSYS) and the computational procedure used to obtain the stress concentration factors for elliptical cross holes is made. The equivalent circular large cross holes (the radius of the circular hole is same as the minor axis radius of the elliptical hole) placed along the radial center line of the main cylinder for 5 b/a ratios are analyzed using ANSYS and keeping all the parameters the same. Figure 5.37 present the principal stress concentration factors obtained for the circular large holes in the present study and the SCFs obtained by Hamilton *et al.*. From the figure it is observed that the results obtained in the present study provide almost same values of SCFs as that of the results obtained by Hamilton *et al.*. The results of both the investigation show around 1-1.5% variation in results, which is quite low. So it can be said that the computational procedure and the finite element software used to analyze the stress concentration effects of elliptical cross holes are valid.

Figure 5.38 illustrates the von Mises equivalent stress concentration factors obtained for the circular large holes in the present study and the SCFs obtained by Hamilton *et al.*.

The figure also shows that the values obtained by both the investigation are rather similar and show a around 1.5-2.5% variation in values.

Now in figures 5.39 to 5.42; the SCFs K_{s1} and K_e for all the larger cross hole configurations (radial and offset) of circumferential orientation are plotted against main cylinder radius ratio for circular cross hole having blended intersection (data taken from reference [11]), circular cross hole having chamfer at the intersection (data taken from reference [11]) and elliptical cross hole having blended intersection (data obtained from the present study). From the figures it is observed that elliptical cross holes give the lowest SCFs for all b/ratios than for those of circular cross hole having blended intersection, circular cross hole having chamfer at the intersection.

Figures 5.43 to 5.46 show the SCFs K_{s1} and K_e for all the smaller cross hole configurations (radial and offset) of circumferential orientation plotted against b/a ratio for plain elliptical cross hole having blended intersection, cross hole having blended intersection, and circular cross hole having chamfer at the intersection. These figures also show that the SCFs are smallest for elliptical cross holes compared to other two cross holes.

So it can be concluded by observing the figures 5.39 to 5.46 that the SCF is reduced when the intersection between the cross hole and main bore surface has an elliptical profile. So the elliptical shaped cross holes should be preferred over the circular ones. Also it can be seen from the results of Hamilton *et al.* [11] that the circular cross holes having blended intersection give less stress concentration factor compared to that of the chamfered one. So in this present study blending of the surface between the cross hole and the inner of the cylinder is used to obtain less stress concentration factor.

A complete set of SCF values for elliptical cross hole geometries considered here has not been previously presented in the literature and it is not therefore possible to make direct comparison with other solutions. Fenner and Nadiri [14] obtained stress concentration factors for ellipse aspect ratios (minor radius to major radius ratio) 0.9 and

51

0.8, but in the present study we obtained stress concentration factors for 0.5 aspect ratio. Again they considered side branch holes, so the effect of the branch pipes are considered as closed end boundary conditions in their literature but in this present study the hole has been considered open. Therefore obviously they results cannot be compared.

CHAPTER 6
CONCLUSIONS

In the present study two relatively small opening are considered, which are typical of an instrumentation tapping, bursting caps or fluid entry/ exit ports in thick walled high pressure vessels. Overall, the stress concentration effect was smaller for smaller hole. Again the results obtained from the analysis demonstrates the increasing nature of the stress concentration factors for both radial and offset elliptical cross holes with the increment of the outer to inner radius ratio of the main cylinder (b/a) for both circumferential and longitudinal orientation.

The Principal SCFs for elliptical smaller radial cross holes having blended intersection obtained from the present study are 1.77, 1.803, 2, 2.11, and 2.2 and von Mises SCFs for the same configuration are 1.71, 1.815, 1.93, 1.95 and 2.01. Similarly the Principal SCFs for equivalent circular smaller radial cross hole having blended intersection are 3.2, 3.4, 3.5, 3.55 and 3.6 and von Mises SCFs for the same configuration are 2.75, 2.75, 2.73, 2.72 and 2.71. The results for the circular cross holes are obtained by Hamilton et al. [11]. Comparing these results obtained for elliptical smaller radial cross holes with those obtained for equivalent circular cross holes by Hamilton et al.[11] show that the both the SCFs are less for elliptical cross holes than the circular ones. All other configurations of holes also show that the SCFs are less for elliptical shaped holes.

Comparing the results of the equivalent circular and elliptical radial larger cross holes, the principal and von Mises SCFs for the elliptical cross holes are seen to vary

around 30% and 28% in contrast to the circular ones. The Principal and von Mises SCFs for equivalent smaller radial cross holes vary around 42% and 30% respectively. Considering offset cross holes, the principal SCFs for larger and smaller elliptical cross holes show around 35% and 41% reduction in values than the equivalent circular cross holes and the von Mises SCFs show around 22% and 34% reduction in values. So cross holes of elliptical shape can be used instead of the circular one, though the manufacturing cost of the elliptical holes are high.

The Principal SCFs for larger radial elliptical cross hole of circumferential orientation found in the present study are 1.92, 2.2, 2.36, 2.45 and 2.52 and the von Mises SCFs are 1.71, 1.75, 1.795, 1.9 and 2.01. Again, the Principal SCFs for the same configuration of cross hole of longitudinal orientation are 4.627, 4.89, 5.1, 5.2 and 5.36 and the von Mises SCFs are 4.15, 4.229, 4.44, 4.5 and 4.4667. Comparing the SCFs, it can be concluded that the circumferential orientation of the cross hole give less SCFs than the longitudinal orientation of holes.

For larger radial cross hole orienting along the circumferential direction of the main cylinder, the Principal SCFs for corresponding b/a ratios of 1.5, 1.75, 2, 2.25 and 2.5 are found to be 1.92, 2.2, 2.36, 2.45 and 2.52 respectively , where as for offset cross holes the SCFs are 1.88, 2.04, 2.1, 2.23 and 2.35 respectively. For the same configuration of cross holes, the von Mises SCFs are 1.71, 1.75, 1.795, 1.9 and 2.01 respectively for radial configuration and 1.65, 1.72, 1.746, 1.77 and 1.82 respectively for offset configuration. So it can be seen from the results that the Principal SCFs and von Mises SCFs for larger offset cross holes show maximum 8% and 9% reduction in values than the radial cross holes. The smaller offset cross holes of circumferential orientation give around 15% and 9% maximum reduction in Principal and von Mises SCF values respectively. From the results obtained and also from the figures it can be concluded that the offset cross holes are a better proposition that the radial ones. Offset cross holes are cheaper to manufacture than elliptical radial cross holes and give some reduction in stress concentration factor compared with a radial cross hole. Offset elliptical cross holes are not generally used in practice but included in this present study as a design possibility.

54

Bar charts from figure 5.32 to 5.36 show all the results, obtained for the entire elliptical hole configurations for each b/a ratio, in a different approach. From the figures it can be concluded for all b/a ratio the smaller offset hole of circumferential orientation gives the smallest Principal and von Mises equivalent stress concentration factors.

Comparing the results obtained in the present study with that of the results obtained by Hamilton *et al.* it is seen that the elliptical cross holes having blended surface in the intersection gives less stress concentration factors than that of the circular cross holes with blended and chamfered intersection. So it can be concluded that the elliptical cross holes both the radial and offset configurations having blended feature in the intersection give less stress concentration factors than those of the circular ones.
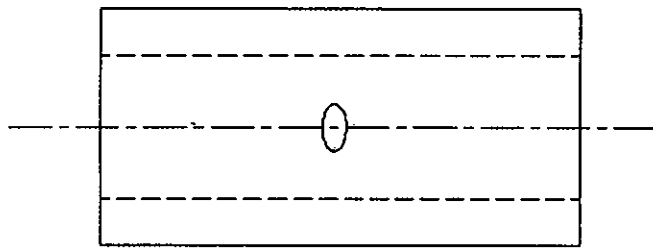
Top view
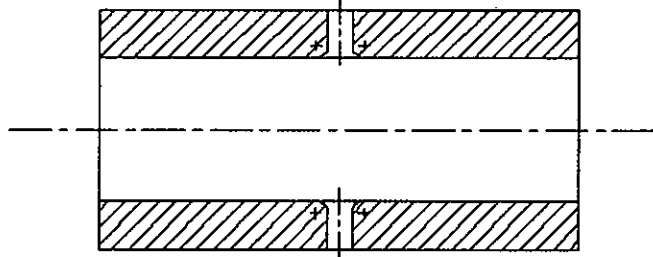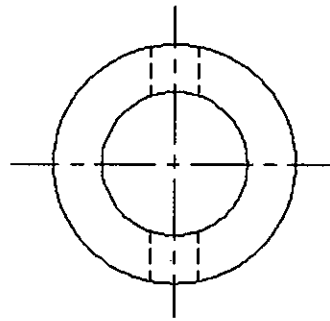
Front view   R.H.S view

Figure 4.1: Circumferential orientation of the cross hole
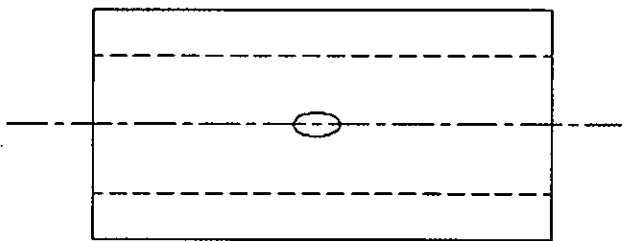
Top view
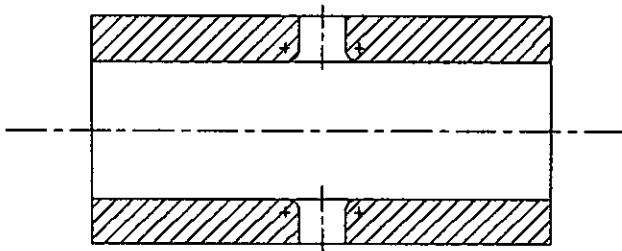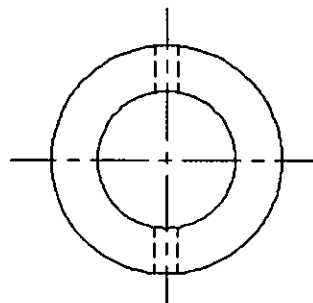
Front view   R.H.S view

Figure 4.2:longitudinal orientation of the cross hole
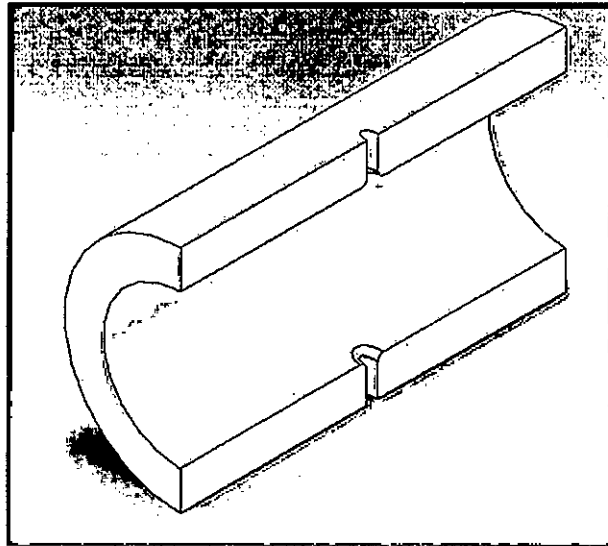
Figure 4.3: A half section of a cylinder containing radial cross hole
(Circumferential orientation)
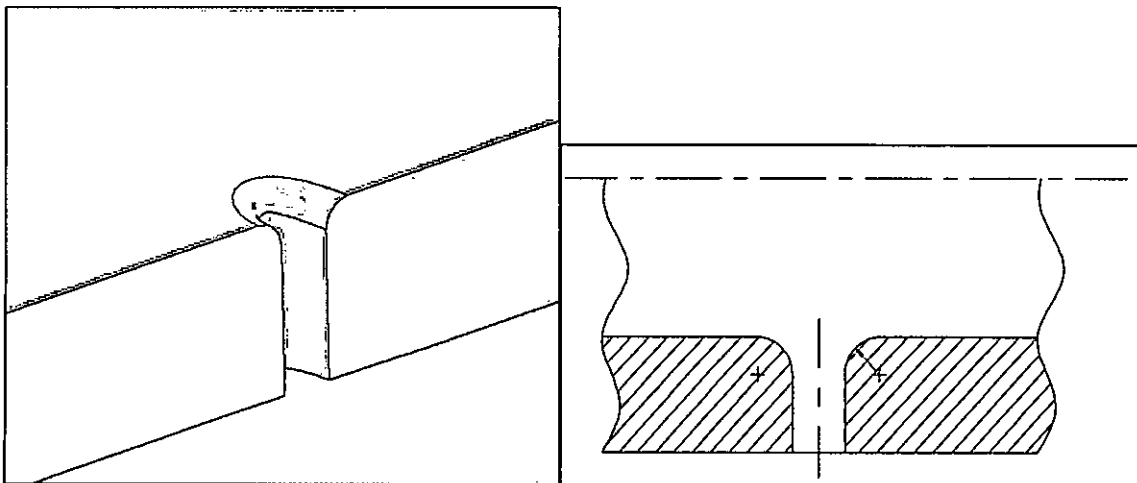
Figure 4.4: Radial cross hole having blended surface between the main bore and the cross
hole intersection
(circumferential orientation)

57
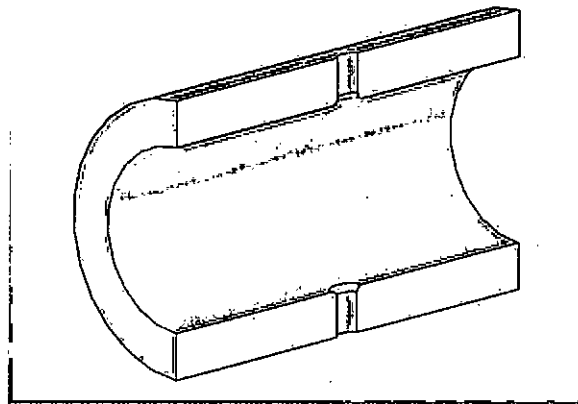
Figure 4.5: A half section of a cylinder containing radial cross hole
(longitudinal orientation)
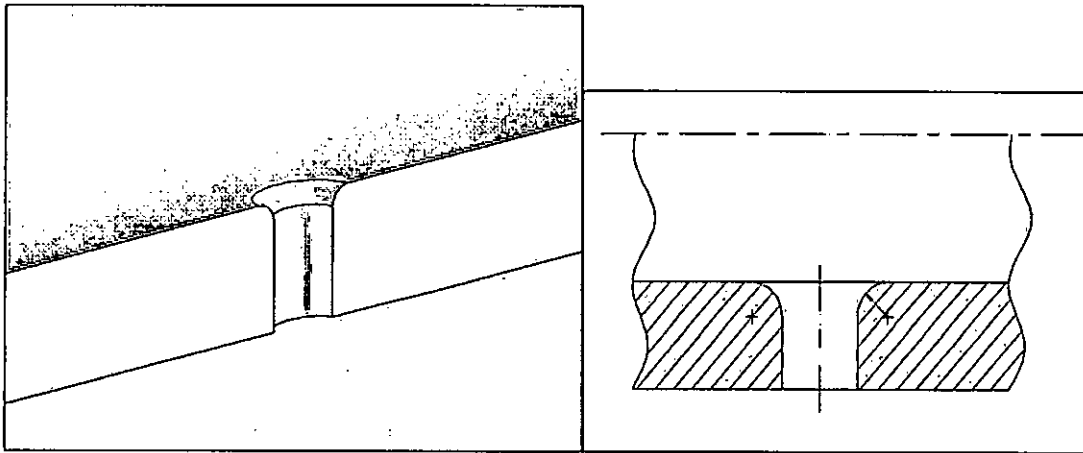
Figure 4.6: Radial cross hole having blended surface between the main bore and the cross
hole intersection
(longitudinal orientation)
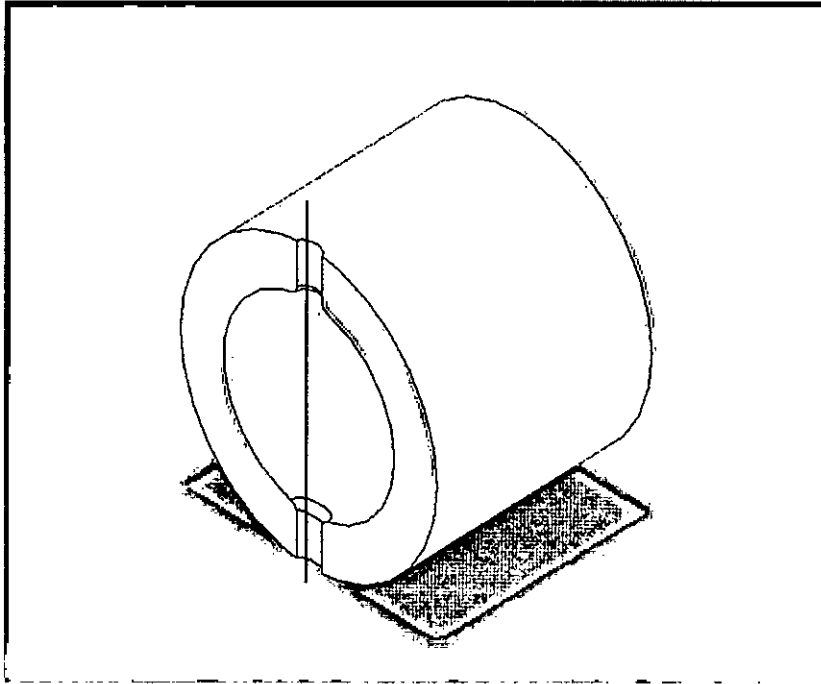
Figure 4.7: A cross section of a cylinder containing radial cross hole
(circumferential orientation)
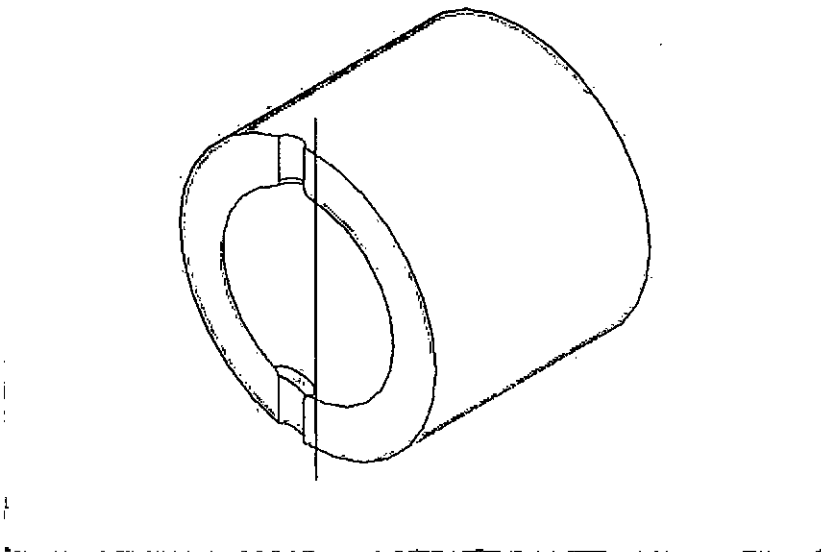
Figure 4.8: A cross section of a cylinder containing offset cross hole
(circumferential orientation)
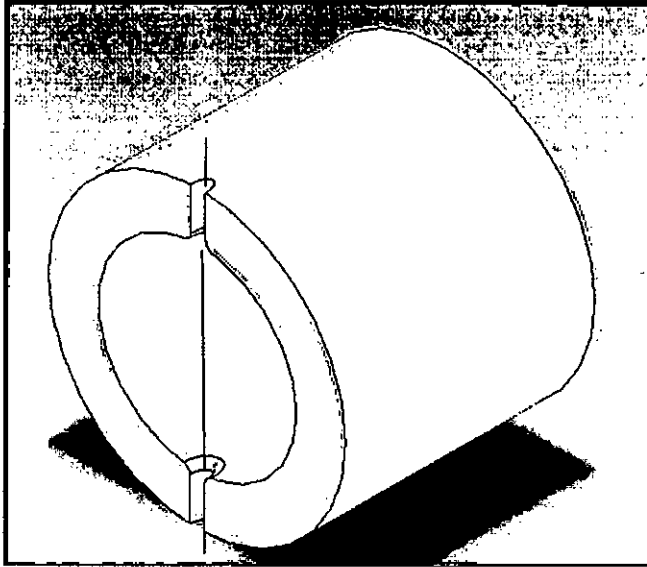
Figure 4.9: A cross section of a cylinder containing radial cross hole
(longitudinal orientation)
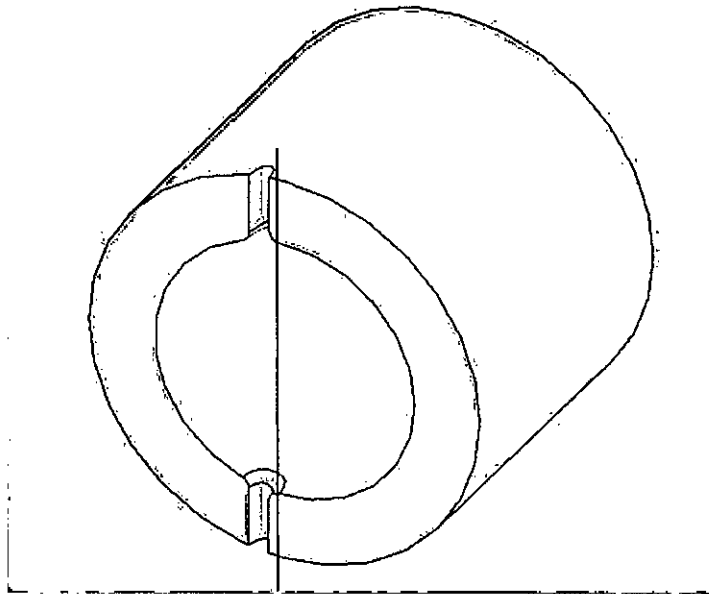
Figure 4.10: A cross section of a cylinder containing offset cross hole
(longitudinal orientation)

```
ANSYS 5.4
DEC 11 2006
13:17:58
NODAL SOLUTION
STEP=1
SUB =1
TIME=1
SEQV      (AVG)
PowerGraphics
EFACET=1
AVRES=Mat
DMX =.001669
SMN =.366687
SMX =175.321
     .366687
     19.806
     39.245
     58.685
     78.124
     97.563
     117.003
     136.442
     155.881
     175.321
```
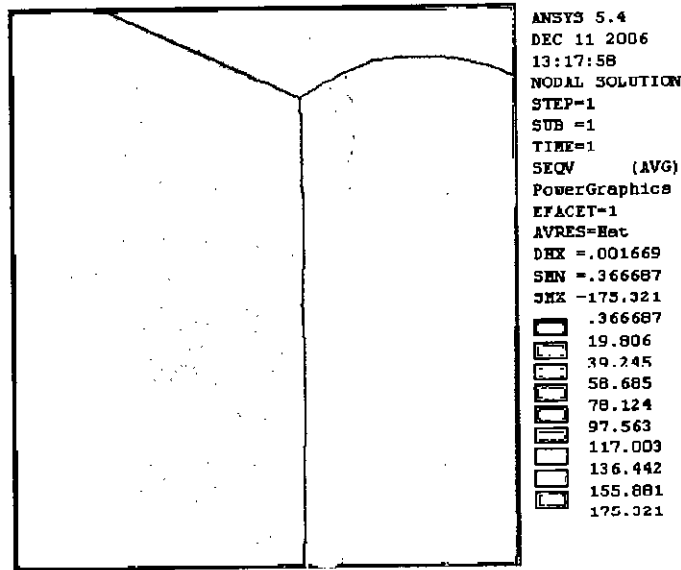
Figure 5.1: The Von Mises equivalent stress distribution is shown as a contour plot for a radial elliptical cross hole; circumferential orientation , main cylinder ratio b/a = 2, R_C = 2 mm and fillet radius R_b = 2 mm


```
ANSYS 5.4
DEC 15 2006
11:15:16
NODAL SOLUTION
STEP=1
SUB =1
TIME=1
S1        (AVG)
PowerGraphics
EFACET=1
AVRES=Mat
DMX =.001669
SMN =-54.118
SMX =149.761
     -54.118
     -31.465
     -8.811
     13.842
     36.495
     59.148
     81.802
     104.455
     127.108
     149.761
```
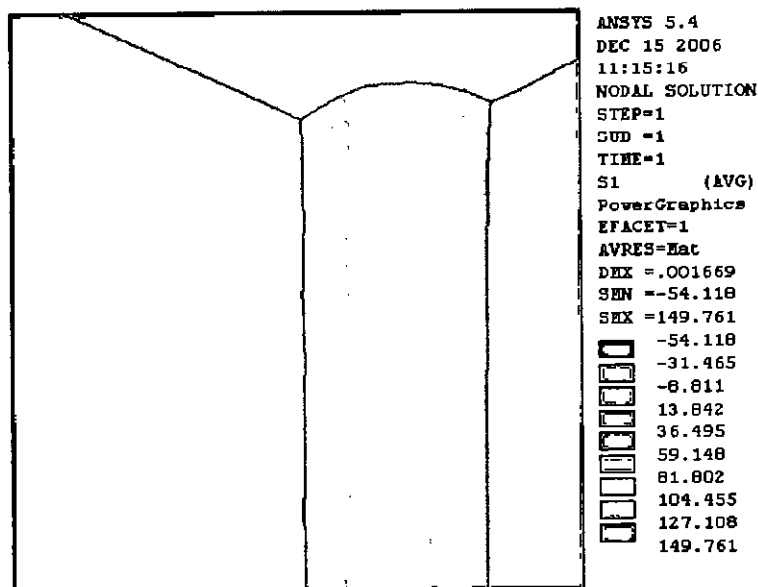
Figure 5.2: The contour plot of Princial stress (σ 1) distribution for a elliptical radial cross hole; circumferential orientation , b/a = 2, R_C = 2 mm and R_b = 2 mm

61
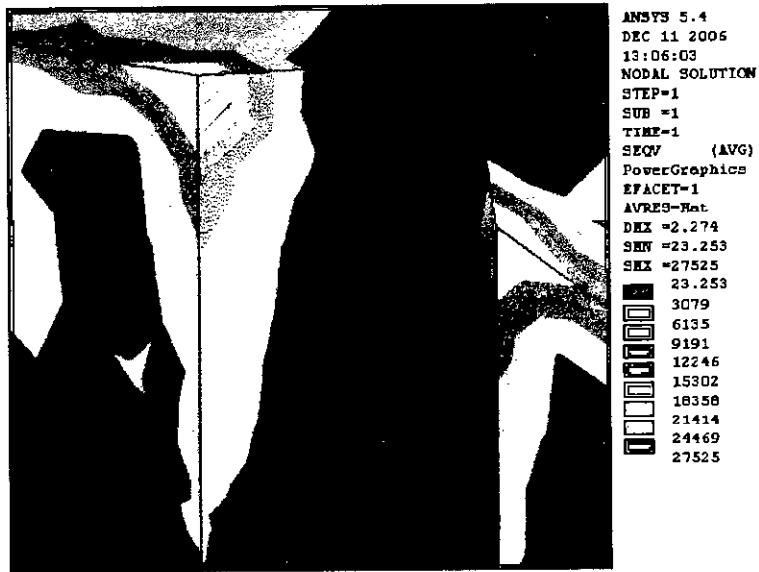
Figure 5.3: The contour plot of Von Mises equivalent stress distribution for a elliptical cross hole offset at a distance 3.36 mm from the radial center line; orientation A, b/a = 1.5, Rc = 0.4 mm and Rb = 0.4 mm
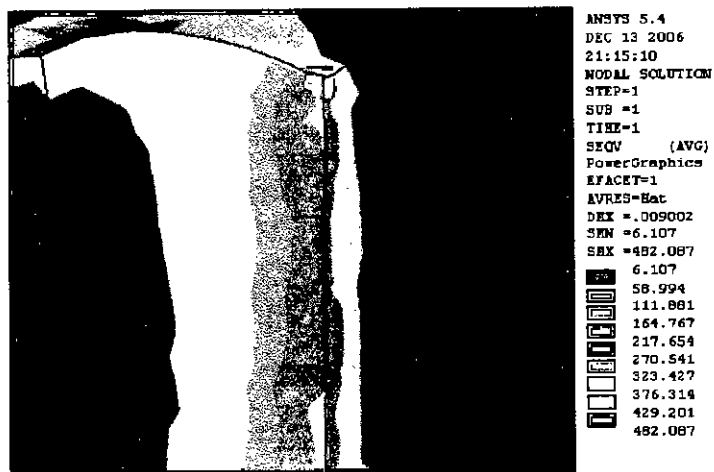
Figure 5.4: The contour plot of Von Mises equivalent stress distribution for a radial elliptical cross hole; orientation B, b/a = 2, Rc = 2 mm and Rb = 2 mm
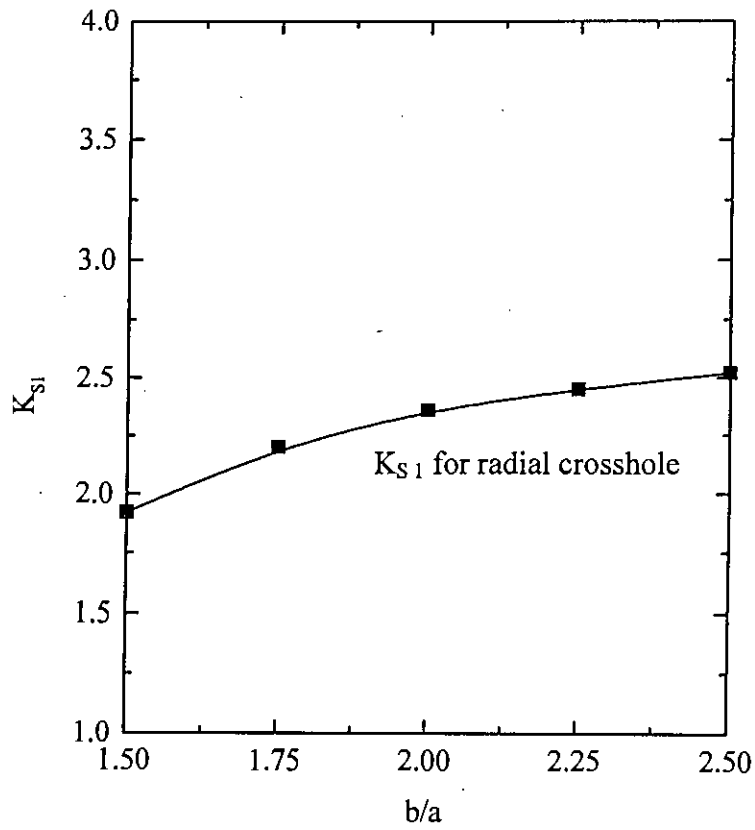
Figure 5.5: The effect of thickness ratio on Principal SCF for larger bore radial crossholes
(Circumferential Orientation)
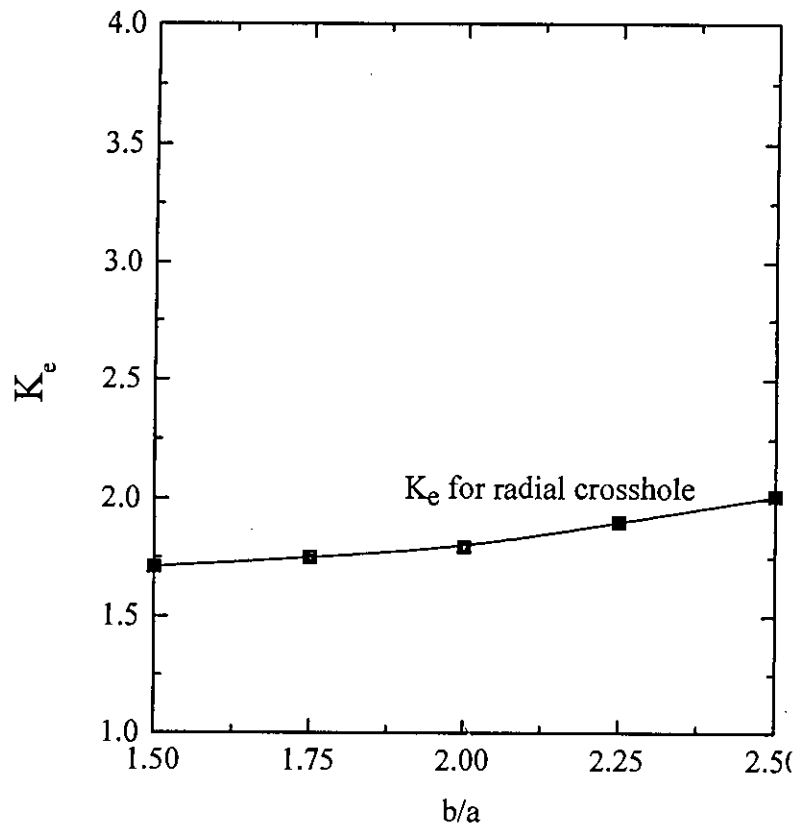
Figure 5.6: The effect of thickness ratio on von Mises SCF for larger radial crosshole
(Circumferential Orientation)
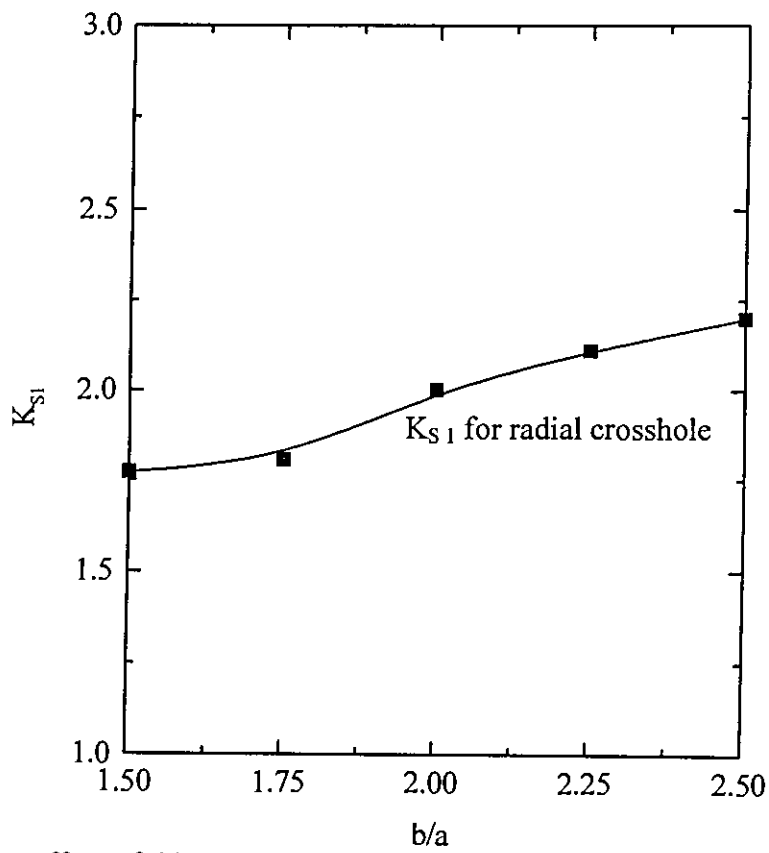
Figure 5.7: The effect of thickness ratio on Principal SCF for smaller radial crossholes
(Circumferential Orientation)
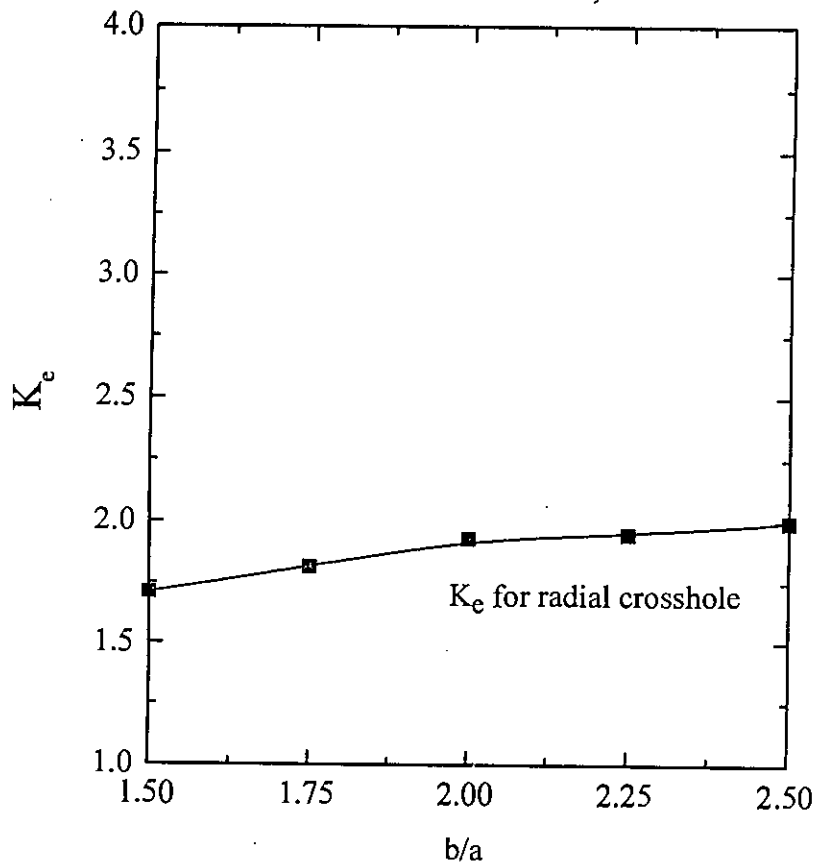
Figure 5.8: The effect of thickness ratio on von Mises equivalent SCFs for smaller radial
crossholes
(Circumferential Orientation)
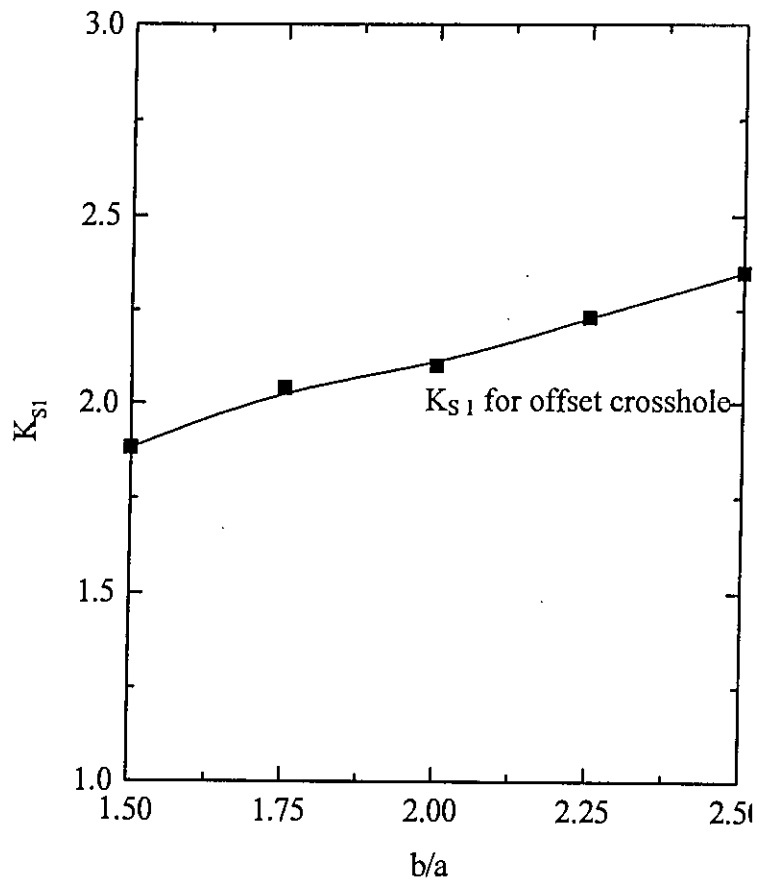
Figure 5.9: The effect of thickness ratio on Principal SCF for larger offset crossbores
(Circumferential Orientation)
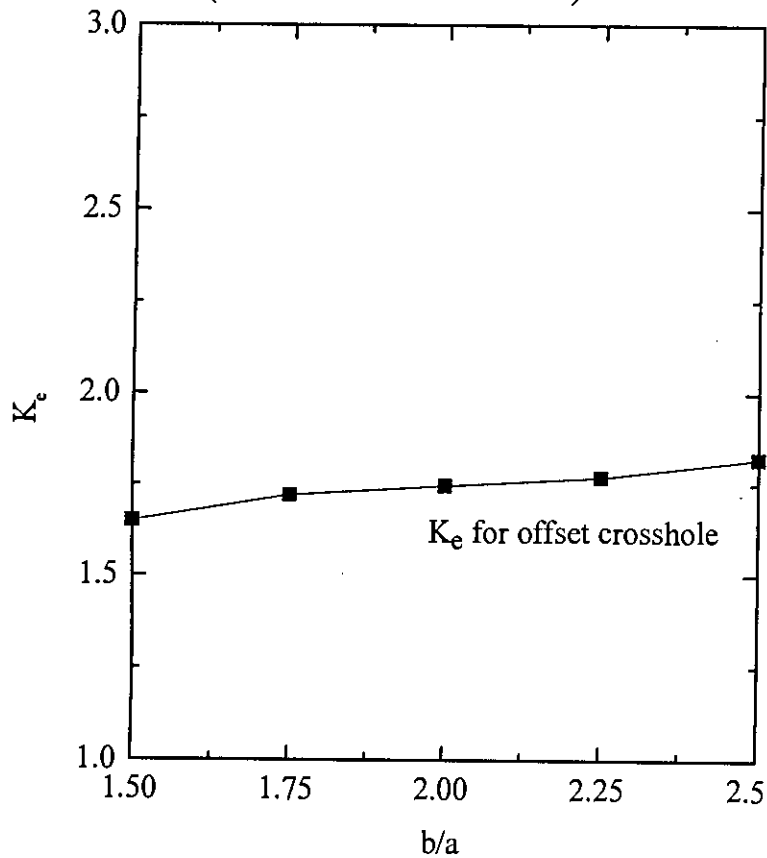
Figure 5.10: The effect of thickness ratio on Von mises SCF for larger offset crossbores
(Circumferential Orientation)
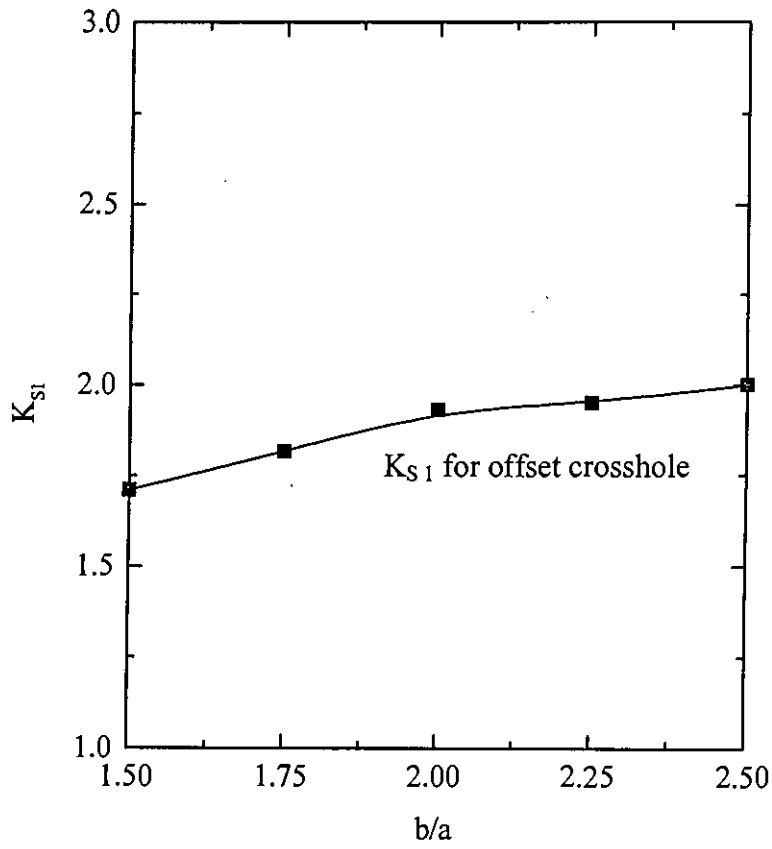
Figure 5.11: The effect of thickness ratio on Principal SCF for smaller offset crossholes
(Circumferential Orientation)
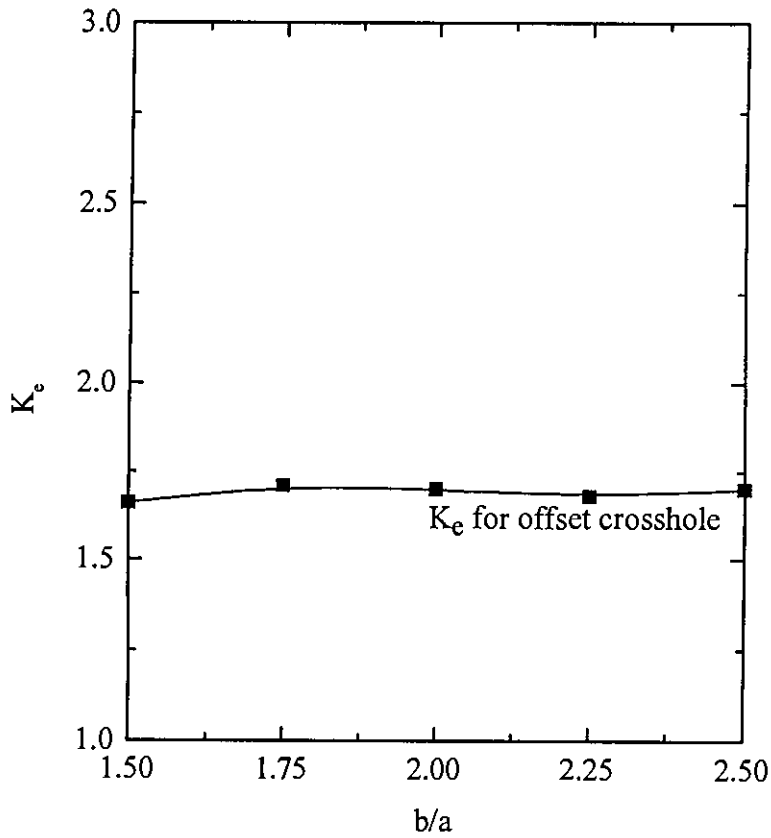
Figure 5.12: The effect of thickness ratio on von Mises SCF for smaller offset crossbores
(Circumferential Orientation)
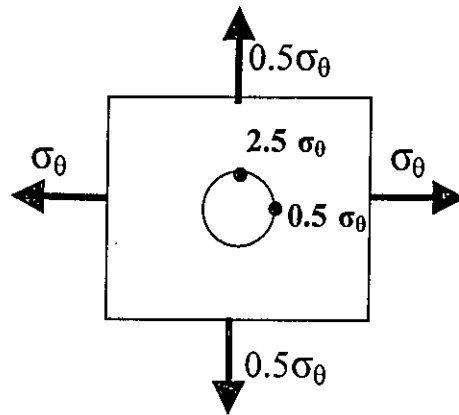
Figure5.13: Stress concentration in a biaxially loaded (σ_0, $\sigma_\theta/2$) flat plate with small central hole
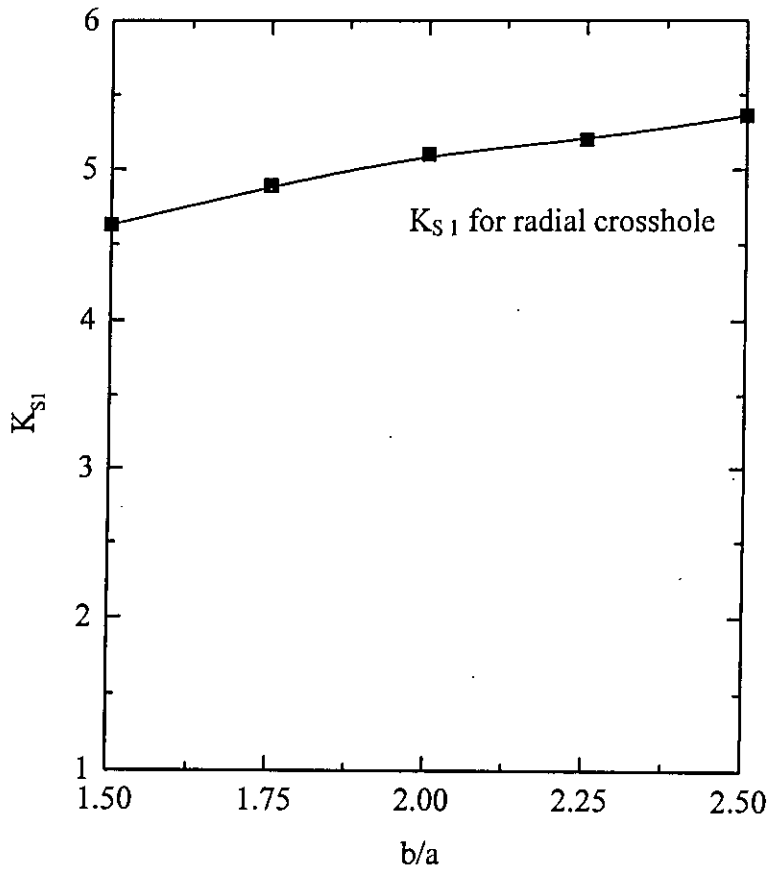
Figure 5.14: The effect of thickness ratio on the principal SCF for larger radial cross holes (longitudinal direction)
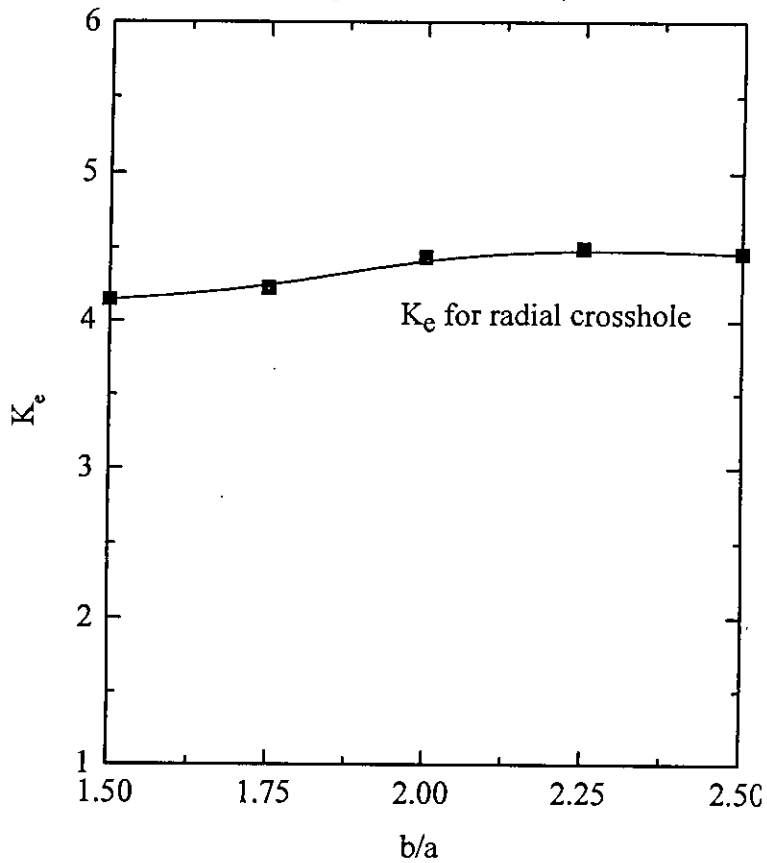
Figure 5.15: The effect of thickness ratio on the von Mises SCF for larger radial crossholes (longitudinal direction)
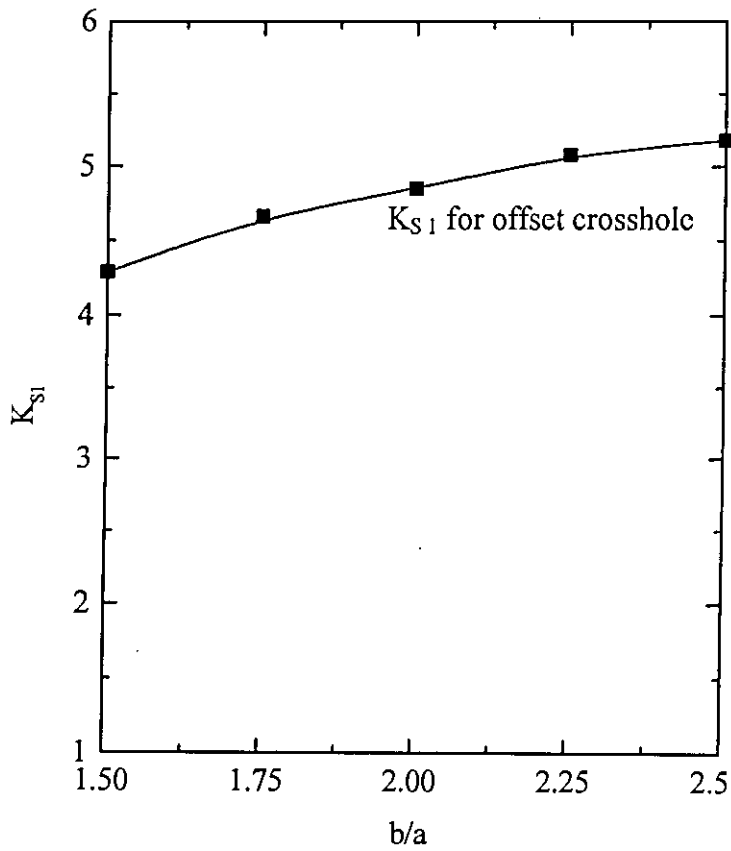
Figure 5.16: The effect of thickness ratio on the Principal SCF for larger offset cross holes (longitudinal direction)
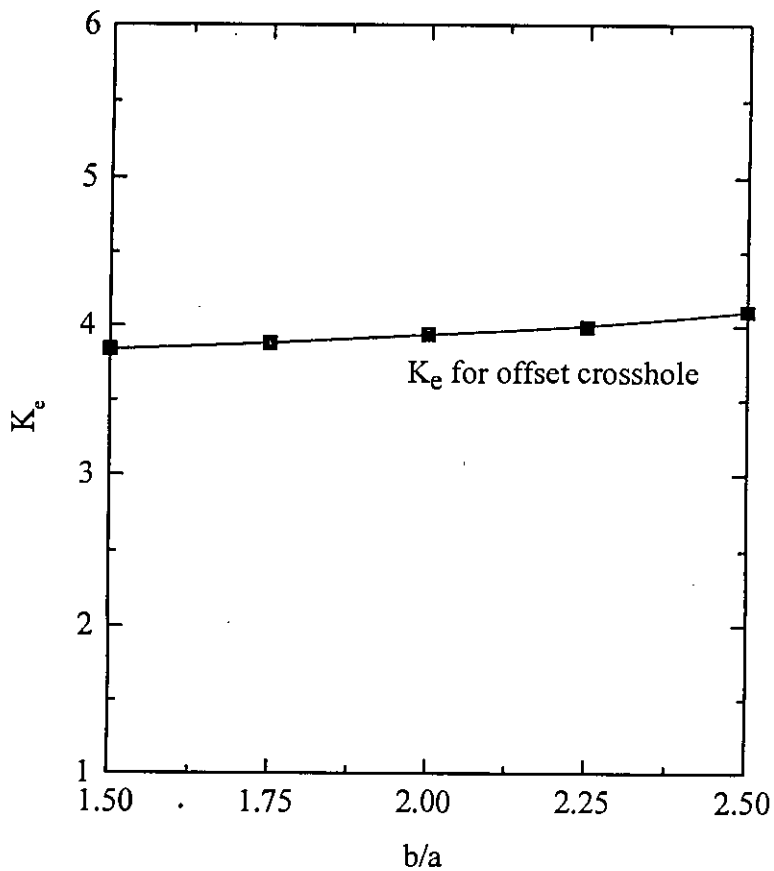
Figure 5.17: The effect of thickness ratio on von Mises equivalent SCF for larger offset cross holes (longitudinal direction)

69
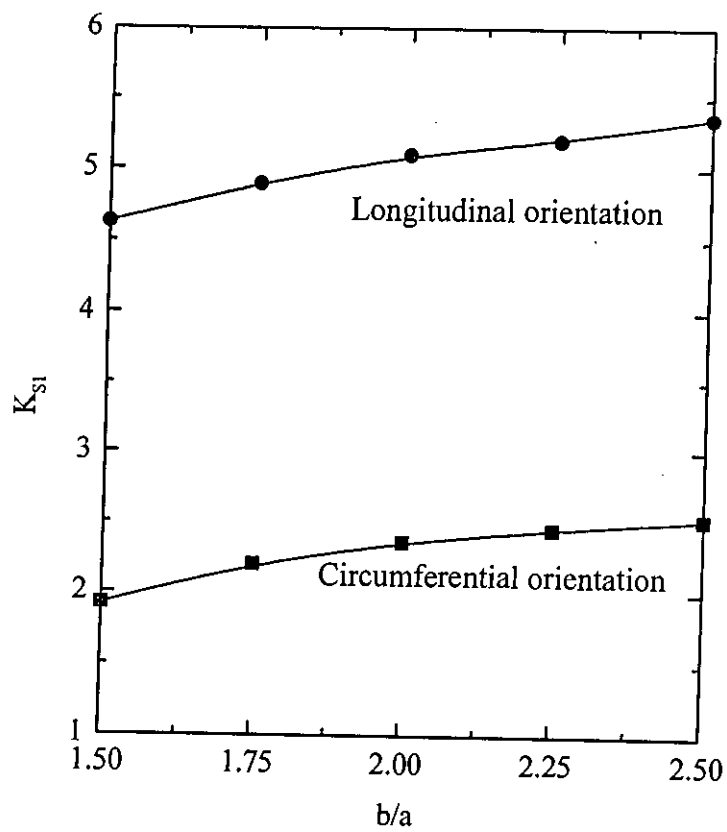
Figure 5.18: Comparison of Principal SCFs for larger radial crossholes between longitudinal and circumferential orientation
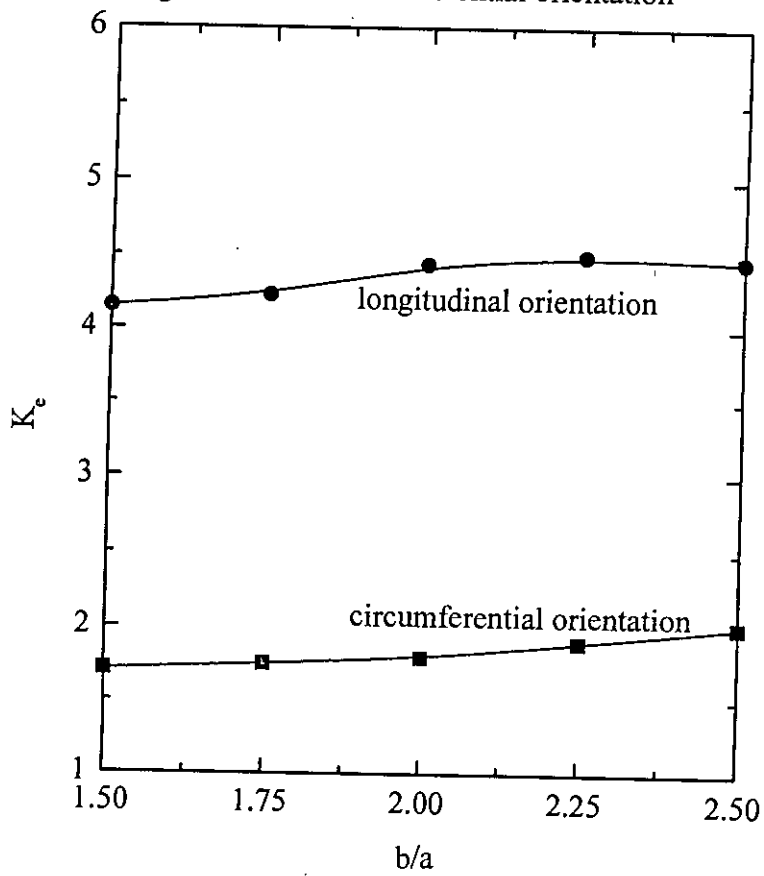
Figure 5.19: Comparison of von Mises Equivalent SCFs for larger radial crossholes between longitudinal and circumferential orientation
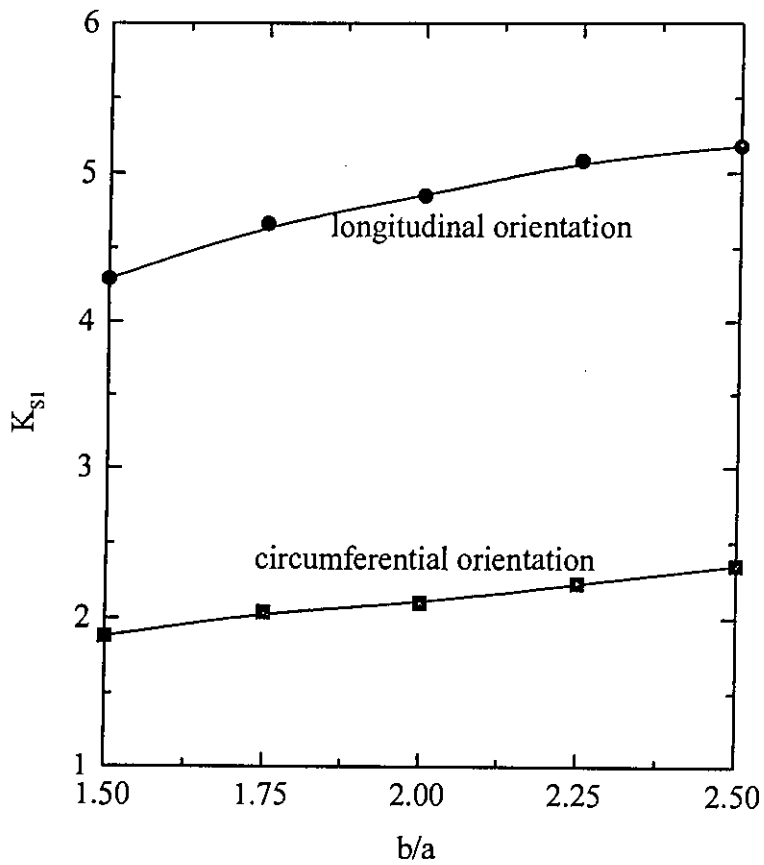
Figure 5.20: Comparison of Principal SCFs for larger offset crossholes between
longitudinal and circumferential orientation
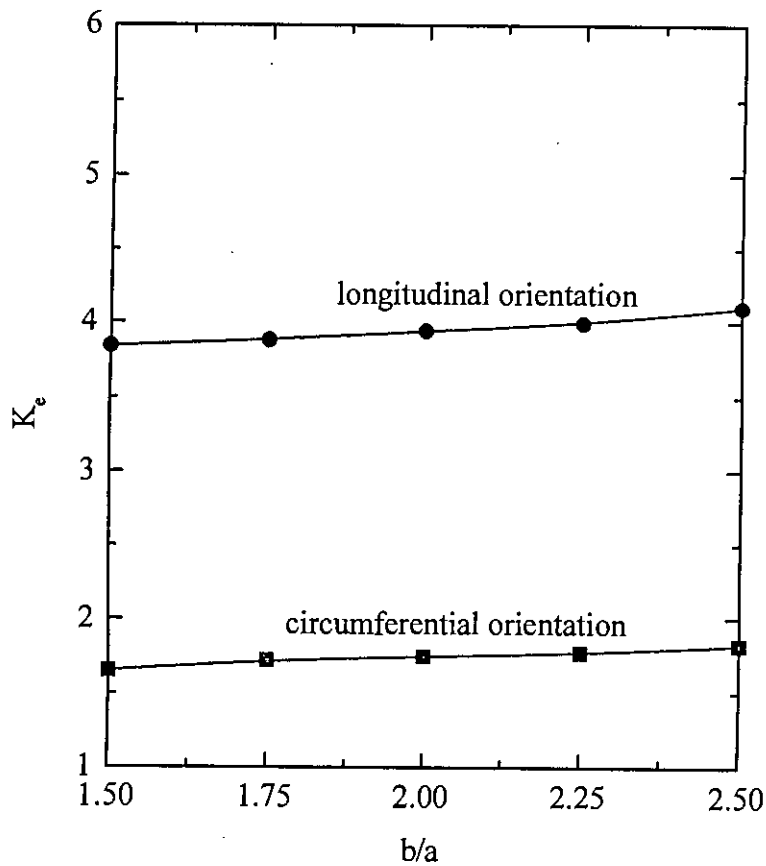
Figure 5.21: Comparison of von Mises Equivalent SCFs for larger offset crossholes
between longitudinal and circumferential orientation
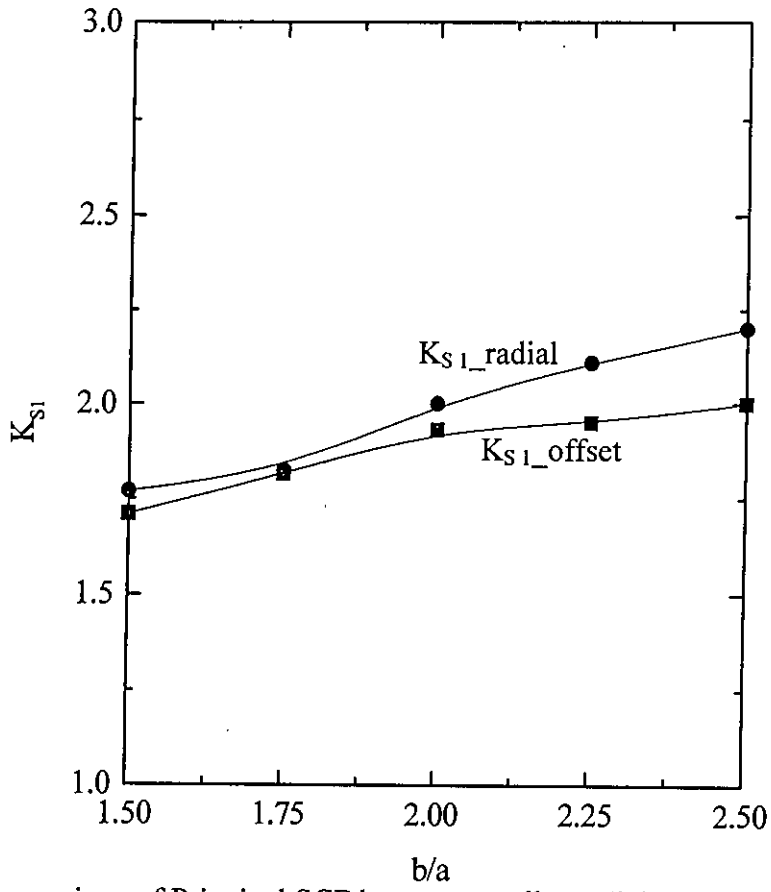
Figure 5.22: Comparison of Principal SCF between smaller radial and offset crosshole
for circumferential orientation
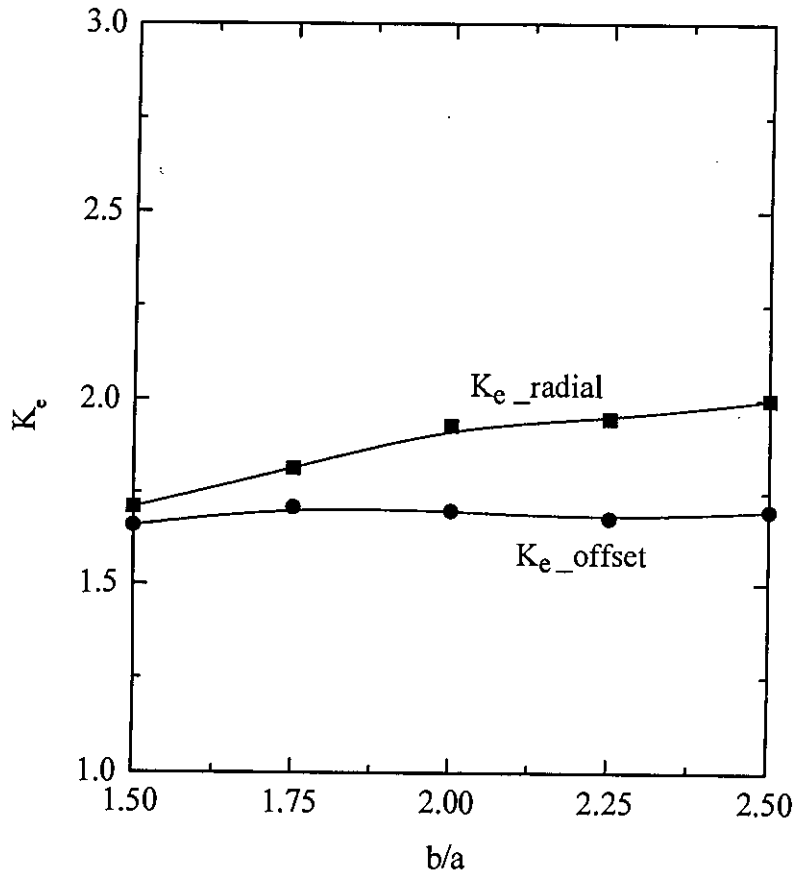
Figure 5.23: Comparison of von Mises SCF between smaller radial and offset crosshole
for circumferential orientation
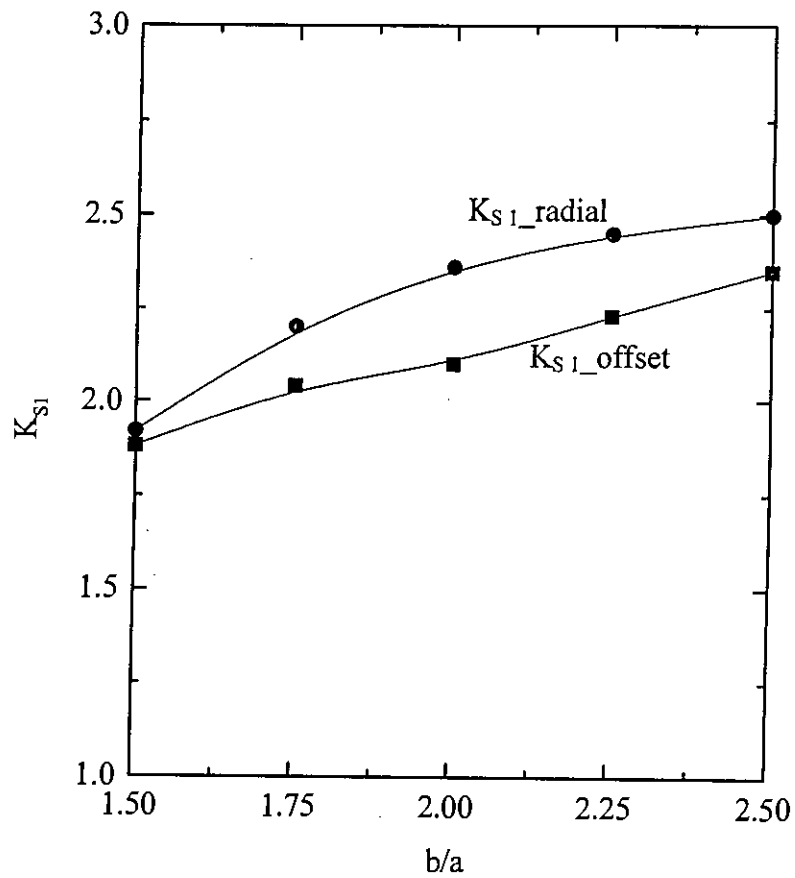
Figure 5.24: Comparison of Principal SCF between large radial and offset crosshole for circumferential orientation
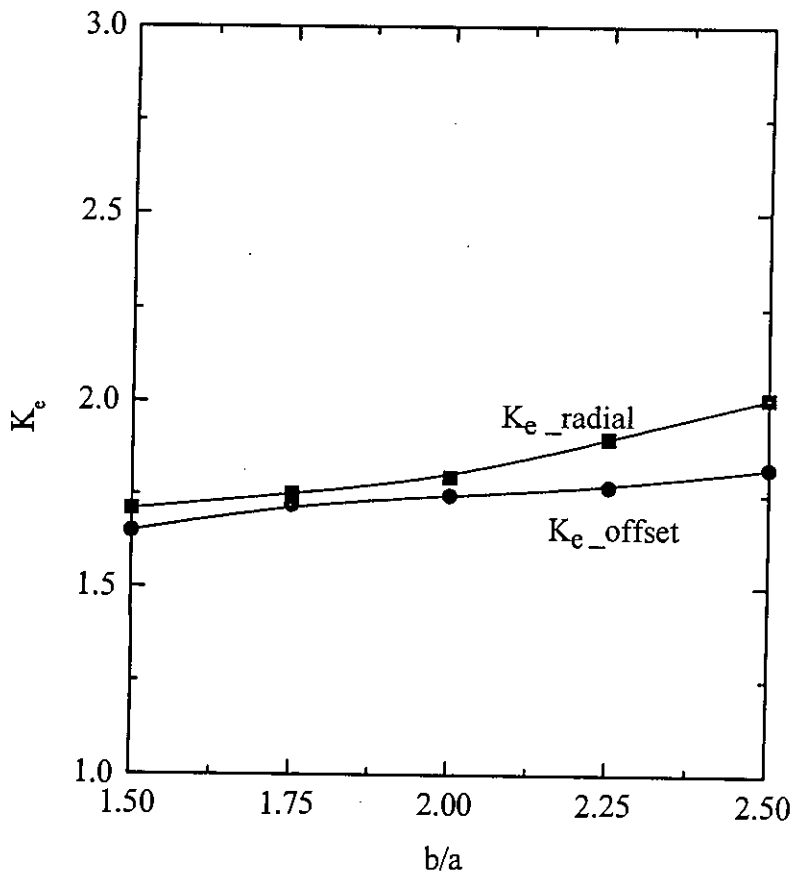
Figure 5.25: Comparison of von Mises SCF between larger radial and offset crosshole for circumferential orientation

73
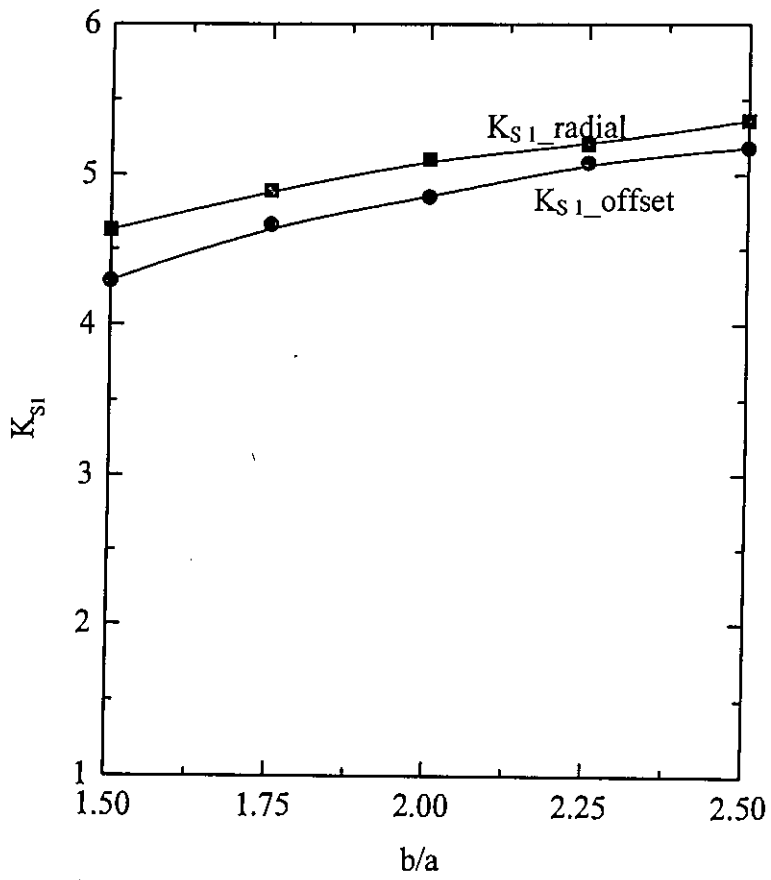
Figure 5.26: Comparison of Principal SCF between large radial and offset crosshole for longitudinal orientation
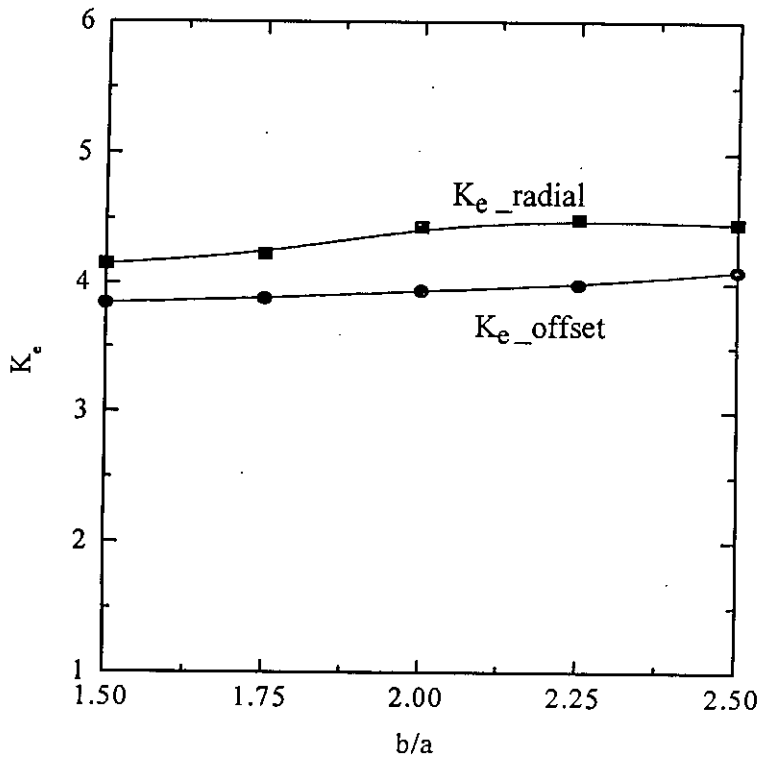
Figure 5.27: Comparison of von Mises SCF between large radial and offset crosshole for longitudinal orientation

74
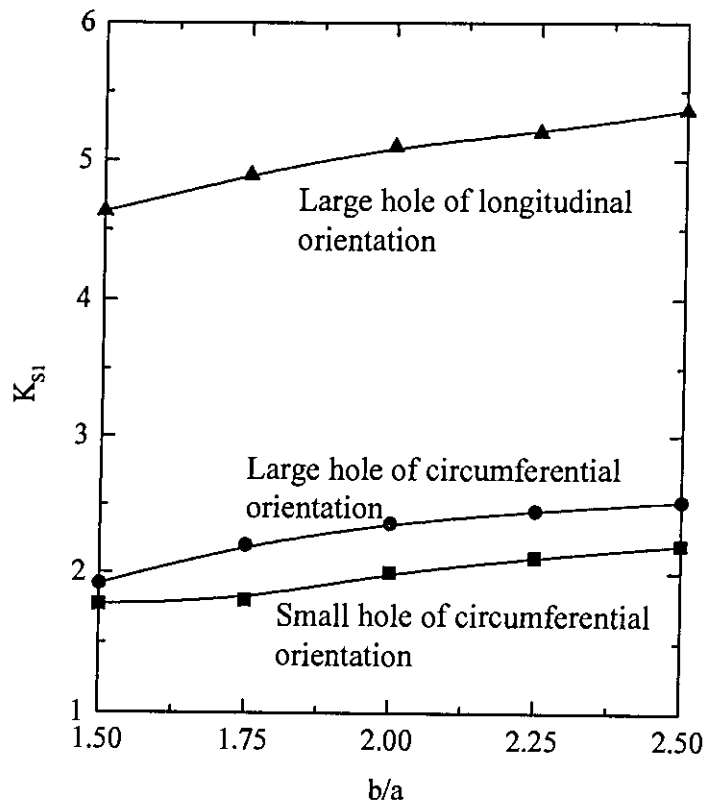
Figure 5.28: Comparison Principal SCFs between smaller and larger radial cross holes
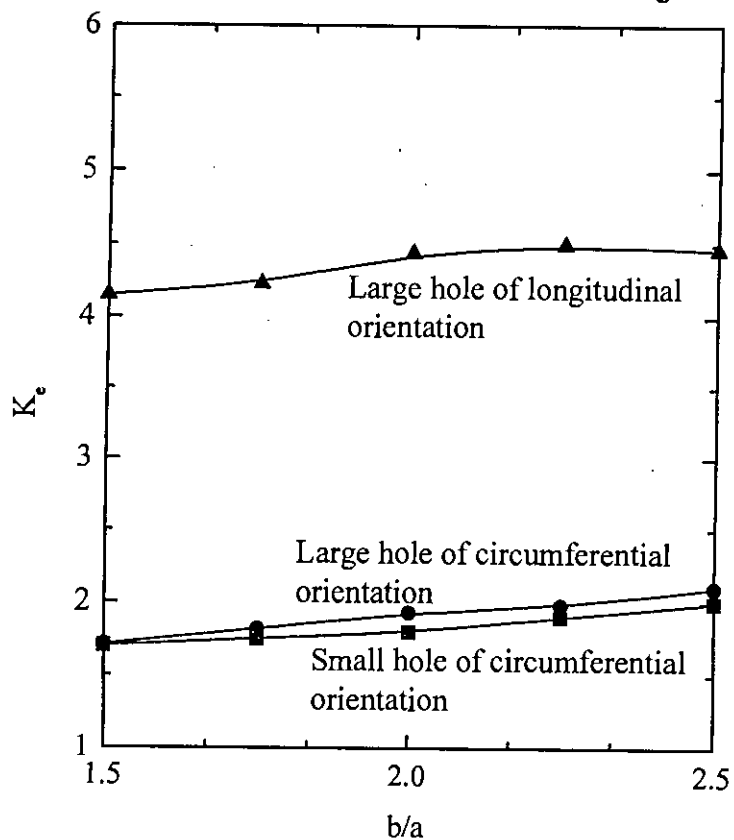
Figure 5.29: Comparison von Mises equivalent SCFs between smaller and larger radial cross holes

75
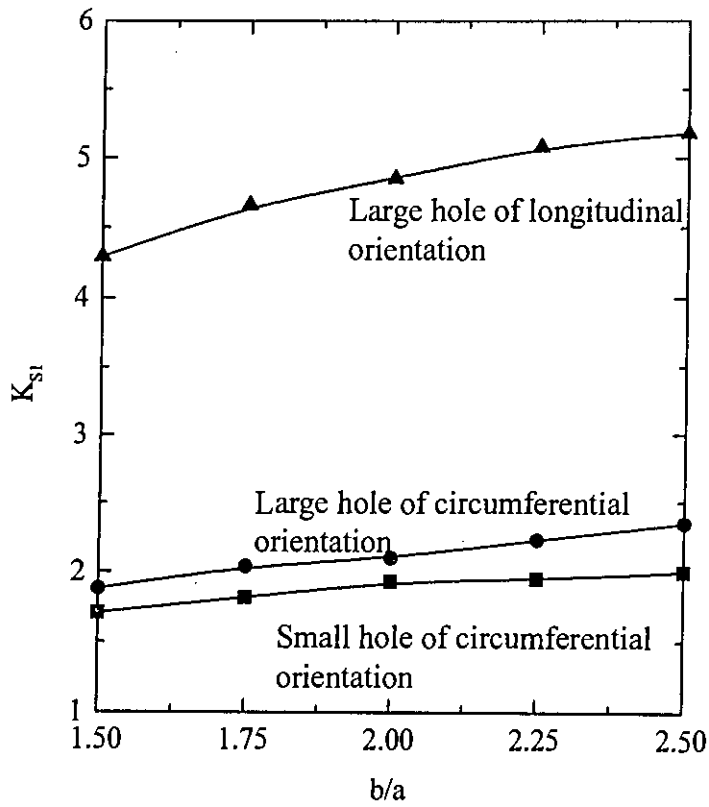
Figure 5.30: Comparison Principal SCFs between smaller and larger offset cross holes
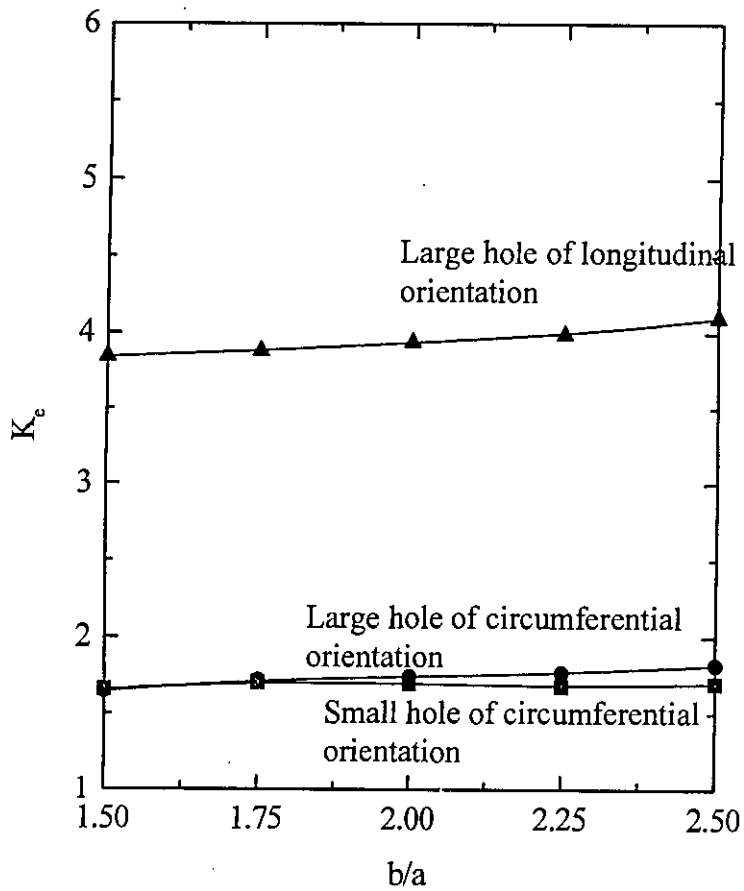
Figure 5.31: Comparison von Mises equivalent SCFs between smaller and larger offset
cross holes
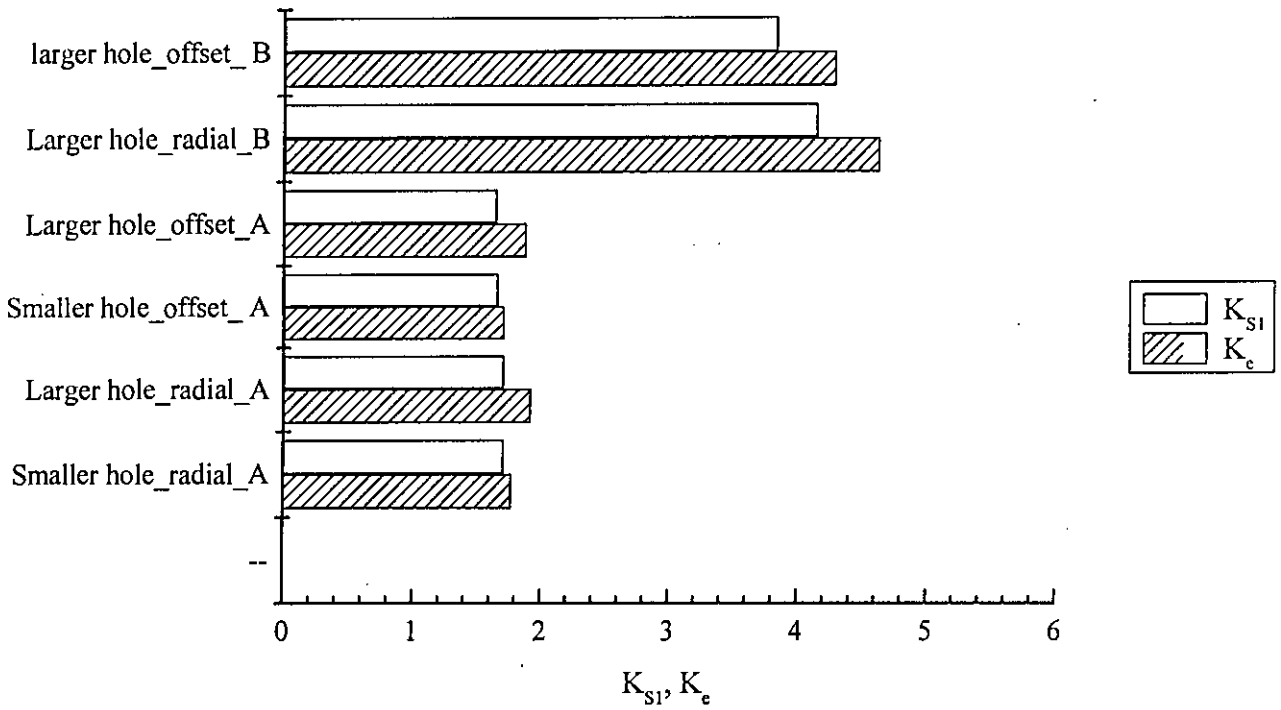
Figure 5.32: Comparison of hole sizes and orientation of the elliptical cross hole for
b/a =1.5
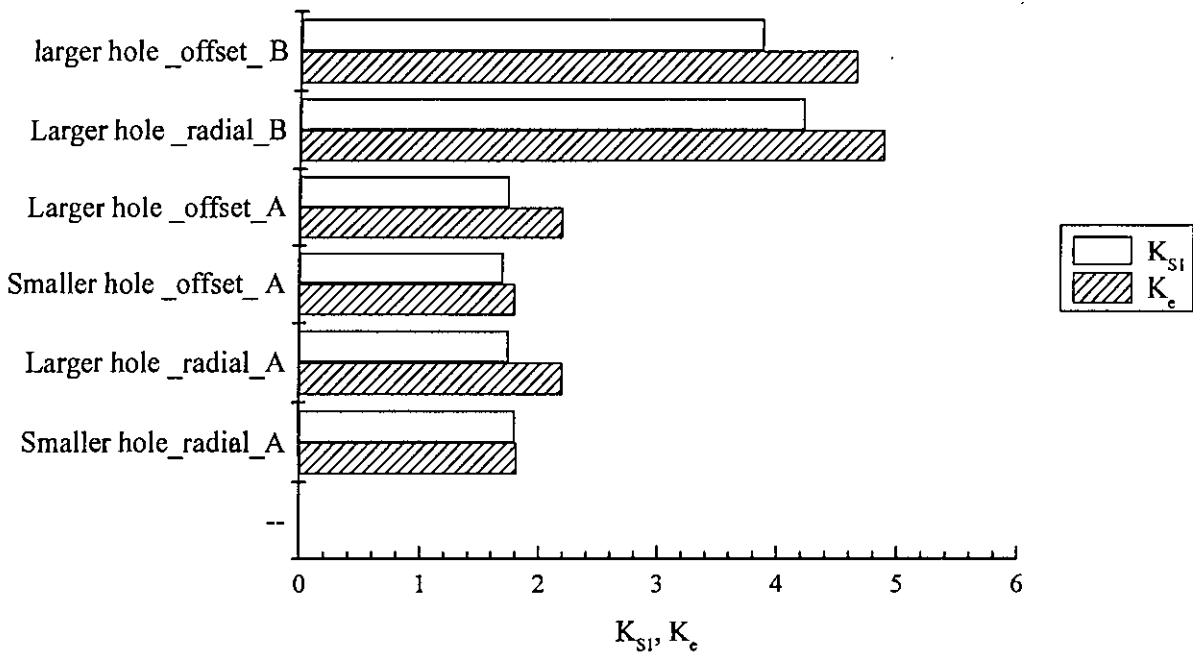
Figure 5.33: Comparison of hole sizes and orientation of the elliptical cross hole for
b/a =1.75
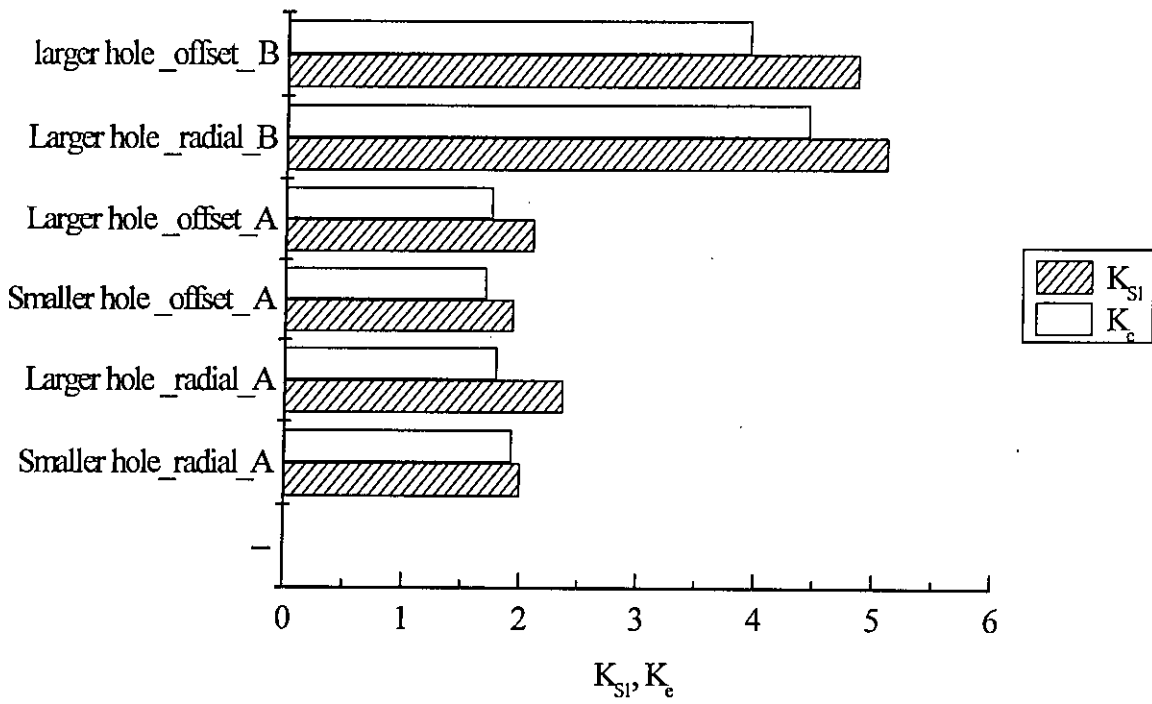
Figure 5.34: Comparison of hole sizes and orientation of the elliptical cross hole for
b/a =2.0
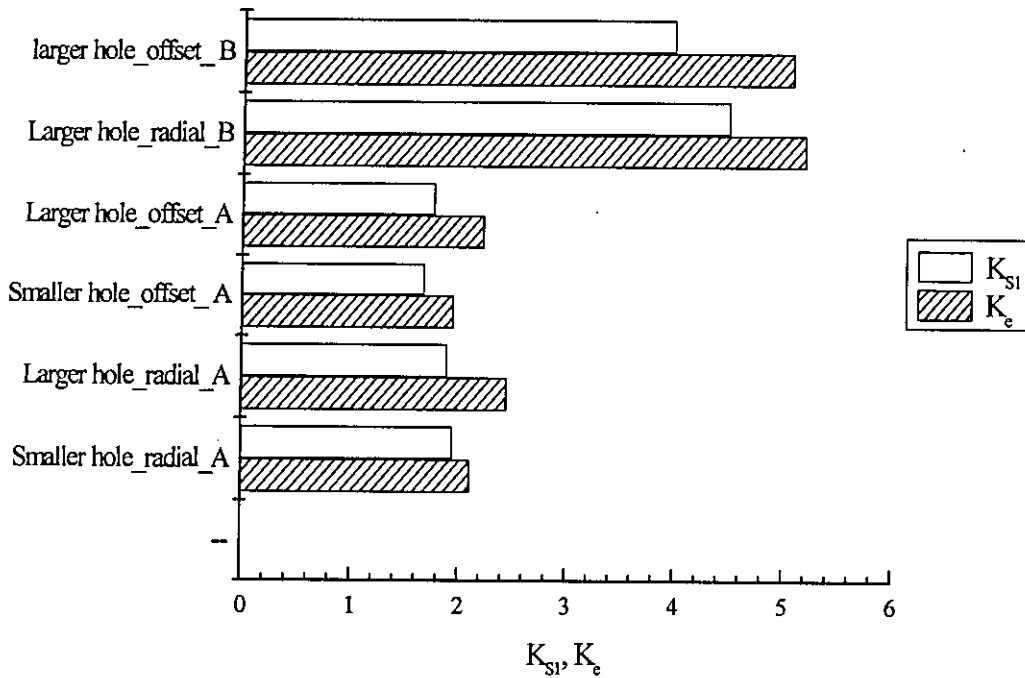
Figure 5.35: Comparison of hole sizes and orientation of the elliptical cross hole for
b/a =2.25
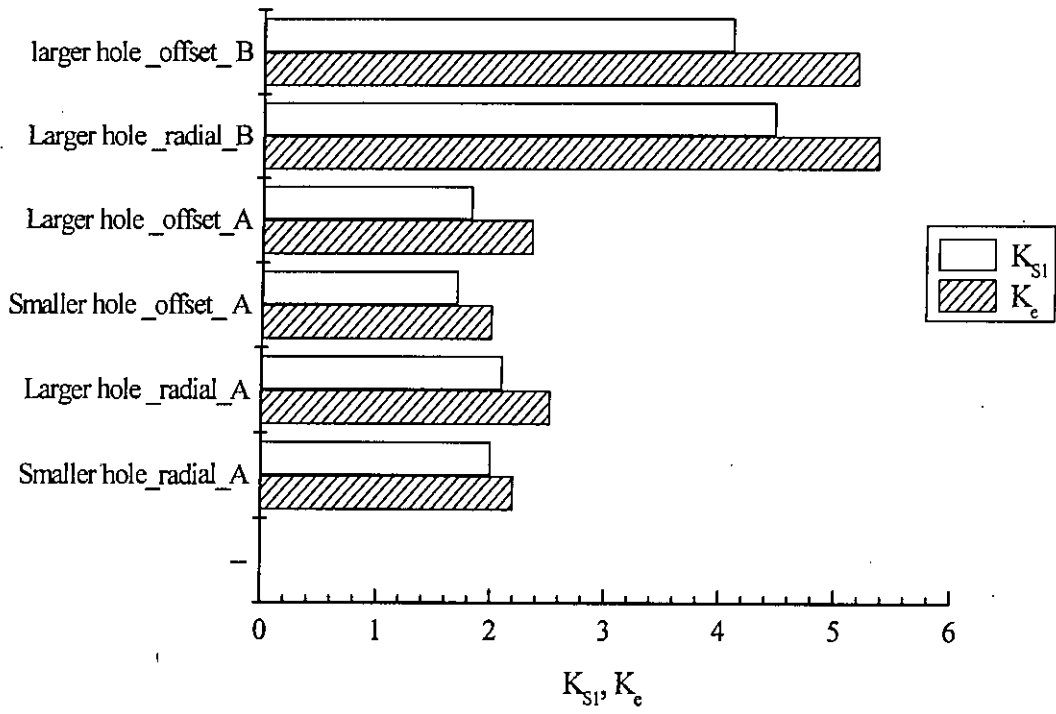
Figure 5.36: Comparison of hole sizes and orientation of the elliptical cross hole for b/a =2.50
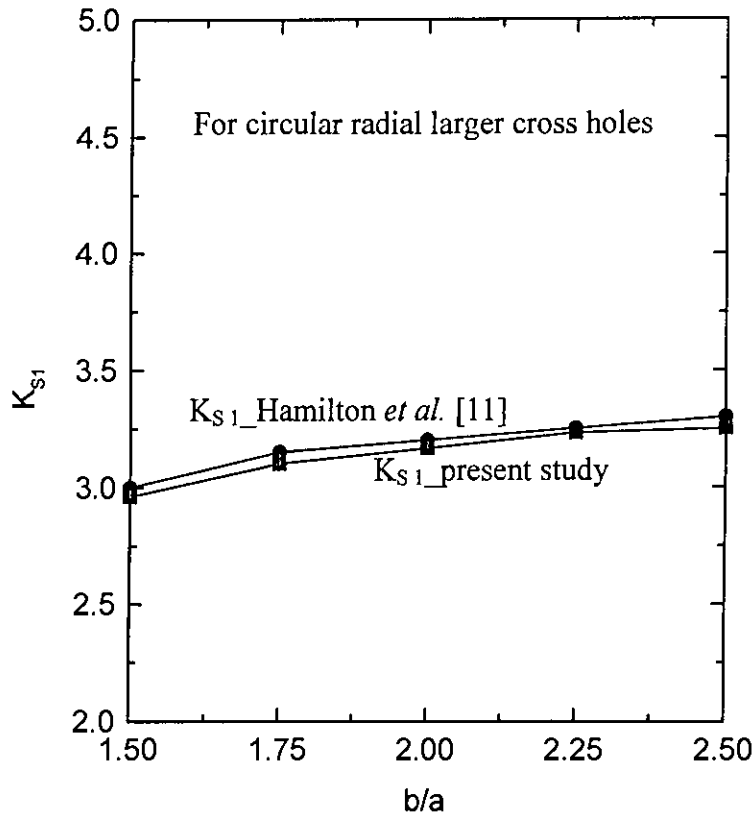
Figure5.37: Comparison of Principal SCFs for circular cross holes between the present study and the results of Hamilton et al.
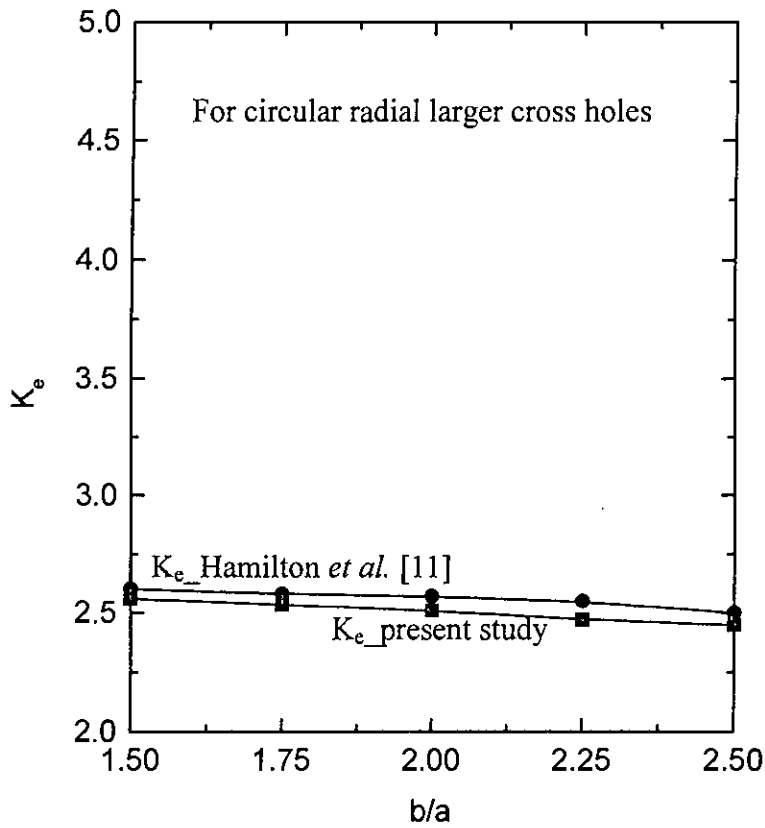
Figure5.38: Comparison of von Mises SCFs for circular cross holes between the present study and the results of Hamilton et al.
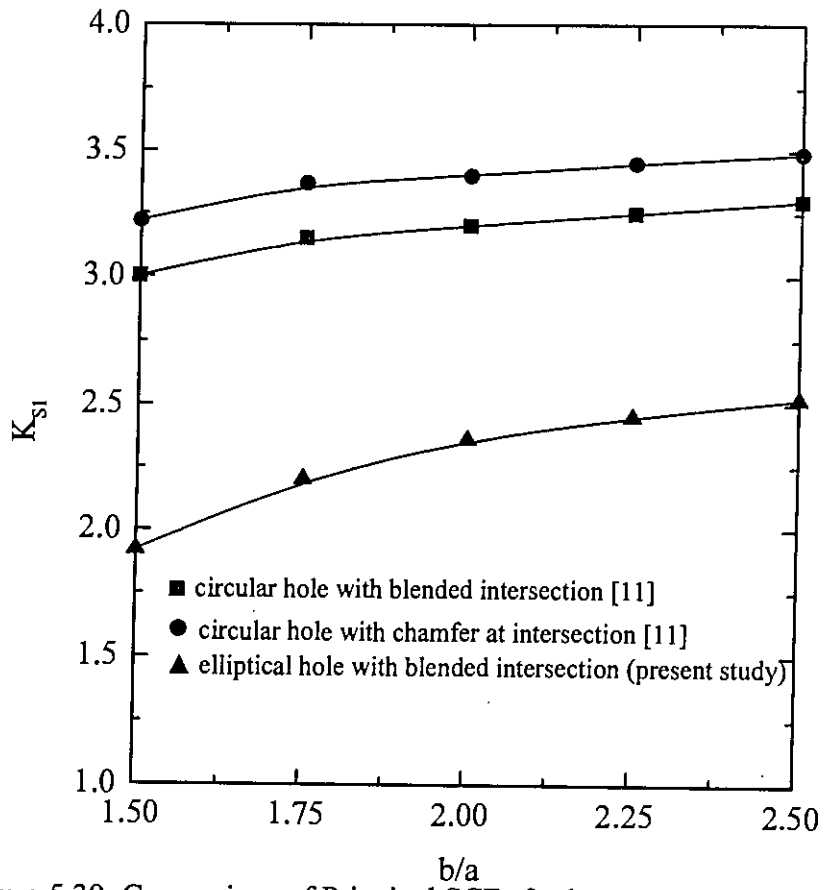
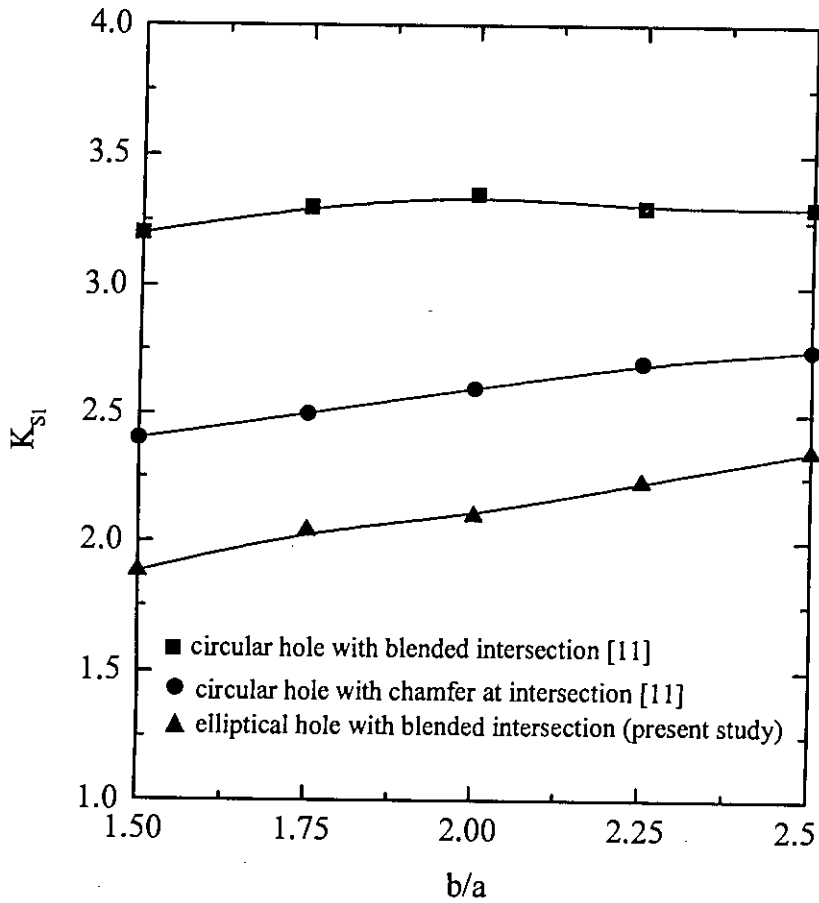Figure 5.39: Comparison of Principal SCFs for larger radial crossbore

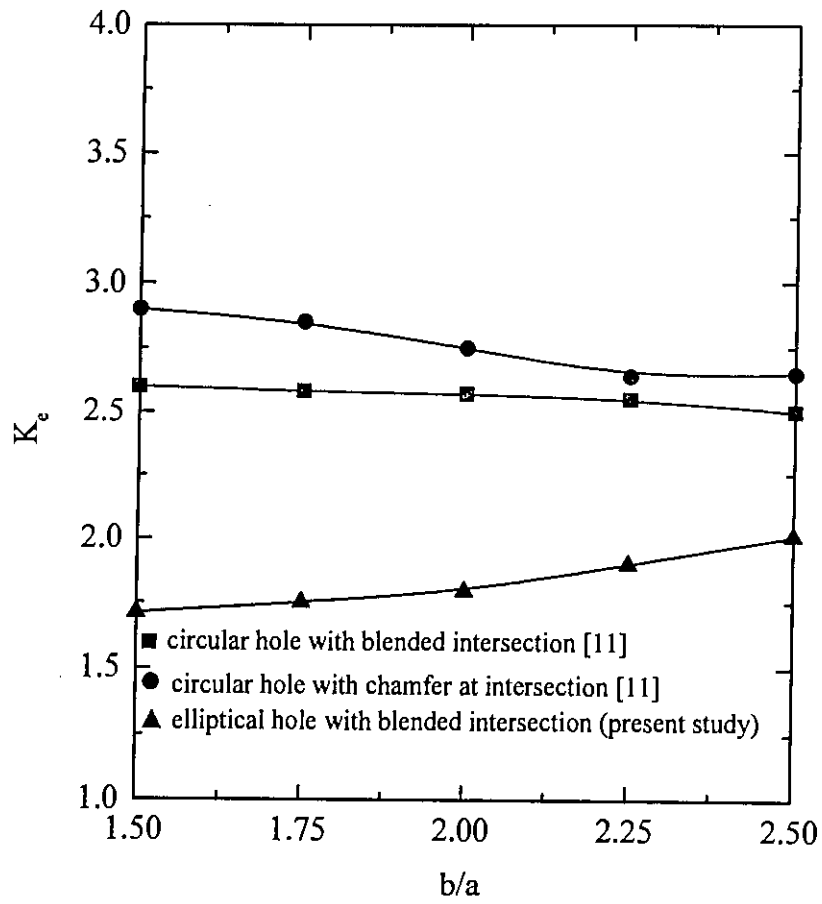Figure 5.40: Comparison of Principal SCFs for large bore offset crossbores

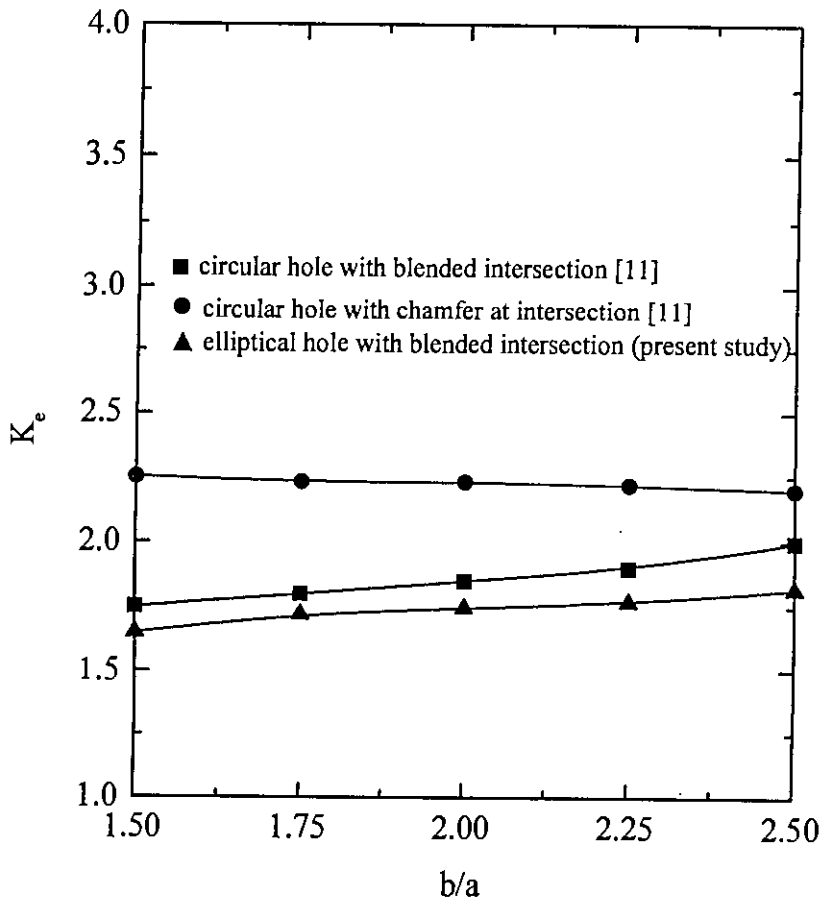Figure 5.41: Comparison of von Mises equivalent SCFs of larger radial crossholes.

Figure 5.42: Comparison of von Mises Equivalent stresses for larger offset cross hole
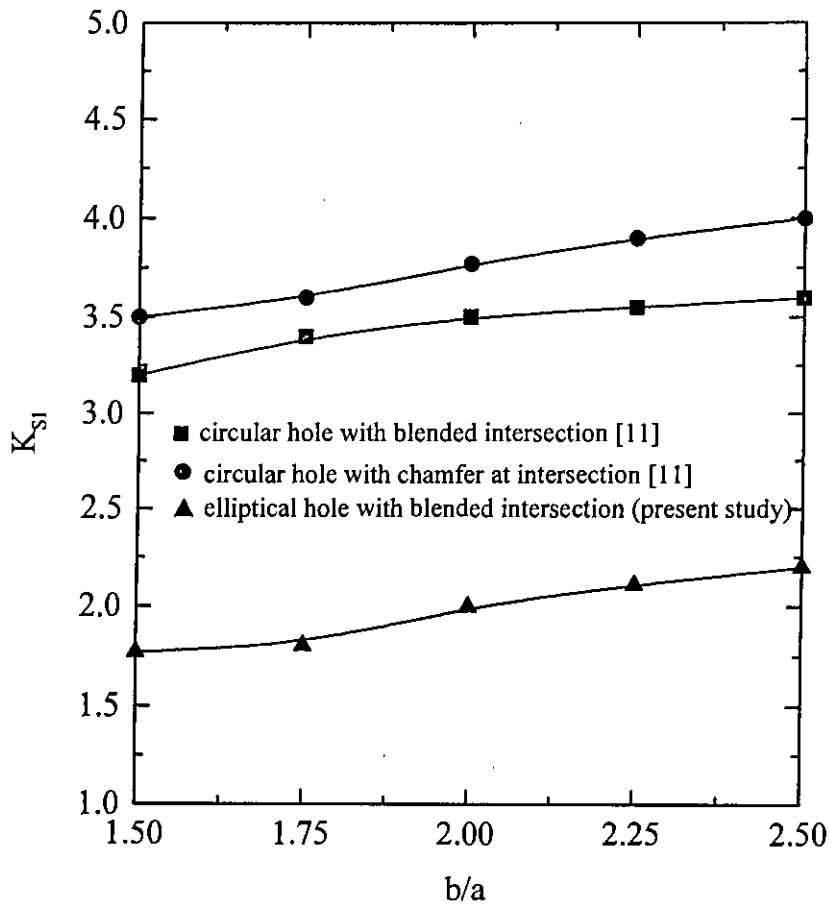
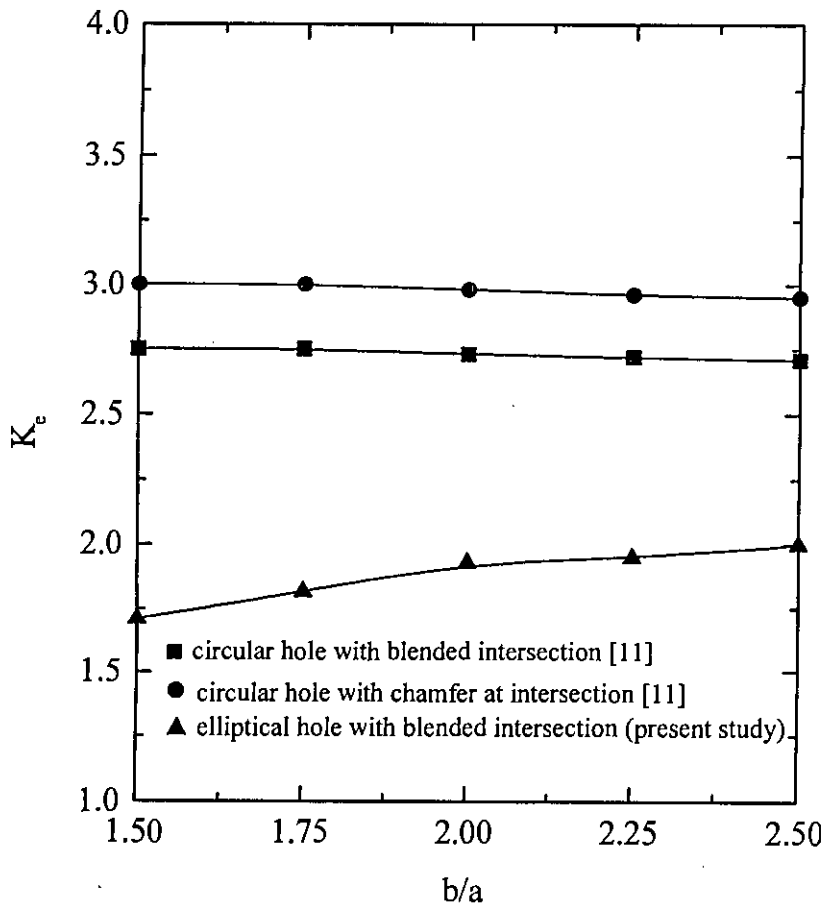Figure 5..43: Comparsion of Principal SCFs between smaller radial crossholes

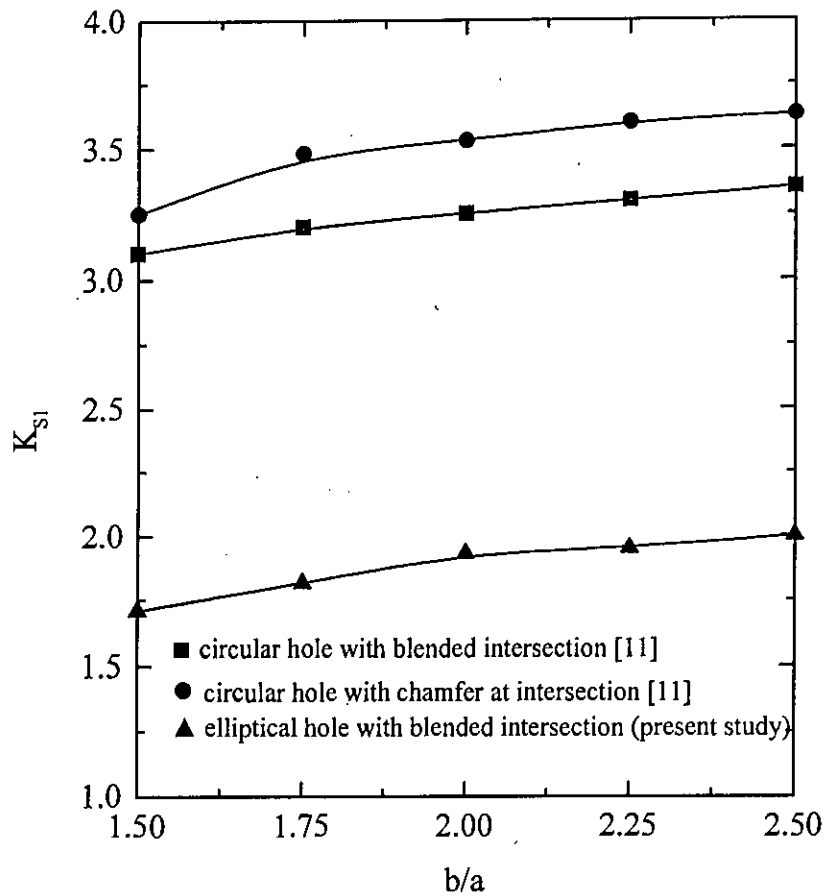Figure 5.44: Comparison of von Mises equivalent SCFs of smaller radial crossholes

Figure 5.45: Comparison of principal SCFs for smaller bore offset crossholes
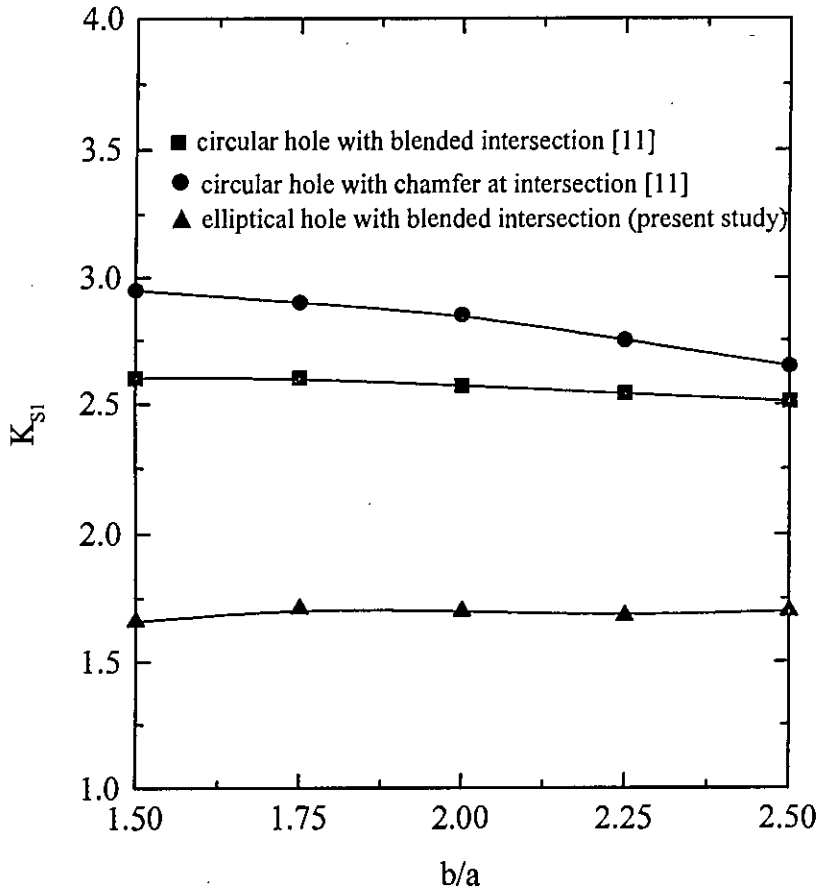

Figure 5.46: Comparison of von Mises Equivalent stresses for smaller bore offset crossholes

REFERENCES:

[1] Fessler, H. and Lewin, B. H., "Stress distribution in the tee junction of thick pipes.", British Jour. of Applied Physics, Vol-7, pp 76-79, 1956.

[2] Lake, G. F.,In Proceedings of IMechE conference on the fatigue of metals, p734, 1956.

[3] Fauple, J. H., and Harris, D. B., "Stress distribution in heavy walled cylindrical vessels.", Ind. Engineering Chemistry, Vol-49(12), pp 1979-1986, 1957.

[4] Morrison, J. L. M., Crossland, B. and Parry, J.S.C., "Fatigue strength of cylinders with branch holes. Journal of Mechanical Engineering Sciences, pp. 207-210, 1959.

[5] Cole, B. N., "Strategy for cross-bored in high pressure containers." J. Mech. Engineering Science., Vol-11(2), pp 151-161, 1969.

[6] Gerdeen, J. C., "Analysis of the stress concentrations in thick cylinders with sideholes and crossholes.", Trans. of ASME J. Engineering for Industry, Vol-94, pp 815-823, 1972.

[7] Gerdeen, J. C. and Smith, R.E.," Experimental determination of stress concentration factors in thick walled cylinders with holes." Expl Mechanics, Vol.-12, pp. 503-526, 1972.

[8] Masu, L. M. and Craggs, G., "Fatigue strength of thick walled cylinders containing cross bores", Journal of Mechanical Engineering Science, Vol-206, pp 299-309, 1997.

[9] .Masu, L. M., "Cross bore configuration and size effects on the stress distribution in thick walled cylinders.", International Journal of Pressure Vessels and Pipings, Vol-72, pp. 171-176, 1997.

[10] Masu, L. M., "Numerical analysis of cylinders containing circular offsets crossbores.", International Journal of Pressure Vessels Piping, Vol-75, pp 191-196, 1998.

[11] Makulsawatudom P., Mackenzie D. and Hamilton R., "Stress Concentration at Crossholes in Thick Cylindrical Vessels", International Journal of Pressure Vessels Piping, Vol-39, pp 471-481, 2004.

[12] Murthy, M.V. V., "Stresses around an elliptic hole in a thin cylindricall shell", Transaction of ASME: Journal of Applied Mechanics, Vol. 36, pp. 39-46, 1972.

[13] Murthy, M.V. V.and Bapu Rao, "Stresses in a thin cylindrical shell weakened by an elliptical hole with major axis perpendicular to shell axis.", Transaction of ASME: Journal of Applied Mechanics, Vol. 37, pp. 539-41, 1972.

[14] Fenner, R.T. and Nadiri, F., " On the use of elliptical side branches to Thick walled cylinders.", International Journal of Pressure Vessels Piping, Vol-20, pp 139-154, 1985.

[15] Ficenec, I., "The influence of cross bores on the bursting strength of high pressure containers." PhD thesis, University of Leeds, 1972.

[16] Ford, H., Watson, E.M. and Cross land, B., "Thoughts on a code of practice for forged high pressures on monobloc design." , Transaction of ASME: Journal of Pressure Vessel Technology., Vol- 103, pp. 2-8, 1981

[17] Iwadate, I., Chiba, K., Watanabe, J., Mima, S., Tokai, K. and Tahade, H., "Safety analysis at cross bore corner of high pressure polyethylene reactors." In proceedings of the ASME Pressure Vessels and piping Conference, Vol-48, pp/ 117, 1981.

[18] Timoshenko, S. P. and Goodier, J. N., "Theory of Elasticity", 3rd edition, Newyork, McGraw Hill Company Limited, 1985

[19] Fong, T., "Statistical aspects of fatigue at microstructure, specimen and component levels" , Fatigue Mechanisms, Proceedings of an ASTM- NBS- NSF Symposium, STP 675, pp. 729, 1975.

[20] Chandrupatla, T. R. & Belegunda, A. D. (2004), "Introduction to Finite Elements in Engineering."

[21] Ottoson, N. S. & Peterson, H. (1992), "Introduction to Finite Element Method."

[22] *ANSYS V 5.4,*1997, ANSYS Incorporation, Canonsberg, Pennsylvania.

[23] Chakrabarty, J.(1987), " Thoery of Plasticity".